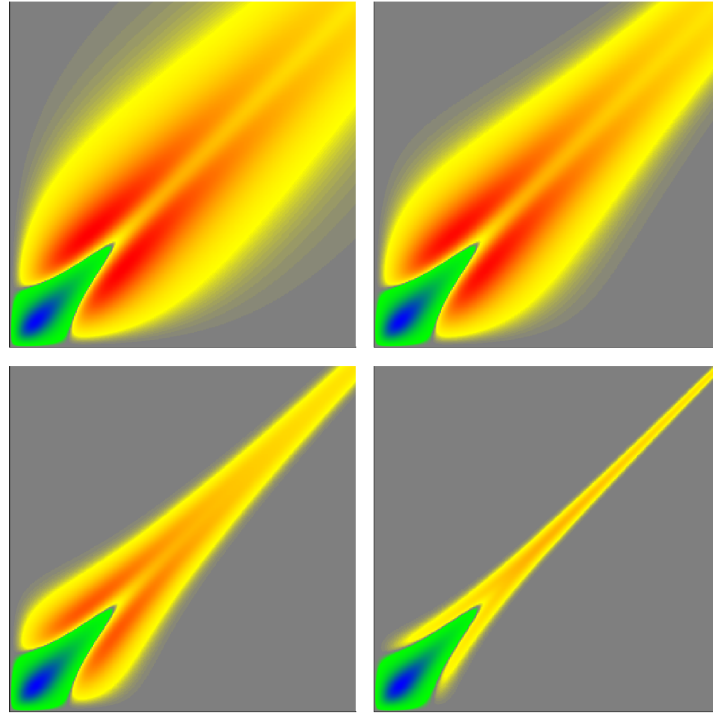


CHALMERS



The Similarity Renormalization Group for three bosons in a momentum-space partial-wave basis

Master's Thesis at the Department of Fundamental Physics

BORIS D. CARLSSON

Department of Fundamental Physics
CHALMERS UNIVERSITY OF TECHNOLOGY
Gothenburg, Sweden 2012
Master's Thesis 2012

The Similarity Renormalization Group for three bosons in a momentum-
space partial-wave basis
BORIS D. CARLSSON

© BORIS D. CARLSSON, 2012.

Technical report 2012
Department of Fundamental Physics
Chalmers University of Technology
SE-412 96 Göteborg
Sweden
Telephone + 46 (0)31-772 1000

Cover:
SRG transformation of the modified Yukawa potential in a momentum-
space partial-wave basis for $L_p = 2$.

Printed by Chalmers Reproservice
Göteborg, Sweden 2012

The Similarity Renormalization Group for three
bosons in a momentum-space partial-wave basis

BORIS D. CARLSSON

Department of Fundamental Physics
CHALMERS UNIVERSITY OF TECHNOLOGY
Göteborg, Sweden 2012

Abstract

The Similarity Renormalization Group (SRG) flow equation is explored for systems of two and three spinless bosons in a momentum-space partial-wave basis. The two- and three-body binding energies as well as the phaseshifts are used to gauge that the transformation is unitary and to study how well the SRG decouples high- and low-energy physics. I consider four different potentials with different characteristics: Two simplified nucleon potentials and two inter-atomic helium potentials (a soft-core potential and the state-of-the-art LM2M2 potential that is fitted to a wealth of experimental data). An initial three-body force is included for two of these potentials. Even with only two-body terms in the initial hamiltonian, SRG induced many-body forces are shown to arise during the transformation. These induced forces are computed for the three-body system and their evolution is studied as a function of the flow parameter. In all cases the SRG transformed potentials display greatly improved decoupling. This is achieved with a three-body binding-energy deviation of less than 0.1% in all cases except for the soft-core helium potential.

Sammanfattning

Egenskaperna för flödesekvationen Similarity Renormalization Group (SRG) undersöks för två och tre partiklar i en partiell-våg-bas i momentrummet. Bindningsenergin för två och tre partiklar samt fasskiften att bekräfta att transformationen är unitär och för att undersöka i vilken utsträckning SRG-transformationen separerar hög- och låg-energifysik. Jag betraktar fyra olika potentialer med olika egenskaper: Två förenklade nukleonpotentialer och två interatomära heliumpotentialer (en svag, fenomenologisk potential och LM2M2-potentialen som reproducerar en mängd experimentell data). En initiala trekropparskraft är inkluderad i två av potentialerna. Jag visar att även med bara tvåkropparstermer i den initiala hamiltonianen så induceras flerkropparskrafter av SRG-transformationen. Dessa inducerade krafter beräknas för trekropparsystem och deras evolution studeras som funktion av flödesparametern. För varje potential jag har arbetat med separeras låg- och högenergifysik i stor utsträckning. Detta uppnås under förutsättningen att bindningsenergin för tre partiklar inte förändras mer än 0.1% förutom för den svaga, fenomenologiska heliumpotentialen.

Acknowledgements

First of all I would like to thank my supervisors Christian Forssén and Lucas Platter for help and guidance. I thank Henrik Gustafsson, Elias Hartvigson, Anton Johansson, Håkan Johansson, Malin Klintefjord, Jonathan Lindgren, Björn Morén and Oscar Åkerlund for help, discussions and feedback. I also want to thank the sub atomic group at Chalmers for providing computers to run the calculations on.

Boris Carlsson, Gothenburg 2012-11-03

Contents

1	Introduction	1
1.1	Specific aim	2
1.2	Method	2
1.3	Reading guide	2
1.3.1	Notation	3
I	Theory	4
2	Quantum few-body states	4
2.1	Jacobi coordinates	4
2.1.1	Normalization	5
2.1.2	Kinetic energy	6
2.2	Partial-wave basis	6
2.2.1	Symmetrical states	7
2.2.2	Three particles	7
2.2.3	Partially symmetric states for three particles	8
2.2.4	The Wigner-Eckart theorem	8
2.3	Harmonic-oscillator basis	9
3	Types of potentials	11
4	Basis transformations	11
4.1	Partial-wave projection for two particles	12
4.2	From position space to partial-wave basis in momentum space for two particles	12
4.3	Partial-wave projection for three particles	13
4.4	From position space to harmonic-oscillator basis for two particles	16
5	Few-body Observables	16
5.1	The transition operator for two particles	16
5.2	The permutation operators	18
5.2.1	Two-body potentials acting on three-body states	19
5.3	Binding energy	20
5.3.1	Two particles in a partial-wave basis	20
5.3.2	Two particles in a harmonic-oscillator basis	21
5.3.3	Three particles in a partial-wave basis	21
5.4	Low-energy scattering parameters	23
6	The SRG flow equation	24
II	Implementation	26

7	Discretization of space	26
7.1	Discretized representation	26
7.2	Discretized integration	27
8	The permutation operator	28
8.1	Interpolation and extrapolation	31
8.2	Matrix representations of the permutation operator	31
9	Calculation of the binding energy	32
9.1	Diagonalization in the harmonic-oscillator basis	32
9.2	Solving the kernel equation	32
9.2.1	Determinant method	33
9.2.2	Power iteration	34
9.2.3	Arnoldi iteration	34
9.3	The Kernels	35
9.3.1	Two-particle kernels	35
9.3.2	Three-particle kernels	35
10	Calculation of low-energy scattering observables	36
11	The SRG flow equation	37
11.1	In two-particle space	37
11.2	In three-particle space	38
III	Results	41
12	Introduction	41
12.1	Choice of units	41
12.2	Choice of grid	41
12.3	Error estimates	42
12.4	SRG evolution	42
13	Nucleon potentials	42
13.1	Three-body potential	43
13.2	Two-body results	46
13.2.1	Determination of the effective range	47
13.2.2	Comparison with a harmonic-oscillator basis	48
13.3	Three-body results	48
13.4	SRG evolution of the potentials	50
13.4.1	Two-body evolution	50
13.4.2	Three-body evolution	50
13.5	Decoupling	51

14 Helium potentials	56
14.1 Three-body potential	57
14.2 Two-body results	61
14.2.1 Comparison with a harmonic-oscillator basis	62
14.3 Three-body results	63
14.4 SRG evolution of the potentials	63
14.4.1 Two-body evolution	63
14.4.2 Three-body evolution	65
14.5 Decoupling	68
IV Conclusions	70
15 Algorithms	70
15.1 Faddeev equation	70
15.2 SRG flow equation	70
16 Results	70
16.1 Nucleon potentials	70
16.2 Helium potentials	71
17 Improvements	71
17.1 Momentum grids and angular momentum cutoff values	71
17.2 SRG flow equation	72
References	74
Appendices	75
A Quadratures	75
A.1 Gauss-Legendre	75
A.2 Gauss-Lobatto	76
A.3 Gauss-Radau	76
B Interpolation and extrapolation	76
C Permutation operators	77
D Software	78

1 Introduction

Strongly interacting few- and many-body systems are difficult to study since the strong interaction induces couplings between states in a wide energy range. There exists methods to decrease this coupling between energy scales, such as renormalization group techniques [1].

One such method is the Similarity Renormalization Group (SRG) [2, 3, 4]. It achieves this separation of energy scales – decoupling – through a continuous unitary transformation of the hamiltonian,

$$\hat{H}(s) = \hat{U}(s)\hat{H}(0)\hat{U}^\dagger(s), \quad (1.1)$$

where s is the flow parameter of the transformation and \hat{U} a unitary operator.

In this thesis, I have made a detailed study of the SRG transformation in a momentum-space partial-wave basis for two and three identical spinless bosons. The decoupling will cause low-energy observables to only depend on low momentum states, which will reduce the size of the matrix-representation of the hamiltonian needed in order to get converged few-body results. This becomes increasingly important when working with more particles.

The SRG transformation and its properties in a momentum-space partial-wave basis has so far not got much attention. The cases of three identical, spinless bosons in one dimension [5] and three identical fermions [6] have both been studied with demonstrated good decoupling properties. It has also been studied using the harmonic oscillator basis in the no-core shell-model (NCSM) [7, 8]. Therefore it is of interest to see how well it will perform in the present case of identical, spinless bosons in three dimensions using a momentum-space partial-wave basis.

I will show results of applying the SRG transformation to several different potentials, including both nuclear potentials and helium potentials.

The helium potentials studied are a simple gaussian potential and the LM2M2 potential [9]. The gaussian potential is constructed to reproduce the binding energy of the helium dimer and low-energy scattering parameters. For these calculations temperatures less than 2 mK are used. The LM2M2 potential was designed to reproduce various experimental data for the second virial coefficient, the viscosity and the thermal conductivity for several temperatures ranging from 1.47 K to 2500 K [9]. To fit high-energy data, a more detailed resolution of the potential at short distances is needed, which results in the need of a strongly repulsive core, a characteristic not present in the everywhere attractive gaussian potential. One of the goals of this thesis is to see how this difference between the construction of the gaussian and LM2M2 potential affects the decoupling behaviour of the SRG transformation.

The low-energy observables I study in this thesis are the two-body and three-body binding energy, the scattering length and the effective range. As for the SRG equation I present detailed theoretical derivations of the equations needed to calculate these observables and describe how I implement and solve them. For the three-body binding energy I use the Faddeev equation, and for the calculation of the scattering parameters I use the transition operator.

1.1 Specific aim

The main task is to implement and apply the SRG flow equation in a momentum-space partial-wave basis to a set of potentials. The goal with this is to demonstrate decoupling, meaning that the high-energy parts of the potential can be ignored when doing low-energy calculations.

Due to the difficulty of evaluating some of the potentials in a momentum-space partial-wave basis, another goal has been to be able to do this in a fast and accurate manner.

1.2 Method

The SRG flow equation is an ordinary differential equation. To solve this I need an ODE solver. I have chosen to use the general-purpose explicit embedded Runge-Kutta-Fehlberg method, since the problem is not stiff.

To verify the unitarity of the SRG transformation, I need to calculate some low-energy two- and three-body observables and make sure the values of these observables do not depend on the value of the SRG flow parameter. I have chosen to calculate the two- and three-body binding energy and also the scattering length and effective range which are two-body observables.

The three-body binding energy is calculated using the Faddeev equation, which is obtained by rewriting the time-independent Schrödinger equation.

To obtain the scattering parameters scattering length and effective range, I need the on-shell transition operator for low energies. These values are not trivial to calculate due to the behaviour of the transition operator for positive energies.

I implement all this in the programming language C, since it is a language for fast computing with many good available libraries. Particularly, I will use the open-source library GNU Scientific Library [10].

1.3 Reading guide

Throughout the report, I have used natural units for which $\hbar = c = 1$. This will make the units for time and length equal. Since energy can be written as $\hbar\omega$, where the unit of ω is inverse time, I can use inverse length as a unit of energy. From the relations $E^2 = m^2c^4 + p^2c^2$ I get that energy, mass and momentum all have the same unit. This means that inverse length will be used as unit for all of these physical quantities.

The report is divided into four parts:

- The first part is the theory, where all the mathematical formulas and relations are shown and derived.
- The second part is about the implementation and how the equations derived in the theory part are realised as algorithms in the computer.
- In the third part I present the results for some potentials.

- The fourth part contains an analysis of the results, a conclusion and an outlook.

1.3.1 Notation

- Quantum operators are written with a hat, \hat{A}
 - Two-body potentials are denoted \hat{V}
 - Three-body potentials are denoted \hat{U}
- Vectors are written in boldface, \mathbf{x}
- Unit vectors are written in boldface with a hat, $\hat{\mathbf{x}}$
- Matrices are written with an inverted hat, \check{A}
- Ordinary matrix multiplication is written without an extra symbol, $\check{A}\check{B}$
- When one of the matrices is diagonal, it is written with a star inbetween, $\check{A}\star\check{B}$
- When one of the matrices is block diagonal, it is written with a star and a letter, $\check{A}\star^x\check{B}$, where x is the non diagonal variable. This will be made clearer in the implementation part.
- The diagonal of matrix \check{A} is written with an arrow above, $\vec{\check{A}}$

Part I

Theory

2 Quantum few-body states

A spinless boson has no internal degrees of freedom, so a complete set of states for one such particle is given by the position eigenstates $|\mathbf{x}_1\rangle$ or the momentum eigenstates $|\mathbf{p}_1\rangle$. A complete set of states for several such particles is simply the tensor product of the one particle basis states. For example, for two particles, the states $|\mathbf{x}_1\rangle \otimes |\mathbf{x}_2\rangle$ could be used as a basis.

2.1 Jacobi coordinates

Jacobi coordinates are a set of coordinates where, instead of using absolute position vectors for all particles, one uses a center of mass vector and relative coordinates between the particles. Since there will be no external forces acting upon the collection of particles, I will have translational invariance, which means that the center of mass location will be irrelevant. That is why Jacobi coordinates are well suited for this problem – I will get one vector less. Since each vector is three degrees of freedom, this will reduce the number of variables by three.

In this report, the Jacobi coordinates in position space for N particles are defined as follows: The last coordinate vector points to the center of mass of the system, relative to some origin. For the rest, the n :th coordinate vector points from the center of mass of the first n particles to the position of the $(n + 1)$:th particle.

For two identical particles with mass m , there will be one relative coordinate vector \mathbf{r} and a center of mass coordinate vector \mathbf{R} , and from the definition it can be seen that they are related to the absolute positions \mathbf{x}_1 and \mathbf{x}_2 of the particles by

$$\begin{aligned} \mathbf{r} &= \mathbf{x}_2 - \mathbf{x}_1 \\ \mathbf{R} &= \frac{1}{m+m}(m\mathbf{x}_1 + m\mathbf{x}_2) = \frac{1}{2}(\mathbf{x}_1 + \mathbf{x}_2) \end{aligned} \iff \begin{aligned} \mathbf{x}_1 &= \mathbf{R} - \frac{1}{2}\mathbf{r} \\ \mathbf{x}_2 &= \mathbf{R} + \frac{1}{2}\mathbf{r} \end{aligned} \quad (2.1)$$

The momentum coordinates \mathbf{p} and \mathbf{P} corresponding to \mathbf{r} and \mathbf{R} respectively, can now be obtained using the quantum mechanical representation of momentum in the position space, $\mathbf{p} = -i\frac{\partial}{\partial\mathbf{r}}$ [11, p. 54]:

$$\begin{aligned} \mathbf{p} &\equiv -i\frac{\partial}{\partial\mathbf{r}} = -i\left(\frac{\partial\mathbf{x}_1}{\partial\mathbf{r}}\frac{\partial}{\partial\mathbf{x}_1} + \frac{\partial\mathbf{x}_2}{\partial\mathbf{r}}\frac{\partial}{\partial\mathbf{x}_2}\right) = \\ &= \frac{\partial\mathbf{x}_1}{\partial\mathbf{r}}\mathbf{p}_1 + \frac{\partial\mathbf{x}_2}{\partial\mathbf{r}}\mathbf{p}_2 = \frac{1}{2}(\mathbf{p}_2 - \mathbf{p}_1) \\ \mathbf{P} &= \frac{\partial\mathbf{x}_1}{\partial\mathbf{R}}\mathbf{p}_1 + \frac{\partial\mathbf{x}_2}{\partial\mathbf{R}}\mathbf{p}_2 = \mathbf{p}_1 + \mathbf{p}_2 \end{aligned} \iff \begin{aligned} \mathbf{p}_1 &= \frac{1}{2}\mathbf{P} - \mathbf{p} \\ \mathbf{p}_2 &= \frac{1}{2}\mathbf{P} + \mathbf{p} \end{aligned} \quad (2.2)$$

where \mathbf{p}_1 and \mathbf{p}_2 are the conjugate momenta corresponding to \mathbf{x}_1 and \mathbf{x}_2 respectively.

The same can be done for three particles, in which case the Jacobi coordinates will consist of two relative coordinates, \mathbf{r} and \mathbf{s} , and the center of mass coordinate \mathbf{R} . They are related to the absolute positions \mathbf{x}_1 to \mathbf{x}_3 by

$$\begin{aligned} \mathbf{r} &= \mathbf{x}_2 - \mathbf{x}_1 \\ \mathbf{s} &= \mathbf{x}_3 - \frac{1}{m+m}(m\mathbf{x}_1 + m\mathbf{x}_2) = \\ &= \mathbf{x}_3 - \frac{1}{2}(\mathbf{x}_1 + \mathbf{x}_2) \\ \mathbf{R} &= \frac{1}{3}(\mathbf{x}_1 + \mathbf{x}_2 + \mathbf{x}_3) \end{aligned} \iff \begin{aligned} \mathbf{x}_1 &= \mathbf{R} - \frac{1}{2}\mathbf{r} - \frac{1}{3}\mathbf{s} \\ \mathbf{x}_2 &= \mathbf{R} + \frac{1}{2}\mathbf{r} - \frac{1}{3}\mathbf{s} \\ \mathbf{x}_3 &= \mathbf{R} + \frac{2}{3}\mathbf{s} \end{aligned} \quad (2.3)$$

The momentum variables \mathbf{p} , \mathbf{q} and \mathbf{P} corresponding to \mathbf{r} , \mathbf{s} and \mathbf{R} respectively are obtained in the same way as for two particles, and the result is

$$\begin{aligned} \mathbf{p} &= \frac{1}{2}(\mathbf{p}_2 - \mathbf{p}_1) \\ \mathbf{q} &= \frac{1}{3}(2\mathbf{p}_3 - \mathbf{p}_2 - \mathbf{p}_1) \\ \mathbf{P} &= \mathbf{p}_1 + \mathbf{p}_2 + \mathbf{p}_3. \end{aligned} \iff \begin{aligned} \mathbf{p}_1 &= \frac{1}{3}\mathbf{P} - \mathbf{p} - \frac{1}{2}\mathbf{q} \\ \mathbf{p}_2 &= \frac{1}{3}\mathbf{P} + \mathbf{p} - \frac{1}{2}\mathbf{q} \\ \mathbf{p}_3 &= \frac{1}{3}\mathbf{P} + \mathbf{q} \end{aligned} \quad (2.4)$$

where \mathbf{p}_1 to \mathbf{p}_3 are the absolute momenta.

This way to define \mathbf{r} , \mathbf{s} , \mathbf{p} and \mathbf{q} corresponds to the configuration in figure 1c. Configuration 1 and 2 can be related to the third:

$$\mathbf{p}^{(1)} = \frac{1}{2}(\mathbf{p}_3 - \mathbf{p}_2) = \frac{1}{2}\left(\mathbf{q} - \mathbf{p} + \frac{1}{2}\mathbf{q}\right) = -\frac{1}{2}\mathbf{p} + \frac{3}{4}\mathbf{q} \quad (2.5a)$$

$$\mathbf{q}^{(1)} = \frac{1}{3}(2\mathbf{p}_1 - \mathbf{p}_3 - \mathbf{p}_2) = -\mathbf{p} - \frac{1}{2}\mathbf{q}$$

$$\mathbf{p}^{(2)} = \frac{1}{2}(\mathbf{p}_1 - \mathbf{p}_3) = -\frac{1}{2}\mathbf{p} - \frac{3}{4}\mathbf{q} \quad (2.5b)$$

$$\mathbf{q}^{(2)} = \frac{1}{3}(2\mathbf{p}_2 - \mathbf{p}_1 - \mathbf{p}_3) = \mathbf{p} - \frac{1}{2}\mathbf{q}$$

As stated earlier, I am not interested in the center of mass coordinate, \mathbf{R} in position space and \mathbf{P} in momentum space. \mathbf{P} will be constant and \mathbf{R} will change linearly with time, due to the absence of external forces. This means that I can choose a frame of reference with origin at the center of mass \mathbf{R} and moving alongside it. So I set $\mathbf{R} = \mathbf{0}$ and $\mathbf{P} = \mathbf{0}$, and they can be excluded from calculations.

2.1.1 Normalization

The normalization of the states $\langle \mathbf{r}\mathbf{s}\mathbf{R} | \mathbf{r}'\mathbf{s}'\mathbf{R}' \rangle$, is calculated by inserting a complete set of states¹,

$$\hat{1} = \int d^3x_1 \int d^3x_2 \int d^3x_3 |\mathbf{x}_1\mathbf{x}_2\mathbf{x}_3\rangle \langle \mathbf{x}_1\mathbf{x}_2\mathbf{x}_3|, \quad (2.6)$$

¹Using the concept of completeness relation [11, p. 19]

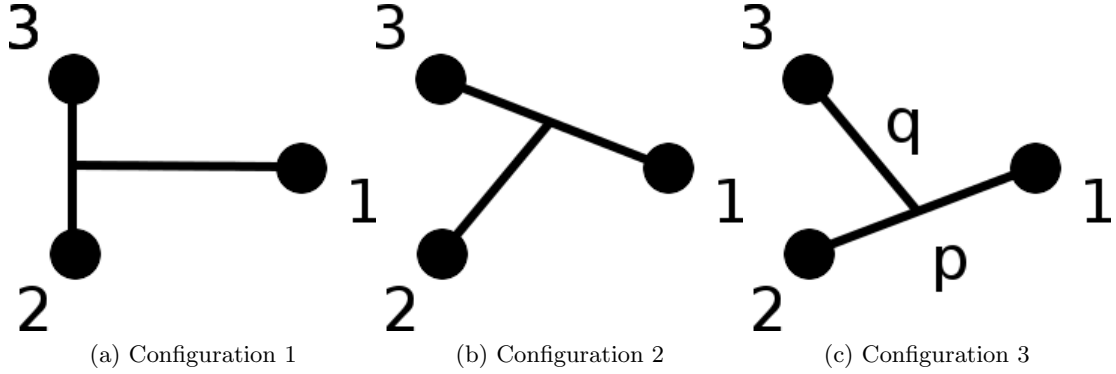


Figure 1: Illustration of the three possible configurations for the Jacobi coordinates.

where $\hat{1}$ is the identity operator. The integrals are assumed to be over the entire space. Doing this gives the result

$$\langle \mathbf{r}\mathbf{s}\mathbf{R} | \mathbf{r}'\mathbf{s}'\mathbf{R}' \rangle = \delta^3(\mathbf{r} - \mathbf{r}')\delta^3(\mathbf{s} - \mathbf{s}')\delta^3(\mathbf{R} - \mathbf{R}'). \quad (2.7)$$

Important to note is that no scale factor is needed, which makes this definition of the Jacobi coordinates particularly easy to use.

2.1.2 Kinetic energy

The kinetic energy function T_N for N particles, I define from the expression

$$\langle \mathbf{p}_1\mathbf{p}_2 \dots \mathbf{p}_N | \hat{T} | \mathbf{p}'_1\mathbf{p}'_2 \dots \mathbf{p}'_N \rangle = T_N \prod_{i=1}^N \delta^3(\mathbf{p}_i - \mathbf{p}'_i) \quad (2.8a)$$

$$T_N = \sum_{i=1}^N \frac{\mathbf{p}_i^2}{2m}. \quad (2.8b)$$

where \mathbf{p}_i are the absolute coordinates. For two and three particles described in a Jacobi coordinate basis, T_j – the kinetic energy function in Jacobi coordinates – can be calculated from eqs. (2.2) and (2.4):

$$T_j(\mathbf{p}, \mathbf{P}) = \frac{\left(\frac{1}{2}\mathbf{P} - \mathbf{p}\right)^2}{2m} + \frac{\left(\frac{1}{2}\mathbf{P} + \mathbf{p}\right)^2}{2m} = \frac{\mathbf{P}^2}{4m} + \frac{\mathbf{p}^2}{m} \quad (2.9)$$

$$T_j(\mathbf{p}, \mathbf{q}, \mathbf{P}) = \frac{\left(\frac{1}{3}\mathbf{P} - \mathbf{p} - \frac{1}{2}\mathbf{q}\right)^2}{2m} + \frac{\left(\frac{1}{3}\mathbf{P} + \mathbf{p} - \frac{1}{2}\mathbf{q}\right)^2}{2m} + \frac{\left(\frac{1}{3}\mathbf{P} + \mathbf{q}\right)^2}{2m} = \frac{\mathbf{P}^2}{6m} + \frac{\mathbf{p}^2}{m} + \frac{3\mathbf{q}^2}{4m} \quad (2.10)$$

2.2 Partial-wave basis

To further reduce the number of variables, I use the partial-wave basis in momentum space. The momentum state $|\mathbf{p}\rangle$ can be decomposed as $|p\rangle \otimes |\hat{\mathbf{p}}\rangle$, where p is the radial

component and $\hat{\mathbf{p}}$ is the direction of the vector. Since I will only use spherically symmetric potentials this is a particularly useful decomposition, and will reduce the number of variables further.

A basis for the directional part is the set of $|L_p M_p\rangle$ states, where L_p and M_p are the quantum numbers associated with the operators for total angular momentum $\hat{\mathbf{L}}_p$ and projected angular momentum $\hat{L}_{z,p}$ respectively. This decomposition using the angular momentum quantum numbers is what is referred to as the partial-wave basis. The angular dependencies of these states are given by the spherical harmonics:

$$\langle \theta \phi | L_p M_p \rangle = Y_{L_p}^{M_p}(\theta, \phi) \quad (2.11)$$

The normalization of the states is

$$\langle p L_p M_p | p' L'_p M'_p \rangle = \frac{\delta(p-p')}{p^2} \delta_{L_p L'_p} \delta_{M_p M'_p} \quad (2.12)$$

and the overlap with $|\mathbf{p}\rangle$ is given by

$$\langle \mathbf{p} | p L_p M_p \rangle = \frac{\delta(|\mathbf{p}| - p)}{p^2} Y_{L_p}^{M_p}(\hat{\mathbf{p}}) \quad (2.13)$$

2.2.1 Symmetrical states

Since the particles under consideration are indistinguishable bosons, the two-body state must be symmetric, that is, the wave function remains unchanged under the exchange of two particles. A two-particle state $|\mathbf{p}\rangle$, where \mathbf{p} is the relative Jacobi coordinate, will transform to $|\mathbf{-p}\rangle$ when permuting the two particles. This is equivalent to applying the parity operator [11, p. 251] to the state.

When using the partial-wave basis, applying the permutation operator will transform $|p L_p M_p\rangle$ to $(-1)^{L_p} |p L_p M_p\rangle$ [11, p. 255]. For spinless particles, without additional quantum numbers, only the states with even L_p are allowed bosonic states, since they are the only states that are symmetric.

2.2.2 Three particles

For three particles, the state of the system will depend on two coordinates, p and q . Remember that the Jacobi momentum coordinate for the center of mass, P , is irrelevant. I want to separate the angular dependence from the radial, so I write

$$|\mathbf{p}\rangle \otimes |\mathbf{q}\rangle = |p\rangle \otimes |q\rangle \otimes |\hat{\mathbf{p}}\hat{\mathbf{q}}\rangle. \quad (2.14)$$

One way to construct a basis for the angular part, is to decompose it further, to $|\hat{\mathbf{p}}\hat{\mathbf{q}}\rangle = |\hat{\mathbf{p}}\rangle \otimes |\hat{\mathbf{q}}\rangle$. Then one could use the four quantum numbers L_p , M_p , L_q and M_q . An alternative way – the way I will do it – is to use the coupled basis with quantum numbers L_p , L_q , L and M , where L and M are the total angular momenta and the projection of the total angular momenta respectively. The normalization can then be written

$$\langle p q L_p L_q L M | p' q' L'_p L'_q L' M' \rangle = \frac{\delta(p-p')}{p^2} \frac{\delta(q-q')}{q^2} \delta_{L_p L'_p} \delta_{L_q L'_q} \delta_{L L'} \delta_{M M'} \quad (2.15)$$

and the overlap with $|\mathbf{p}\mathbf{q}\rangle$ is

$$\langle \mathbf{p}\mathbf{q} | p q L_p L_q L M \rangle = \frac{\delta(|p| - p)}{p^2} \frac{\delta(|q| - q)}{q^2} \mathcal{Y}_{L_p L_q}^{LM}(\hat{\mathbf{p}}, \hat{\mathbf{q}}) \quad (2.16)$$

where \mathcal{Y} is the eigenfunction for L_p , L_q , L and M , which exists since the operators $\hat{\mathbf{L}}_p$, $\hat{\mathbf{L}}_q$, $\hat{\mathbf{L}}$ and \hat{L}_z all commute with each other. The relation between \mathcal{Y} and the spherical harmonics is [12]

$$\mathcal{Y}_{L_p L_q}^{LM}(\hat{\mathbf{p}}, \hat{\mathbf{q}}) = \sum_{M_p=-L_p}^{L_p} \sum_{M_q=-L_q}^{L_q} \langle L_p M_p L_q M_q | L M \rangle Y_{L_p}^{M_p}(\hat{\mathbf{p}}) Y_{L_q}^{M_q}(\hat{\mathbf{q}}) \quad (2.17)$$

where the overlaps are the Clebsch-Gordan coefficients.

The angular momenta L_p and L_q must obey

$$|L_p - L_q| \leq L \leq L_p + L_q. \quad (2.18)$$

I will only consider the case $L = 0$, which means that

$$L_p = L_q \quad (2.19)$$

2.2.3 Partially symmetric states for three particles

By requiring that L_p is even, the three-particle states are symmetric in the first two particles. The states are however not symmetric under exchange of the third particle with any of the other two. For that reason, the states are called partially symmetric.

These partially symmetric states are used in favor of totally symmetric states since the former are easy to work with and allows for an easy representation of the two-body potential.

2.2.4 The Wigner-Eckart theorem

The number of variables is the same for the Jacobi-coordinate basis as for the corresponding partial-wave basis – three for two particles and six for three particles. However, when evaluating matrix elements of tensor operators in the partial-wave basis one can employ the Wigner-Eckart theorem. This will reduce the number of integration variables. The theorem in the two-particle case states that, for spherically symmetric operators, the values $\langle p L_p M_p | \hat{A} | p' L_p' M_p' \rangle$ will be independent of M_p and M_p' and diagonal in L_p . More specifically, it says that

$$\langle p L_p M_p | \hat{A} | p' L_p' M_p' \rangle = \delta_{L_p L_p'} \delta_{M_p M_p'} \frac{\langle p L_p \| \hat{A} \| p' L_p' \rangle}{\sqrt{2L_p + 1}}, \quad (2.20)$$

where the double bar is a reduced matrix element. Since the right hand side is independent of M_p and M_p' , the left hand side must be too. For this reason, the quantum number M_p will be omitted in most cases.

For a three-particle system the theorem says that the states

$$\langle pqL_pL_qLM | \hat{A} | p'q'L'_pL'_qL'M' \rangle \quad (2.21)$$

will be independent of M and M' and diagonal in the quantum number L .

In the two-body case, setting $L_p = L'_p$ and $M_p = M'_p$ and summing over M_p I get

$$\sum_{M_p=-L_p}^{L_p} \langle pL_pM_p | \hat{A} | p'L_pM_p \rangle = (2L_p + 1) \langle pL_pM_p | \hat{A} | p'L_pM_p \rangle, \quad (2.22)$$

which will be used later in section 4.1.

Since the potentials will be spherically symmetric, this means that for two particles, there will only be one non-diagonal variable. For three particles there will be three non-diagonal variables, since i only consider the case when $L = 0$ which means that $L_p = L_q$.

2.3 Harmonic-oscillator basis

I will mainly use the momentum-space partial-wave basis, but some two-body potentials will also be evaluated in a harmonic-oscillator (HO) basis for comparison.

The HO-basis states are the eigenvectors of the hamiltonian with an isotropic harmonic oscillator potential:

$$\hat{H} = \frac{\hat{\mathbf{p}}^2}{2m} + \frac{1}{2}m\omega^2\hat{\mathbf{r}}^2 = \frac{1}{2}\omega (\hat{\xi}_p^2 + \hat{\xi}_r^2) \quad (2.23a)$$

$$\hat{\xi}_r = \frac{|\hat{\mathbf{r}}|}{r_0} \quad \hat{\xi}_p = \frac{|\hat{\mathbf{p}}|}{p_0} \quad (2.23b)$$

$$r_0 = \sqrt{\frac{1}{m\omega}} \quad p_0 = \sqrt{m\omega} = \frac{1}{r_0}. \quad (2.23c)$$

r_0 is usually called the oscillator length.

The eigenvalues and eigenvectors are

$$\hat{H} |nLM_L\rangle = E_N |nLM_L\rangle \quad (2.24a)$$

$$E_N = \omega \left(N + \frac{3}{2} \right) \quad (2.24b)$$

$$N = 2n + L \quad (2.24c)$$

$$\langle r\theta\phi | nLM_L \rangle = H_L(\xi_r, n) Y_L^{M_L}(\theta, \phi) \quad (2.24d)$$

$$\langle rLM_L | nL'M'_L \rangle = H_L(\xi_r, n) \delta_{LL'} \delta_{M_L M'_L} \quad (2.24e)$$

$$H_L(\xi_r, n) = C_{nL} \xi_r^L e^{-\frac{1}{2}\xi_r^2} L_n^{L+\frac{1}{2}}(\xi_r^2) \quad (2.24f)$$

$$C_{nL} = e^{i\delta_r(r,n,L)} 2^{n+L+1} \sqrt{\frac{(n+L)!n!}{r_0^3 \sqrt{\pi} (2n+2L+1)!}} \quad (2.24g)$$

where $\delta_r(r, n, L) \in \mathbb{R}$ is a phase factor, which I choose to be 0. $L_n^k(x)$ are the associated Laguerre polynomials. $Y_L^{ML}(\theta, \phi)$ are the spherical harmonics. The difference between the harmonic-oscillator basis and the momentum-space partial-wave basis is that p is replaced by n , but the angular quantum numbers are the same.

In order to evaluate the kinetic energy operator in the harmonic-oscillator basis, I will need to calculate the overlaps $\langle p\theta\phi | nLM_L \rangle$. To find these, I begin by noting that the a differential equation can be obtained from eq. (2.23a),

$$\langle \mathbf{r} | \hat{H} | \psi \rangle = -\frac{1}{2m} \Delta \psi_r(\mathbf{r}) + \frac{1}{2} m \omega^2 r^2 \psi_r(\mathbf{r}) = E \psi_r(\mathbf{r}). \quad (2.25)$$

If I instead of applying $\langle \mathbf{r} |$, applies $\langle \mathbf{p} |$, and use that $\langle \mathbf{p} | \hat{\mathbf{r}} | \psi \rangle = i \frac{\partial}{\partial p} \langle p | \psi \rangle$, I get

$$\langle \mathbf{p} | \hat{H} | \psi \rangle = \frac{1}{2m} p^2 \psi_p(\mathbf{p}) - \frac{1}{2} m \omega^2 \Delta_p \psi_p(\mathbf{p}) = E \psi_p(\mathbf{p}). \quad (2.26)$$

Defining $\tilde{\omega} = 1/(\omega m^2)$ and $\tilde{E} = E/(\omega^2 m^2)$ the equation becomes

$$\langle \mathbf{p} | \hat{H} | \psi \rangle = -\frac{1}{2m} \Delta \psi_p(\mathbf{p}) + \frac{1}{2} m \tilde{\omega}^2 \mathbf{p}^2 \psi_p(\mathbf{p}) = \tilde{E} \psi_p(\mathbf{p}). \quad (2.27)$$

This is the same differential equation and I will therefore get the same solution, by replacing ω with $\tilde{\omega}$ and E with \tilde{E} . So I will get the overlaps $\langle p\theta\phi | nLM_L \rangle$ by letting $r_0 \rightarrow p_0$, $\xi \rightarrow \xi_p$ and $\delta_r \rightarrow \delta_p$ in eq. (2.24d). Note that eq. (2.24b) remains unchanged, since $\tilde{E}/\tilde{\omega} = E/\omega$. The phase factor, $\exp(i\delta_p)$, I set to $(-1)^n$, since this will make the kinetic energy operator non-negative.

The kinetic energy operator \hat{T} is not diagonal in the harmonic-oscillator basis, but it can be calculated analytically. I start by inserting a complete set of states:

$$\begin{aligned} \langle nLM_L | \hat{T} | n' L' M'_L \rangle &= \sum_{L''} \sum_{M''_L} \sum_{L'''} \sum_{M'''_L} \int_0^\infty p^2 dp \int_0^\infty p'^2 dp' \\ &\times \langle nLM_L | p L'' M''_L \rangle \langle p L'' M''_L | \hat{T} | p' L''' M'''_L \rangle \langle p' L''' M'''_L | n' L' M'_L \rangle. \end{aligned} \quad (2.28)$$

From eq. (2.24e), with p instead of r , I see that the angular parts will only be delta-functions, and the kinetic energy operator is also diagonal in the angular part. This means that the overlap is zero unless $L = L'$ and $M_L = M'_L$ and the expression in this case is

$$\begin{aligned} \langle nLM_L | \hat{T} | n' LM_L \rangle &\equiv T_L(n, n') = \int_0^\infty p^2 dp H_L^*(\xi_p, n) \frac{p^2}{m} H_L(\xi_p, n') = \\ &= \frac{p_0^2}{m} \int_0^\infty p^2 dp H_L(\xi_p, n) \xi_p^2 H_L(\xi_p, n'). \end{aligned} \quad (2.29)$$

To simplify this, I use the following recurrence relation for the generalized Laguerre polynomials [13, eq. 22.7.(29, 31)],

$$\begin{aligned} x L_n^{L+1/2}(x) &= -\left(n + L + \frac{1}{2}\right) L_{n-1}^{L+1/2}(x) + \\ &+ \left(2n + L + \frac{3}{2}\right) L_n^{L+1/2}(x) - (n+1) L_{n+1}^{L+1/2}(x). \end{aligned} \quad (2.30)$$

This yields the relation

$$\begin{aligned}
H_L(\xi_p, n)\xi_p^2 = & -\left(n + L + \frac{1}{2}\right) \frac{C_{nL}}{C_{n-1,L}} H_L(\xi_p, n-1) + \\
& + \left(2n + L + \frac{3}{2}\right) H_L(\xi_p, n) - (n+1) \frac{C_{nL}}{C_{n+1,L}} H_L(\xi_p, n+1).
\end{aligned} \tag{2.31}$$

Inserting this, and using the orthonormality of the $|nLM_L\rangle$ states the final expression for the kinetic energy matrix elements is

$$\begin{aligned}
T_L(n, n') = & \frac{p_0^2}{m} \left(-\left(n + L + \frac{1}{2}\right) \frac{C_{nL}}{C_{n-1,L}} \delta_{n-1, n'} + \right. \\
& \left. + \left(2n + L + \frac{3}{2}\right) \delta_{nn'} - (n+1) \frac{C_{nL}}{C_{n+1,L}} \delta_{n+1, n'} \right) = \\
= & \frac{p_0^2}{m} \left(\sqrt{n' \left(n' + L + \frac{1}{2}\right)} \delta_{n-1, n'} + \left(2n' + L + \frac{3}{2}\right) \delta_{nn'} + \right. \\
& \left. + \sqrt{(n'+1) \left(n' + L + \frac{3}{2}\right)} \delta_{n+1, n'} \right).
\end{aligned} \tag{2.32}$$

3 Types of potentials

An expression for a potential between two particles can be constructed in different ways. Most of the time approximations need to be done. For example, when solving the equations of motion for a planet with a moon orbiting a sun, the bodies could be approximated as point particles with different masses. Another way to construct the potential would be to do it phenomenologically, that is, make up a potential that works for the specific case, but not necessarily for any other cases.

The problem is that maybe not all the physics will be captured by the model. In the example, the moon will cause tidal effects reshaping the planet, which will affect the gravitational field. This effect is not present using point particles. A way to get around this, is to include in the calculations a three body force.

A three body force is a simultaneous interaction between three bodies that is not present when only two bodies exist, such as the gravitational effect on the sun of the tidal effect caused by the moon. The importance of such three-body forces depends on the model.

In this report, I will consider both two-body and three-body forces.

4 Basis transformations

Frequently the matrix elements of an operator, for example of a potential-energy operator, need to be converted from one basis to another. In the following subsections I will show the details for some particular cases that will come in use later.

4.1 Partial-wave projection for two particles

Assuming that I know the expression for a spherically symmetrical two body potential in Jacobi momentum coordinates, $\langle \mathbf{p} | \hat{V} | \mathbf{p}' \rangle$ and I want to calculate $\langle pL_p | \hat{V} | p'L_p \rangle$. Note that I have omitted the quantum number M_p here since it will be independent of M_p . In the intermediate calculations, I will need to use the M_p quantum number, so I will temporarily include it below. Using eq. (2.22), I can write

$$\begin{aligned}
\langle pL_p M_p | \hat{V} | p'L_p M_p \rangle &= \frac{1}{2L_p + 1} \sum_{M'_p=-L_p}^{L_p} \langle pL_p M'_p | \hat{V} | p'L_p M'_p \rangle = \\
&= \frac{1}{2L_p + 1} \sum_{M'_p=-L_p}^{L_p} \int_{\mathbb{R}^3} d^3 \mathbf{q} \int_{\mathbb{R}^3} d^3 \mathbf{q}' \langle pL_p M'_p | \mathbf{q} \rangle \langle \mathbf{q} | \hat{V} | \mathbf{q}' \rangle \langle \mathbf{q}' | p'L_p M'_p \rangle = \\
&= \frac{1}{2L_p + 1} \sum_{M'_p=-L_p}^{L_p} \int_0^{2\pi} d\phi \int_0^\pi \sin(\theta) d\theta \int_0^{2\pi} d\phi' \int_0^\pi \sin(\theta') d\theta' \\
&\quad \times Y_{L_p}^{M'_p*}(\theta, \phi) V(p\hat{\mathbf{q}}, p'\hat{\mathbf{q}}') Y_{L_p}^{M'_p}(\theta', \phi')
\end{aligned} \tag{4.1}$$

where $\hat{\mathbf{q}} = (\sin(\theta) \cos(\phi), \sin(\theta) \sin(\phi), \cos(\theta))$.

To simplify this, the addition theorem for spherical harmonics is used [14, eq. 5.83]:

$$\frac{1}{2L_p + 1} \sum_{M'_p=-L_p}^{L_p} Y_{L_p}^{M'_p*}(\theta, \phi) Y_{L_p}^{M'_p}(\theta', \phi') = \frac{1}{4\pi} P_{L_p}(\hat{\mathbf{q}} \cdot \hat{\mathbf{q}}'), \tag{4.2}$$

where $P_n(x)$ are the Legendre polynomials. I will also assume that the potential only depends on the magnitudes p and p' and the angle between the vectors. This is a safe assumption since \hat{V} is assumed to be spherically symmetric.

Since there is no preferred direction, $\hat{\mathbf{q}}'$ can be fixed in the direction $\theta' = 0$ and $\phi' = 0$, yielding a factor 4π from the integration. Furthermore, a rotation around the fixed $\hat{\mathbf{q}}'$ vector will not affect the angle between the vectors or the magnitudes, so the ϕ integral will just give a factor of 2π . With the substitution $x = \cos(\theta)$ and again omitting the M_p quantum number, the expression becomes

$$\langle pL_p | \hat{V} | p'L_p \rangle = 2\pi \int_{-1}^1 dx P_{L_p}(x) V\left((p\sqrt{1-x^2}, 0, px), (0, 0, p')\right). \tag{4.3}$$

I will only encounter the case where the potential only depends on $|\mathbf{p} - \mathbf{p}'|$, so I can write $V = V(|\mathbf{p} - \mathbf{p}'|)$, and the above expression becomes

$$\langle pL_p | \hat{V} | p'L_p \rangle = 2\pi \int_{-1}^1 dx P_{L_p}(x) V\left(\sqrt{p^2 + p'^2 - 2pp'x}\right). \tag{4.4}$$

4.2 From position space to partial-wave basis in momentum space for two particles

In the last section I converted from momentum space to a partial-wave basis in momentum space. If I instead have the potential in position space, $\langle \mathbf{r} | \hat{V} | \mathbf{r}' \rangle$, I need to do an

extra step where I first convert to momentum space via a Fourier transform. Then I can use the same expression as in the last section to do the last part to partial-wave basis in momentum space. I will assume that the potential is diagonal in the position basis and only depends on the magnitude of \mathbf{r} , so $\langle \mathbf{r} | \hat{V} | \mathbf{r}' \rangle = \tilde{V}(|\mathbf{r}|) \delta^3(\mathbf{r} - \mathbf{r}')$.

Converting to momentum space is done as follows,

$$\begin{aligned}
\langle \mathbf{p} | \hat{V} | \mathbf{p}' \rangle &= \int_{\mathbb{R}^3} d^3\mathbf{r} \int_{\mathbb{R}^3} d^3\mathbf{r}' \langle \mathbf{p} | \mathbf{r} \rangle \langle \mathbf{r} | \hat{V} | \mathbf{r}' \rangle \langle \mathbf{r}' | \mathbf{p}' \rangle = \\
&= \int_{\mathbb{R}^3} d^3\mathbf{r} \left(\frac{1}{(2\pi)^{3/2}} \exp(-i\mathbf{r} \cdot \mathbf{p}) \right) \tilde{V}(|\mathbf{r}|) \left(\frac{1}{(2\pi)^{3/2}} \exp(i\mathbf{r} \cdot \mathbf{p}') \right) = \\
&= \frac{1}{(2\pi)^3} \int_0^\infty r^2 dr \int_0^\pi \sin(\theta) d\theta \int_0^{2\pi} d\phi \exp\left(ir \overbrace{|\mathbf{p} - \mathbf{p}'| \cos(\theta)}^{\equiv q} \right) \tilde{V}(r) = \\
&= \frac{1}{(2\pi)^2} \int_0^\infty r^2 dr \int_0^\pi \sin(\theta) d\theta \exp(irq \cos(\theta)) \tilde{V}(r) = \\
&= \frac{1}{(2\pi)^2} \int_0^\infty r^2 dr \tilde{V}(r) \left[\frac{\exp(irq \cos(\theta))}{-irq} \right]_0^\pi = \\
&= \frac{1}{2\pi^2 q} \int_0^\infty dr r \tilde{V}(r) \left(\frac{\exp(irq) - \exp(-irq)}{2i} \right) = \\
&= \frac{1}{2q\pi^2} \int_0^\infty dr \sin(rq) r \tilde{V}(r) = \left\{ \begin{array}{l} r = qx \\ dr = q dx \end{array} \right\} = \\
&= \frac{1}{2\pi^2} \int_0^\infty dx \sin(q^2 x) qx V(qx) \equiv V(q) = V(|\mathbf{p} - \mathbf{p}'|).
\end{aligned} \tag{4.5}$$

Inserting this in eq. (4.4), I get

$$\begin{aligned}
\langle pL_p | \hat{V} | p'L_p \rangle &= \frac{1}{\pi} \int_{-1}^1 dt P_{L_p}(t) \int_0^\infty dx \\
&\quad \times \sin(x(p^2 + p'^2 - 2pp't)) x \sqrt{p^2 + p'^2 - 2pp't} \tilde{V}(x \sqrt{p^2 + p'^2 - 2pp't}).
\end{aligned} \tag{4.6}$$

4.3 Partial-wave projection for three particles

In this section I will do the same thing as in the last section, but for a three body potential instead. Assuming I have the expression for $\langle \mathbf{p}\mathbf{q} | \hat{U} | \mathbf{p}'\mathbf{q}' \rangle$ and I want to evaluate the spherically symmetric potential \hat{U} in partial-wave basis, then I can write

$$\begin{aligned}
\langle pqL_pL_q | \hat{U} | p'q'L_p'L_q \rangle &= \int_{\mathbb{R}^3} d^3\mathbf{p} \int_{\mathbb{R}^3} d^3\mathbf{q} \int_{\mathbb{R}^3} d^3\mathbf{p}' \int_{\mathbb{R}^3} d^3\mathbf{q}' \\
&\quad \times \langle pqL_pL_q | \mathbf{p}\mathbf{q} \rangle \tilde{U}(\mathbf{p}, \mathbf{q}, \mathbf{p}', \mathbf{q}') \langle \mathbf{p}'\mathbf{q}' | p'q'L_p'L_q \rangle,
\end{aligned} \tag{4.7}$$

where I have written \tilde{U} to distinguish the function given in momentum space from the function given in partial-wave basis. Using eq. (2.16) and using spherical coordinates for

the four volume integrations, this becomes

$$\begin{aligned}
U(p, q, L_p, L_q, L, M, p', q', L'_p, L'_q, L', M') &= \\
&= \int_0^{2\pi} d\phi_1 \int_0^\pi \sin(\theta_1) d\theta_1 \int_0^{2\pi} d\phi_2 \int_0^\pi \sin(\theta_2) d\theta_2 \\
&\quad \times \int_0^{2\pi} d\phi_3 \int_0^\pi \sin(\theta_3) d\theta_3 \int_0^{2\pi} d\phi_4 \int_0^\pi \sin(\theta_4) d\theta_4 \\
&\quad \times \mathcal{Y}_{L_p L_q}^{LM*}(\hat{\mathbf{p}}(\phi_1, \theta_1), \hat{\mathbf{q}}(\phi_2, \theta_2)) \mathcal{Y}_{L'_p L'_q}^{L'M'}(\hat{\mathbf{p}}'(\phi_3, \theta_3), \hat{\mathbf{q}}'(\phi_4, \theta_4)) \\
&\quad \times \tilde{U}(\mathbf{p}(p, \phi_1, \theta_1), \mathbf{q}(q, \phi_2, \theta_2), \mathbf{p}'(p', \phi_3, \theta_3), \mathbf{q}'(q', \phi_4, \theta_4)).
\end{aligned} \tag{4.8}$$

As stated in section 2.2.2, I will only consider the case $L = 0$. The two angular momenta L_p and L_q will then be equal.

Assuming $L = 0$ allows for a simplification of eq. (4.8). Using eq. (2.17) with $L = M = 0$ and eq. (4.2) (the addition theorem) and the relations [13, eq. 27.9.1]

$$\langle L_p M_p L_q M_q | L_p L_q 00 \rangle = \delta_{L_p L_q} \delta_{M_p, -M_q} \frac{(-1)^{L_p - M_p}}{\sqrt{2L_p + 1}} \tag{4.9}$$

and [11, eq. 3.6.38]

$$Y_{L_p}^{-M_p}(\hat{\mathbf{p}}) = (-1)^{M_p} Y_{L_p}^{M_p*}(\hat{\mathbf{p}}) \tag{4.10}$$

I get the expression

$$\mathcal{Y}_{L_p L_p}^{00}(\hat{\mathbf{a}}, \hat{\mathbf{b}}) = (-1)^{L_p} \frac{\sqrt{2L_p + 1}}{4\pi} P_{L_p}(\hat{\mathbf{a}} \cdot \hat{\mathbf{b}}), \tag{4.11}$$

where $P_n(x)$ are the Legendre polynomials. Furthermore I do a change of variables in the θ variables, doing $t_i = \cos(\theta_i)$. So at this point I have

$$\begin{aligned}
U(p, q, L_p, p', q', L'_p) &= \frac{\sqrt{(2L_p + 1)(2L'_p + 1)}}{16\pi^2} \\
&\quad \times \int_{-1}^1 dt_1 \int_{-1}^1 dt_2 \int_0^{2\pi} d\phi_1 \int_0^{2\pi} d\phi_2 \\
&\quad \times P_{L_p}(\sqrt{(1-t_1^2)(1-t_2^2)} \cos(\phi_1 - \phi_2) + t_1 t_2) \\
&\quad \times \int_{-1}^1 dt_3 \int_{-1}^1 dt_4 \int_0^{2\pi} d\phi_3 \int_0^{2\pi} d\phi_4 \\
&\quad \times P_{L'_p}(\sqrt{(1-t_3^2)(1-t_4^2)} \cos(\phi_3 - \phi_4) + t_3 t_4) \\
&\quad \times \tilde{U}(\mathbf{p}(p, \phi_1, t_1), \mathbf{q}(q, \phi_2, t_2), \mathbf{p}'(p', \phi_3, t_3), \mathbf{q}'(q', \phi_4, t_4)).
\end{aligned} \tag{4.12}$$

Since L_p must be even – see section 2.2.3 – I omitted the term $(-1)^{L_p + L'_p}$.

Just like in the two particle case, I can fix one of the vectors in the positive z direction. I choose to fix the \mathbf{p} vector. This gives a factor of 4π . The function \tilde{U} will also only

depend on the magnitudes of the vectors and the angles between them, so I can instead write \tilde{U} as

$$\tilde{U} = \tilde{U}(p, q, p', q', \hat{\mathbf{p}} \cdot \hat{\mathbf{p}}', \hat{\mathbf{q}} \cdot \hat{\mathbf{q}}', \hat{\mathbf{p}} \cdot \hat{\mathbf{q}}, \hat{\mathbf{p}}' \cdot \hat{\mathbf{q}}', \hat{\mathbf{p}} \cdot \hat{\mathbf{q}}', \hat{\mathbf{p}}' \cdot \hat{\mathbf{q}}). \quad (4.13)$$

Introducing the definitions,

$$S_{ij} = \sqrt{(1-t_i^2)(1-t_j^2)} \cos(\phi_i - \phi_j) + t_i t_j \quad (4.14a)$$

$$\tilde{S}_{ij} = \sqrt{(1-t_i^2)(1-t_j^2)} \cos(\phi_i) + t_i t_j, \quad (4.14b)$$

the expression is

$$\begin{aligned} U(p, q, L_p, p', q', L'_p) &= \\ &= \frac{\sqrt{(2L_p+1)(2L'_p+1)}}{4\pi} \int_{-1}^1 dt_2 P_{L_p}(t_2) \int_{-1}^1 dt_3 \int_{-1}^1 dt_4 \int_0^{2\pi} d\phi_4 \\ &\quad \times \int_0^{2\pi} d\phi_3 P_{L'_p}(S_{34}) \int_0^{2\pi} d\phi_2 \tilde{U}(p, q, p', q', t_3, S_{24}, t_2, S_{34}, t_4, S_{23}). \end{aligned} \quad (4.15)$$

Thus, the ϕ variables only appear in S_{ij} , and there only as the difference between two different ϕ variables. So I can for example set $\phi_4 = 0$ and multiply with 2π instead. In the end I get the expression

$$\begin{aligned} U(p, q, L_p, p', q', L'_p) &= \\ &= \frac{\sqrt{(2L_p+1)(2L'_p+1)}}{2} \int_{-1}^1 dt_2 P_{L_p}(t_2) \int_{-1}^1 dt_3 \int_{-1}^1 dt_4 \int_0^{2\pi} d\phi_3 \\ &\quad \times P_{L'_p}(\tilde{S}_{34}) \int_0^{2\pi} d\phi_2 \tilde{U}(p, q, p', q', t_3, \tilde{S}_{24}, t_2, \tilde{S}_{34}, t_4, S_{23}). \end{aligned} \quad (4.16)$$

In the special case of a potential only depending on $(\mathbf{p} - \mathbf{p}')^2$ and $(\mathbf{q} - \mathbf{q}')^2$, the expression can be simplified further. In this case \tilde{U} only depends on the angle between \mathbf{p} and \mathbf{p}' and the angle between \mathbf{q} and \mathbf{q}' . This means that the dependencies of \tilde{U} are

$$\tilde{U} = \tilde{U}(p, q, p', q', t_3, \tilde{S}_{24}). \quad (4.17)$$

Thus, \tilde{U} is independent of ϕ_3 , and the only dependence of ϕ_3 is in one of the Legendre polynomials. The integration can be performed analytically, and I am left with four integrals:

$$\begin{aligned} U(p, q, L_p, p', q', L'_p) &= \frac{\sqrt{(2L_p+1)(2L'_p+1)}}{2} \int_{-1}^1 dt_2 P_{L_p}(t_2) \int_{-1}^1 dt_3 \int_{-1}^1 dt_4 \\ &\quad \times \int_0^{2\pi} d\phi_2 \tilde{U}(p, q, p', q', t_3, \tilde{S}_{24}) \int_0^{2\pi} d\phi_3 P_{L'_p}(\tilde{S}_{34}). \end{aligned} \quad (4.18)$$

4.4 From position space to harmonic-oscillator basis for two particles

Here I will consider the case of expressing a local, spherically symmetric potential given in position space in a harmonic-oscillator basis. Local and spherically symmetric means that

$$\langle \mathbf{r} | \hat{V} | \mathbf{r}' \rangle = V(|\mathbf{r}|) \delta^3(\mathbf{r} - \mathbf{r}'). \quad (4.19)$$

Using the results from section 2.3, I get

$$\begin{aligned} \langle nL | \hat{V} | n'L' \rangle &= \int_{\mathbb{R}^3} d^3\mathbf{r} \langle nL | \mathbf{r} \rangle V(|\mathbf{r}|) \langle \mathbf{r} | n'L' \rangle = \\ &= \sum_{L''} \int_0^\infty r^2 dr \langle nL | rL'' \rangle V(r) \langle rL'' | n'L' \rangle = \\ &= \delta_{LL'} \int_0^\infty r^2 dr H_L(\xi_r, n) V(r) H_L(\xi_r, n'). \end{aligned} \quad (4.20)$$

5 Few-body Observables

5.1 The transition operator for two particles

The transition operator \hat{t}_E is used in the context of elastic scattering, to describe the behaviour of a particle with energy E when it scatters against a local potential. For example, the matrix elements $\langle \mathbf{p} | \hat{t}_E | \mathbf{p}' \rangle$ determines the differential cross section. The specific case I will assume here is that of two identical spinless bosons scattering from each other. For more information about the transition operator, see chapter 7 in Modern Quantum Mechanics by Sakurai [11].

The transition operator \hat{t}_E , depending on the incident energy $E = p_0^2/m = T(p_0)$, is defined through the relation

$$\hat{t}_E = \hat{V} + \hat{V} \left((E + i\epsilon) \hat{1} - \hat{T} \right)^{-1} \hat{t}_E. \quad (5.1)$$

The $i\epsilon$ is introduced to avoid the singularity that otherwise would be present. It is only necessary for the case $E > 0$ – which I will consider here – since otherwise there will not be any singularity.

By using the partial-wave basis I can turn this into a matrix equation. Due to the Wigner-Eckart theorem, I have

$$\langle pL_p M_p | \hat{t}_E | p'L'_p M'_p \rangle = t_{L_p E}(p, p') \delta_{L_p L'_p} \delta_{M_p M'_p}. \quad (5.2)$$

The equation for $t_{L_p E}$ is then

$$t_{L_p E}(p, p') = V_{L_p}(p, p') + \int_{p''} p''^2 dp'' V_{L_p}(p, p'') \left(T(p_0) - T(p'') + i\epsilon \right)^{-1} t_{L_p E}(p'', p'). \quad (5.3)$$

To eliminate the $i\epsilon$, I use the identity [14]

$$\int_x dx \frac{f(x)}{g(x) + i\epsilon} = \mathcal{P} \int_x dx \frac{f(x)}{g(x)} - i\pi \int_x dx f(x) \delta(g(x)), \quad (5.4)$$

where the \mathcal{P} denotes that it is a principal value integral. In this case it will result in

$$t_{L_p E}(p, p') = V_{L_p}(p, p') + \mathcal{P} \overbrace{\int_{p''} p''^2 dp'' \frac{V_{L_p}(p, p'') t_{L_p E}(p'', p')}{T(p_0) - T(p'')}}^A - \underbrace{i\pi \int_{p''} p''^2 dp'' V_{L_p}(p, p'') t_{L_p E}(p'', p') \delta(T(p_0) - T(p''))}_B. \quad (5.5)$$

The delta function in term B is evaluated using the formula [14]

$$\delta(g(x)) = \sum_{\{x_0 | g(x_0)=0\}} \frac{\delta(x - x_0)}{g'(x_0)}. \quad (5.6)$$

There is one zero, $p'' = p_0$, so the term B is

$$B = i\pi p_0^2 V_{L_p}(p, p_0) t_{L_p E}(p_0, p') \frac{m}{2p_0}. \quad (5.7)$$

The term A is handled by adding and subtracting $p_0^2 V_{L_p}(p, p_0) t_{L_p E}(p_0, p')$ to the numerator,

$$A = \overbrace{\int_{p''} dp'' \frac{V_{L_p}(p, p'') t_{L_p E}(p'', p') p''^2 - V_{L_p}(p, p_0) t_{L_p E}(p_0, p') p_0^2}{T(p_0) - T(p'')}}^C + \underbrace{+ p_0^2 V_{L_p}(p, p_0) t_{L_p E}(p_0, p') \mathcal{P} \int_{p''} \frac{dp''}{T(p_0) - T(p'')}}_D. \quad (5.8)$$

The first integral is no longer a principal value integral since the pole is canceled by the numerator. That means that the term C can be integrated numerically as it is, as long as the point p_0 is not included in the quadrature. The integral D can be solved analytically. To evaluate the integral C , I will use a quadrature over the interval $[0, p_m]$, where $p_m > p_0$ is called the cut off momenta. So when calculating D , I need to use the same limits of integration. I will use the relation

$$\mathcal{P} \int_{x_0-L}^{x_0+L} \frac{dx}{x - x_0} = 0 \quad (5.9)$$

to remove the principal value prescription. Using that, I get

$$\begin{aligned}
D &= m\mathcal{P} \int_0^{p_m} \frac{dp''}{p_0^2 - p''^2} = \frac{m}{2p_0} \mathcal{P} \int_0^{p_m} dp'' \left(\frac{1}{p_0 - p''} + \frac{1}{p_0 + p''} \right) = \\
&= \frac{m}{2p_0} \left(\overbrace{\mathcal{P} \int_0^{2p_0} \frac{dp''}{p_0 - p''}}^{=0} + \int_{2p_0}^{p_m} \frac{dp''}{p_0 - p''} + \left[\log(p_0 + p'') \right]_{p''=0}^{p''=p_m} \right) = \\
&= \frac{m}{2p_0} \left(\left[-\log(|p_0 - p''|) \right]_{p''=2p_0}^{p''=p_m} + \log(p_0 + p_m) - \log(p_0) \right) = \frac{m}{2p_0} \log \left(\frac{p_m + p_0}{p_m - p_0} \right)
\end{aligned} \tag{5.10}$$

Collecting all the terms, I have

$$\begin{aligned}
t_{L_p E}(p, p') &= V_{L_p}(p, p') + A - B = \\
&= V_{L_p}(p, p') + C + p_0^2 V_{L_p}(p, p_0) t_{L_p E}(p_0, p') D - B = \\
&= V_{L_p}(p, p') + \\
&\quad + \int_{p''} dp'' \frac{V_{L_p}(p, p'') t_{L_p E}(p'', p') p''^2 - V_{L_p}(p, p_0) t_{L_p E}(p_0, p') p_0^2}{T(p_0) - T(p'')} + \\
&\quad + \frac{mp_0}{2} V_{L_p}(p, p_0) t_{L_p E}(p_0, p') \left(\log \left(\frac{p_m + p_0}{p_m - p_0} \right) - i\pi \right).
\end{aligned} \tag{5.11}$$

This constitutes an integral equation. The integral will be discretized, which will result in a matrix equation that will be solved for $t_{L_p E}$. The implementation of this is presented in section 10.

Since it is elastic scattering, the energy of the particle will be the same before and after the scattering process. Therefore, I am only interested in the elements where $p = p'$. Also, p should be equal to p_0 , since E is the energy for the particle that scatters.

5.2 The permutation operators

I define the permutation operator \hat{P}_{ij} as the operator that interchange the states of particle i and particle j . For example,

$$\hat{P}_{12} |\psi_1\rangle \otimes |\psi_2\rangle = |\psi_2\rangle \otimes |\psi_1\rangle. \tag{5.12}$$

An operator $\hat{A} \otimes \hat{1}$ acting on the first particle will then obey

$$\hat{P}_{12} (\hat{A} \otimes \hat{1}) \hat{P}_{12}^{-1} = \hat{1} \otimes \hat{A}. \tag{5.13}$$

Note that $\hat{P}_{ij}^{-1} = \hat{P}_{ij}$.

Furthermore, since I have a system of identical bosons, the permutation of any two particles will yield the same state, due to the symmetrization postulate.

An identity that will be needed later is

$$\hat{P}_{12} \hat{P}_{12} \hat{P}_{23} \hat{P}_{12} = \hat{P}_{13} \hat{P}_{23}. \tag{5.14}$$

This can be seen by applying the permutation operators to a state $|\psi_1\psi_2\psi_3\rangle$:

$$\begin{aligned}\hat{P}_{12}\hat{P}_{12}\hat{P}_{23}\hat{P}_{12}|\psi_1\psi_2\psi_3\rangle &= \hat{P}_{12}\hat{P}_{12}\hat{P}_{23}|\psi_2\psi_1\psi_3\rangle = \\ &= \hat{P}_{12}\hat{P}_{12}|\psi_2\psi_3\psi_1\rangle = \hat{P}_{12}|\psi_3\psi_2\psi_1\rangle = \\ &= |\psi_2\psi_3\psi_1\rangle\end{aligned}\quad (5.15a)$$

$$\hat{P}_{13}\hat{P}_{23}|\psi_1\psi_2\psi_3\rangle = \hat{P}_{13}|\psi_1\psi_3\psi_2\rangle = |\psi_2\psi_3\psi_1\rangle. \quad (5.15b)$$

5.2.1 Two-body potentials acting on three-body states

In a three-body system of distinguishable, each pair of particles can have a different two-body potential. I work with identical particles so each two-body potential will be the same. In the Jacobi basis for three particles, there are two relative coordinates, \mathbf{r} and \mathbf{s} . I can number the particles, in the same way as in section 2.1, so that \mathbf{r} points from particle one to particle two, and \mathbf{s} points to particle three from the center of mass of the first two particles. The third particle is called the odd one.

In the Jacobi basis, the two-body potential between the first two particles is easy to express,

$$\langle \mathbf{rs} | \hat{V}_3 | \mathbf{r}' \mathbf{s}' \rangle = V_3(\mathbf{r}, \mathbf{r}') \delta^3(\mathbf{s} - \mathbf{s}'). \quad (5.16)$$

The index 3 is to indicate that the third particle is the odd one. I will also need expressions for \hat{V}_1 and \hat{V}_2 .

Given a state for the three particles, $|\psi_1\psi_2\psi_3\rangle$, where $|\psi_i\rangle$ is the state for particle i , then \hat{V}_3 acting on the state $|\psi_1\psi_2\psi_3\rangle$ will be the same as \hat{V}_2 acting on the state $|\psi_2\psi_3\psi_1\rangle$, since the state $|\psi_3\rangle$ in both cases is the odd one. It appears to be two possibilities here though: \hat{V}_2 could just as well act on the state $|\psi_1\psi_3\psi_2\rangle$, and the state $|\psi_3\rangle$ would still be in the odd position. For bosons it would indeed not matter, but when dealing with fermions, this last case would give a minus sign since (1,3,2) is an odd permutation of (1,2,3). So for generality, I choose the first case.

Using the permutation operators defined in section 5.2, I can write

$$\hat{V}_1|\psi_1\psi_2\psi_3\rangle = (\hat{P}_{23}\hat{P}_{12})^{-1}\hat{V}_3\hat{P}_{23}\hat{P}_{12}|\psi_1\psi_2\psi_3\rangle = \hat{P}_{12}\hat{P}_{23}\hat{V}_3|\psi_2\psi_3\psi_1\rangle \quad (5.17a)$$

$$\hat{V}_2|\psi_1\psi_2\psi_3\rangle = (\hat{P}_{23}\hat{P}_{13})^{-1}\hat{V}_3\hat{P}_{23}\hat{P}_{13}|\psi_1\psi_2\psi_3\rangle = \hat{P}_{13}\hat{P}_{23}\hat{V}_3|\psi_3\psi_1\psi_2\rangle. \quad (5.17b)$$

Note that the inverse permutations are needed in order to return the state to the same configuration as before.

A symmetric wave function, $|\Psi\rangle$, remains the same after applying a permutation operator to it, that is, $\hat{P}_{ij}|\Psi\rangle = |\Psi\rangle$. By replacing $|\psi_1\psi_2\psi_3\rangle$ in the above equation by the symmetric state $|\Psi\rangle$, I get

$$\hat{V}_1|\Psi\rangle = \hat{P}_{12}\hat{P}_{23}\hat{V}_3|\Psi\rangle \quad (5.18a)$$

$$\hat{V}_2|\Psi\rangle = \hat{P}_{13}\hat{P}_{23}\hat{V}_3|\Psi\rangle. \quad (5.18b)$$

This means that

$$\begin{aligned} (\hat{V}_1 + \hat{V}_2 + \hat{V}_3) |\Psi\rangle &= (\hat{P}_{12}\hat{P}_{23}\hat{V}_3 + \hat{P}_{13}\hat{P}_{23}\hat{V}_3 + \hat{V}_3) |\Psi\rangle = \\ &= (\hat{P}_{12}\hat{P}_{23} + \hat{P}_{13}\hat{P}_{23} + \hat{1}) \hat{V}_3 |\Psi\rangle \equiv (\hat{1} + \hat{P}) \hat{V}_3 |\Psi\rangle, \end{aligned} \quad (5.19)$$

where I defined the important \hat{P} operator

$$\hat{P} \equiv \hat{P}_{12}\hat{P}_{23} + \hat{P}_{13}\hat{P}_{23}. \quad (5.20)$$

From section 2.2.3, I showed that permuting the first two particles in a partial-wave basis will give the same state. This means that

$$\hat{P}_{12} |pqL_p\rangle = |pqL_p\rangle. \quad (5.21)$$

Using the identity

$$\hat{P}_{13}\hat{P}_{23} = \hat{P}_{12}\hat{P}_{12}\hat{P}_{23}\hat{P}_{12} \quad (5.22)$$

The two terms in eq. (5.20) are equal in the partial-wave basis, since

$$\langle pqL_p | \hat{P}_{13}\hat{P}_{23} | p'q'L'_p \rangle = \langle pqL_p | \hat{P}_{12}\hat{P}_{12}\hat{P}_{23}\hat{P}_{12} | p'q'L'_p \rangle = \langle pqL_p | \hat{P}_{12}\hat{P}_{23} | p'q'L'_p \rangle. \quad (5.23)$$

5.3 Binding energy

The binding energy $E < 0$ is calculated from the time-independent Schrödinger equation,

$$\hat{H} |\psi\rangle = (\hat{T} + \hat{V}) |\psi\rangle = E |\psi\rangle. \quad (5.24)$$

In the computer implementation, operators will be matrices and the Schrödinger equation can be seen as an eigenvalue problem for the matrix representations of the operators. However, solving eq. (5.24) directly is not always the best alternative. In this section I will derive the different forms of the Schrödinger equation that I will use.

So the problem of finding the binding energy can be decomposed into two tasks. First, one must choose a formulation of the Schrödinger equation and compute the matrix that will appear in the corresponding matrix equation. The second task will be to solve the eigenvalue equation using an appropriate algorithm. In the following I will concentrate on the first task of finding a good formulation. The different algorithms I use are described later in section 9.2.

5.3.1 Two particles in a partial-wave basis

One problem, which exists when using the partial-wave basis, is that the kinetic energy operator \hat{T} will be diagonal. This means that a Dirac delta will appear in the equation, and that can not be discretized. To get around this, I do

$$\begin{aligned} (\hat{V} + \hat{T}) |\psi\rangle = E |\psi\rangle &\implies \hat{V} |\psi\rangle = (E\hat{1} - \hat{T}) |\psi\rangle \implies \\ \implies |\psi\rangle &= (E\hat{1} - \hat{T})^{-1} \hat{V} |\psi\rangle \equiv \hat{G}_0(E) \hat{V} |\psi\rangle \equiv \hat{K}_1(E) |\psi\rangle \end{aligned} \quad (5.25)$$

where $\hat{G}_0(E) \equiv (E\hat{1} - \hat{T})^{-1}$ is the free propagator of the system and $\hat{K}_1(E)$ is the kernel operator. Here I assumed that I can take the inverse of the operator $(E\hat{1} - \hat{T})$. This is not a problem for bound states since $E < 0$ and the kinetic energy is always positive.

In this form, it is not an issue that \hat{T} is diagonal, since it will only appear under an integral sign, which will cancel the Dirac delta. The problem is now to find $E < 0$ such that the kernel operator $\hat{K}_1(E)$ has eigenvalue 1.

5.3.2 Two particles in a harmonic-oscillator basis

In the harmonic-oscillator basis I do not have the difficulty with Dirac delta functions, since I neither have a continuous basis, nor is \hat{T} diagonal. This means that the hamiltonian \hat{H} can be diagonalized directly. I can also use the same method as in the partial-wave basis, solving $\hat{K}_1(E)|\psi\rangle = |\psi\rangle$. This means that the two methods can be compared.

One could argue that instead of finding E such that $\hat{K}_1(E)$ has eigenvalue 1, I could define

$$\hat{K}_2(E) \equiv \frac{1}{E}(\hat{V} + \hat{T}) \quad (5.26)$$

and find E such that $\hat{K}_2(E)$ has eigenvalue 1 instead. Theoretically it is just as good, but as will be seen in the implementation part, this equation is not well suited for computer implementation.

5.3.3 Three particles in a partial-wave basis

To calculate the binding energy of a three-particle bound state, I will use the Faddeev equation, which I will derive here.

The general hamiltonian for three identical bosons is

$$\hat{H} = \hat{T} + \sum_{i=1}^3 \hat{V}_i + \hat{U}, \quad (5.27)$$

where \hat{V}_i is the potential between the other two particles, so \hat{V}_1 is the two-body interaction between particles two and three and \hat{U} is the total three-body potential. The three-body potential \hat{U} is assumed to be totally symmetric. To make the hamiltonian look more symmetric, I define $\hat{U}_i \equiv (1/3)\hat{U}$ for $i = 1, 2, 3$. Then the hamiltonian will be

$$\hat{H} = \hat{T} + \sum_{i=1}^3 (\hat{V}_i + \hat{U}_i). \quad (5.28)$$

The time-independent Schrödinger equation is

$$\hat{H}|\Psi\rangle = E|\Psi\rangle. \quad (5.29)$$

Now I rewrite this equation like in eq. (5.25), so that I have

$$|\Psi\rangle = \hat{G}_0(E) \left(\sum_{i=1}^3 (\hat{V}_i + \hat{U}_i) \right) |\Psi\rangle. \quad (5.30)$$

I decompose the full wave function into three parts, by defining

$$|\Psi\rangle \equiv \sum_{i=1}^3 |\psi_i\rangle \quad (5.31a)$$

$$|\psi_i\rangle \equiv \hat{G}_0(E)(\hat{V}_i + \hat{U}_i)|\Psi\rangle. \quad (5.31b)$$

Notice that each operator $\hat{G}_0(E)(\hat{V}_i + \hat{U}_i)$ is symmetric in the two other particles, that is, particle i is the odd one, and I can use the results from section 5.2.1 to write

$$|\psi_1\rangle = \hat{P}_{12}\hat{P}_{23}|\psi_3\rangle \quad (5.32a)$$

$$|\psi_2\rangle = \hat{P}_{13}\hat{P}_{23}|\psi_3\rangle. \quad (5.32b)$$

This means that $|\Psi\rangle = \sum_i |\psi_i\rangle$ can be written like

$$|\Psi\rangle = (\hat{1} + \hat{P})|\psi_3\rangle. \quad (5.33)$$

Inserting this in eq. (5.31b) for $i = 3$ I get

$$|\psi_3\rangle = \hat{G}_0(E)(\hat{V}_3(\hat{1} + \hat{P}) + \hat{U})|\psi_3\rangle. \quad (5.34)$$

Since the other two equations will look the same, it is enough to solve this one. This equation is called the Faddeev equation. I used that

$$\hat{U}_i(\hat{1} + \hat{P}) = \hat{U}_1 + \hat{U}_2 + \hat{U}_3 = \hat{U}. \quad (5.35)$$

The equation as it is written now is not suitable for implementation though – for the same reason that eq. (5.24) was not appropriate for partial-wave basis – since \hat{V}_3 is diagonal in the quantum numbers for the third particle, I get a Dirac delta from the $\hat{G}_0(E)\hat{V}_3|\psi_3\rangle$ term which I cannot implement. Removing the index 3, and moving this term to the left hand side, I get

$$\begin{aligned} (\hat{1} - \hat{G}_0(E)\hat{V})|\psi\rangle &= \hat{G}_0(E)(\hat{V}\hat{P} + \hat{U})|\psi\rangle \implies \\ \implies |\psi\rangle &= (\hat{1} - \hat{G}_0(E)\hat{V})^{-1}\hat{G}_0(E)(\hat{V}\hat{P} + \hat{U})|\psi\rangle = \\ &= (\hat{1} - (E\hat{1} - \hat{T})^{-1}\hat{V})^{-1}(E\hat{1} - \hat{T})^{-1}(\hat{V}\hat{P} + \hat{U})|\psi\rangle = \\ &= \left((E\hat{1} - \hat{T})(\hat{1} - (E\hat{1} - \hat{T})^{-1}\hat{V}) \right)^{-1} (\hat{V}\hat{P} + \hat{U})|\psi\rangle = \\ &= (E\hat{1} - \hat{T} - \hat{V})^{-1}(\hat{V}\hat{P} + \hat{U})|\psi\rangle \equiv \hat{K}_3(E)|\psi\rangle. \end{aligned} \quad (5.36)$$

This expression is well suited for implementation.

5.4 Low-energy scattering parameters

From the on-shell transition matrix two important observables can be calculated, namely the scattering length a_0 and the effective range r_0 . See the book Modern Quantum Mechanics by Sakurai for more details about these parameters [11, p. 413].

At low energies, only S-wave scattering is important, that is $L_p = 0$. Therefore I will omit the index L_p , assuming it is zero.

According to Sakurai, the on-shell transition matrix is related to the partial-wave amplitude $f(p_0)$ by

$$f(p_0) \equiv -\frac{\pi \tilde{t}_E}{p_0} \quad (5.37a)$$

$$E = \frac{p_0^2}{m}. \quad (5.37b)$$

Here, \tilde{t}_E is the matrix element $\langle E00 | \hat{t}_E | E00 \rangle$. The relationship between \tilde{t}_E and the matrix element I calculate, $t_E \equiv \langle p_0 00 | \hat{t}_E | p_0 00 \rangle$ is [11, eq. (7.5.21a)]

$$\begin{aligned} \tilde{t}_E &= \langle E00 | \hat{t}_E | E00 \rangle = \int_{p'} p'^2 dp' \int_{p''} p''^2 dp'' \langle E | p' \rangle \langle p' 00 | \hat{t}_E | p'' 00 \rangle \langle p'' | E \rangle = \\ &= t_E \frac{2}{mp_0} \left(\int_{p'} p'^2 dp' \delta \left(\frac{p_0^2}{m} - \frac{p'^2}{m} \right) \right)^2 = t_E \frac{2}{mp_0} \left(\frac{mp_0}{2} \right)^2 = \\ &= t_E \frac{mp_0}{2}. \end{aligned} \quad (5.38)$$

The partial-wave amplitude determines the phase shift, δ of the reflected wave, through the relation

$$\begin{aligned} 1 + 2ip_0 f(p_0) &= \exp(2i\delta) \implies \\ \implies f(p_0) &= \frac{1}{p_0 \cot(\delta) - ip_0}. \end{aligned} \quad (5.39)$$

The parameters a_0 and r_0 are then defined through a Taylor expansion of $p_0 \cot(\delta)$ around $p_0 = 0$,

$$\begin{aligned} p_0 \cot(\delta) &= -\frac{1}{a_0} + \frac{1}{2} r_0 p_0^2 + \mathcal{O}(p_0^4) \implies \\ \implies \frac{m\pi i \sqrt{mE} |t_E|^2 - 2t_E^*}{m\pi |t_E|^2} &= -\frac{1}{a_0} + \frac{1}{2} r_0 mE + \mathcal{O}(E^2). \end{aligned} \quad (5.40)$$

Writing $t_E = t_R + t_I i$, I get

$$\frac{-2t_R}{m\pi(t_R^2 + t_I^2)} = -\frac{1}{a_0} + \frac{1}{2} r_0 mE + \mathcal{O}(E^2) \quad (5.41a)$$

$$1 + \frac{2t_I}{m\pi(t_R^2 + t_I^2)} = \mathcal{O}(E^2). \quad (5.41b)$$

The last of these two equations is good for checking that the calculations have been done correctly, since it should tend to zero.

The parameter a_0 determines the cross section at low momenta, which is $4\pi a_0^2$ [11].

6 The SRG flow equation

The main goal of this project is to transform a given potential \hat{V} to another potential $\tilde{\hat{V}}$ in such a way that the values of observables stay the same, and with the intent that $\tilde{\hat{V}}$ will have decoupled the low and high-energy physics. This means that only a small number of matrix elements will be needed when doing low-energy calculations.

This is achieved with the SRG transformation. It is a continuous, unitary transformation. The unitarity ensures that the values of observables stay the same.

I will now derive the SRG flow equation. I start by defining the transformed hamiltonian $\tilde{\hat{H}}$ from the unevolved hamiltonian \hat{H} .

$$\tilde{\hat{H}} = \hat{U}^\dagger \hat{H} \hat{U} \quad (6.1a)$$

$$\hat{U}^\dagger \hat{U} = \hat{1} \quad (6.1b)$$

In order to find a good \hat{U} with the desired property that the off diagonal elements of $\tilde{\hat{V}}$ becomes less significant, a flow parameter s is introduced, so that

$$\tilde{\hat{H}} \equiv \hat{H}_s = \hat{U}_s^\dagger \hat{H} \hat{U}_s \quad (6.2a)$$

$$\hat{U}_s^\dagger \hat{U}_s = \hat{1}. \quad (6.2b)$$

These equations can now be differentiated with respect to s :

$$\frac{d}{ds} \hat{1} = \hat{0} = \frac{d}{ds} (\hat{U}_s^\dagger \hat{U}_s) = \hat{U}_s^{\dagger'} \hat{U}_s + \hat{U}_s^\dagger \hat{U}_s' \equiv \hat{\eta}_s + \hat{\eta}_s^\dagger \quad (6.3a)$$

$$\begin{aligned} \frac{d}{ds} \hat{H}_s &= \hat{U}_s^{\dagger'} \hat{H} \hat{U}_s + \hat{U}_s^\dagger \hat{H} \hat{U}_s' = \\ &= \hat{U}_s^{\dagger'} \hat{U}_s \hat{U}_s^\dagger \hat{H} \hat{U}_s + \hat{U}_s^\dagger \hat{H} \hat{U}_s \hat{U}_s^\dagger \hat{U}_s' = \\ &= \hat{\eta}_s \hat{H}_s - \hat{H}_s \hat{\eta}_s = \\ &= [\hat{\eta}_s, \hat{H}_s]. \end{aligned} \quad (6.3b)$$

Now I need an operator $\hat{\eta}$ which obeys the relation $\hat{\eta} = -\hat{\eta}^\dagger$. Given a hermitian operator \hat{G}_s , I can use $\hat{\eta}_s = [\hat{G}_s, \hat{H}_s]$, so the equation looks like

$$\hat{H}_s' = [[\hat{G}_s, \hat{H}_s], \hat{H}_s]. \quad (6.4)$$

\hat{G}_s is called the propagator.

I am interested in the potential, and $\hat{H} = \hat{T} + \hat{V}$. I am not interested in a transformed kinetic energy operator, so I define

$$\hat{V}_s \equiv \hat{H}_s - \hat{T}. \quad (6.5)$$

This means that eq. (6.4) expressed in \hat{V}_s will be

$$\hat{H}_s' = \hat{V}_s' = [[\hat{G}_s, \hat{T} + \hat{V}_s], \hat{T} + \hat{V}_s]. \quad (6.6)$$

In this report I will only consider the propagator $\hat{G}_s = \hat{T}$. To motivate this, I write the equation in the partial-wave basis in momentum space for two particles:

$$V'_{Lp,s}(p,p') = -V_{Lp,s}(p,p') \frac{(p^2 - p'^2)^2}{m^2} + \int_0^\infty p''^2 dp'' V_{Lp,s}(p,p'') V_{Lp,s}(p'',p') \frac{p^2 + p'^2 - 2p''^2}{m}. \quad (6.7)$$

The first term will quickly drive off-diagonal terms towards zero since the factor $(p^2 - p'^2)^2$ is large for the off-diagonal elements. Furthermore, if one considers only the first term, the evolution would directly be given by

$$V_{Lp,s}(p,p') = V_{Lp,0}(p,p') \exp\left(-s \frac{(p^2 - p'^2)^2}{m^2}\right). \quad (6.8)$$

This suppresses off-diagonal elements, since $p^2 - p'^2$ is large for those elements. This will decouple the high- and low-energy states. For this reason, another flow parameter Λ is often used, which relates to s through

$$\Lambda^{-4} = \frac{s}{m^2}. \quad (6.9)$$

This means that the unit for Λ is the same as that for p and Λ will be a measure on how close to band diagonal the potential is. $\Lambda = \infty$ corresponds to the unevolved potential.

Using the linearity of the commutator, eq. (6.4) becomes

$$\begin{aligned} \hat{V}'_s &= [[\hat{T}, \hat{T} + \hat{V}_s], \hat{T} + \hat{V}_s] = \\ &= [[\hat{T}, \hat{T}] + [\hat{T}, \hat{V}_s], \hat{T} + \hat{V}_s] = \\ &= [\hat{T}, \hat{V}_s](\hat{T} + \hat{V}_s) + ([\hat{T}, \hat{V}_s](\hat{T} + \hat{V}_s))^\dagger. \end{aligned} \quad (6.10)$$

Defining

$$S(\hat{A}) \equiv \hat{A} + \hat{A}^T \quad (6.11)$$

the equation can be written as

$$\hat{V}'_s = S([\hat{T}, \hat{V}_s](\hat{T} + \hat{V}_s)) \quad (6.12)$$

since the potential is assumed to be real valued.

Part II

Implementation

In this part I will show how the major algorithms and equations are implemented. The most important task is to construct a discretized representation of the operators. For this, both how to store the operators as matrices and how the discretization will be handled are important aspects.

Since the amount of data that needs to be handled is often very large, care must be taken that the implementation can be done with relatively low memory usage. But the main goal is of course a fast, stable algorithm, which will allow more accurate calculations.

Details about the actual software and programming environment I have used in order to implement the calculations, can be seen in appendix D. When I have used algorithms that are part of a software library, that will be stated in the text.

7 Discretization of space

7.1 Discretized representation

Non-diagonal operators will be stored as matrices. The bases I work with are either continuous and ranging from zero to infinity – as in the case of the position and momentum variables – or discrete, as in the case of the angular momentums. In both cases a cut off must be chosen, so that only states below this limit are included in the discretized basis.

In the continuous case, a finite number of states – grid points – between zero and the cut off limit must be chosen too. Since the operators often must be integrated, a natural choice is to choose grid points according to some quadrature rule, which will be discussed more in detail in section 7.2.

For an operator \hat{A} depending on one variable x – discrete or continuous – with a chosen grid $\{x_i\}_{i=1}^n$, the matrix representation \check{A} with elements $\check{A}_{ii'}$ will be defined as

$$\check{A}_{ii'} \equiv \langle x_i | \hat{A} | x_{i'} \rangle. \quad (7.1)$$

In the general case, the matrix entries could be complex numbers. In most cases though, the operators I work with allow for a pure real representation, so unless otherwise stated, the matrices will be real. Many of the operators are also hermitian. This means that the matrix representation also will be hermitian, which in the real case is the same as the matrix being symmetric, $\check{A} = \check{A}^T$. In this case, only the upper or lower triangle need to be stored and calculated. This means that at most n^2 elements need to be stored, and only $n(n+1)/2$ elements if the operator is hermitian.

When an operator \hat{B} depends on two variables x and y , with grids $\{x_i\}_{i=1}^n$ and $\{y_j\}_{j=1}^m$, the discretized representation will still be a matrix. A combined grid is constructed,

$\{z_k\}_{k=1}^{nm}$, with grid point $im + j$ corresponding to the state $|x_i\rangle \otimes |y_j\rangle$, so the matrix elements will be

$$\check{B}_{im+j, i'm+j'} = \langle x_i y_j | \hat{B} | x'_i y'_j \rangle. \quad (7.2)$$

Note that if \hat{B} is hermitian, only $nm(nm+1)/2$ elements need to be stored and computed. For more than two variables, I do in the same fashion. For diagonal operators, \hat{D} with matrix representation \check{D} , only the diagonal is stored, in the form of a vector, \vec{D} . For a diagonal operator \hat{D} depending on a single variable x with a chosen grid $\{x_i\}_{i=1}^n$, the operator looks like

$$\langle x_i | \hat{D} | x'_i \rangle = D(i) \tilde{\delta}(x_i - x'_i). \quad (7.3)$$

The delta function should be interpreted as either a Dirac delta of the correct dimension or a Kronecker delta. The vector \vec{D} with elements \vec{D}_i will then be defined as

$$\vec{D}_i \equiv D(i). \quad (7.4)$$

An operator \hat{A} depending on two variables, x and y , can be diagonal in one of the variables, y . In this case, the discretized representation will be a vector of matrices, where element j of the vector will be the matrix \check{A}_j with elements

$$\check{A}_{j; i i'} = A_{y_j}(x_i, x'_i) \quad (7.5a)$$

$$\langle x_i y_j | \hat{A} | x'_i y'_j \rangle \equiv A_{y_j}(x_i, x'_i) \tilde{\delta}(y_j - y'_j). \quad (7.5b)$$

I call this that the operator \hat{A} is decomposed in y .

7.2 Discretized integration

In order to evaluate the product of two operators, $\langle \alpha | \hat{A} \hat{B} | \alpha' \rangle$, where α represents all the quantum numbers, a complete set of states, $\int_{\alpha''} w_I(\alpha'') |\alpha''\rangle \langle \alpha''|$ is inserted between the operators:

$$\langle \alpha | \hat{A} \hat{B} | \alpha' \rangle = \int_{\alpha''} \langle \alpha | \hat{A} | \alpha'' \rangle w_I(\alpha'') \langle \alpha'' | \hat{B} | \alpha' \rangle. \quad (7.6)$$

The \int symbol indicates that it can either be a discrete sum over a discrete quantum number, or an integral over a continuous variable. The $w_I(\alpha'')$ term is the integration weight, if any. For example, when integrating the p or q variable in the partial-wave basis, $w_I(p) = p^2$ and $w_I(q) = q^2$, since it is three dimensions. In the case of a discrete variable, it is an ordinary matrix multiplication between the two matrix representations of the operators. When dealing with continuous operators however, the integral need to be discretized. For this, a quadrature rule is used.

A quadrature is defined over some interval $[a, b]$, or possibly over an infinite interval. It also has a set of discrete points contained in the interval, $\{x_i\}_{i=1}^N$, where N is the order

of the quadrature and a set of weights $\{w_{q,i}\}_{i=1}^N$. This is used to create an approximation of the integral:

$$\int_a^b dx f(x) \approx \sum_{i=1}^N w_{q,i} f(x_i). \quad (7.7)$$

Using this, and defining $w(\alpha'') \equiv w_q(\alpha'')w_I(\alpha'')$, eq. (7.6) can be discretized as

$$\langle \alpha | \hat{A} \hat{B} | \alpha' \rangle \rightarrow \check{A} * \check{W}_\alpha \check{B}, \quad (7.8)$$

where \check{W}_α is a diagonal matrix with diagonal entries $\check{W}_{\alpha''\alpha''} = w(\alpha'')$. Only the diagonal of \check{W}_α will be stored, as a vector \vec{W}_α . The star between \check{A} and \check{W}_α signify that no real matrix multiplication need to be done, since \check{W}_α is diagonal.

For operators $\hat{A} = 1 \otimes \hat{A}_y$ and \hat{B} depending on two variables, x and y , where \hat{A} is decomposed in x , the matrix multiplication will simplify due to the delta function,

$$\begin{aligned} \langle xy | \hat{A} \hat{B} | x' y' \rangle &= \int_{x'' y''} \left(\frac{\tilde{\delta}(x - x'')}{w_I(x'')} \otimes \langle y | \hat{A}_y | y'' \rangle \right) w_I(x'', y'') \langle x'' y'' | \hat{B} | x' y' \rangle = \\ &= \int_{y''} \langle y | \hat{A}_y | y'' \rangle w_I(y'') \langle x y'' | \hat{B} | x' y' \rangle. \end{aligned} \quad (7.9)$$

To explicitly show when the matrix multiplications are done only over some variables, I write the discretization as

$$\langle xy | \hat{A} \hat{B} | x' y' \rangle \rightarrow \check{A} * \check{W}_y \overset{y}{*} \check{B}, \quad (7.10)$$

where the y over the star means that there is only a matrix multiplication in the y variable.

The different quadratures I use are described in appendix A.

Matrix multiplications are the main time consumers in the algorithms, so minimizing the number of such multiplications is always important to make the algorithms go faster. The BLAS routine dgemm is used to do matrix multiplications.

8 The permutation operator

The permutation operator that I need to discretize is

$$\hat{P} \equiv \hat{P}_{12} \hat{P}_{23} + \hat{P}_{13} \hat{P}_{23}. \quad (8.1)$$

As will be seen, this can be done in a few different ways.

I will not show the derivation of the discretized expressions, for these I refer to the book “The quantum mechanical few-body problem” by W. Glöckle [15].

In a three-particle system using the parital-wave basis in momentum space [15, eq. 3.349],

$$\begin{aligned}
 \langle pqL_\alpha L | \hat{P} | p'q'L'_\alpha L \rangle &= \\
 &= \int_{-1}^1 dx \frac{\delta(p - \pi_p^1(q, q', x))}{\pi_p^1(q, q', x)^{L_p+2}} \frac{\delta(p' - \pi_p^2(q, q', x))}{\pi_p^2(q, q', x)^{L'_p+2}} G_p(q, q', L_\alpha, L'_\alpha, L) = \\
 &= \int_{-1}^1 dx \frac{\delta(p - \pi_L^p(p', q', x))}{\pi_L^p(p', q', x)^{L_p+2}} \frac{\delta(q - \pi_L^q(p', q', x))}{\pi_L^q(p', q', x)^{L_q+2}} G_L(p', q', L_\alpha, L'_\alpha, L) = \\
 &= \int_{-1}^1 dx \frac{\delta(p' - \pi_R^p(p, q, x))}{\pi_R^p(p, q, x)^{L'_p+2}} \frac{\delta(q' - \pi_R^q(p, q, x))}{\pi_R^q(p, q, x)^{L'_q+2}} G_R(p, q, L_\alpha, L'_\alpha, L).
 \end{aligned} \tag{8.2}$$

L_α stands for both L_p and L_q . The difference between the three expressions is which two momentum variables are singled out in the delta functions and this also affects the factor G . The expressions for G_p , G_L and G_R are in appendix C. When the two p variables are singled out, I call it “acting on the p variables”, and when p and q are removed, I call it “acting to the left”, which also should explain the L (left) and R (right) notation for the π functions. I have not included the case when it acts on the q variables, since I will not need it.

Which expression that is most suitable depends on the equation where the permutation operator appears, since each delta function must be canceled by an integration. For example, consider the following equation,

$$|\psi\rangle = \hat{P} |\psi\rangle. \tag{8.3}$$

In the partial-wave basis this becomes

$$\begin{aligned}
 \psi(p, q, L_\alpha, L) &= \sum_{L'_\alpha} \int_{p'} p'^2 dp' \int_{q'} q'^2 dq' \int_{-1}^1 dx \\
 &\quad \times \frac{\delta(p' - \pi_R^p(p, q, x))}{\pi_R^p(p, q, x)^{L'_p+2}} \frac{\delta(q' - \pi_R^q(p, q, x))}{\pi_R^q(p, q, x)^{L'_q+2}} \\
 &\quad \times G_R(p, q, L_\alpha, L'_\alpha, L) \psi(p', q', L'_\alpha, L) = \\
 &= \sum_{L'_\alpha} \int_{-1}^1 dx \frac{G_R(p, q, L_\alpha, L'_\alpha, L) \psi(\pi_R^p(p, q, x), \pi_R^q(p, q, x), L'_\alpha, L)}{\pi_R^p(p, q, x)^{L'_p} \pi_R^q(p, q, x)^{L'_q}}.
 \end{aligned} \tag{8.4}$$

In this case, the permutation operator has to act to the right, since the variables p and q are not integration variables.

In most cases, the values of the π -functions will not correspond to a chosen grid point. This means that either interpolation or extrapolation will be necessary. To see when it is enough with interpolation, I need the explicit expressions for the π -functions.

They are given by

$$\pi_p^1(q, q', x) = \sqrt{\frac{1}{4}q^2 + q'^2 + xqq'} \quad (8.5a)$$

$$\pi_p^2(q, q', x) = \pi_p^1(q', q, x) \quad (8.5b)$$

$$\pi_L^p(p', q', x) = \sqrt{\frac{1}{4}p'^2 + \frac{9}{16}q'^2 - \frac{3}{4}xp'q'} \quad (8.5c)$$

$$\pi_L^q(p', q', x) = \sqrt{p'^2 + \frac{1}{4}q'^2 + xp'q'} \quad (8.5d)$$

$$\pi_R^p(p, q, x) = \pi_L^p(p, q, -x) \quad (8.5e)$$

$$\pi_R^q(p, q, x) = \pi_L^q(p, q, -x). \quad (8.5f)$$

For the case when the permutation operator acts on the p variables the extreme values of π_p^1 and π_p^2 will be when $x = \pm 1$. This gives the values

$$\sqrt{\frac{1}{4}q^2 + q'^2 \pm xqq'} = \sqrt{\left(\frac{1}{2}q \pm q'\right)^2} = \left|\frac{1}{2}q \pm q'\right|. \quad (8.6)$$

Of course I have that $0 \geq \pi_p^x(q, q', x)$, but since not all quadrature rules include the zero in the quadrature, it could happen that the lowest off-grid value is lower than the lowest quadrature point. To avoid this, I use a quadrature rule which includes the endpoints of integration. For a given momentum cutoff q_m , the largest p momentum value that will be needed is $1.5q_m$. This means that extrapolation can be avoided by letting $p_m \geq 1.5q_m$.

Now for the case when the permutation operator acts to just one side. For a given p_m and q_m , the maximum values that π_L^p and π_L^q can attain are

$$\max_{p', q', x} \pi_L^p(p', q', x) = \sqrt{\frac{1}{4}p_m^2 + \frac{9}{16}q_m^2 + \frac{3}{4}p_mq_m} = \frac{1}{2}p_m + \frac{3}{4}q_m \quad (8.7a)$$

$$\max_{p', q', x} \pi_L^q(p', q', x) = \sqrt{p_m^2 + \frac{1}{4}q_m^2 + p_mq_m} = p_m + \frac{1}{2}q_m. \quad (8.7b)$$

Now I would like to find p_m and q_m such that

$$\frac{1}{2}p_m + \frac{3}{4}q_m \leq p_m \quad (8.8a)$$

$$p_m + \frac{1}{2}q_m \leq q_m, \quad (8.8b)$$

but the problem is that it reduces to the inequalities $p_m \geq 1.5q_m$ and $p_m \leq 0.5q_m$. So extrapolation is unavoidable in this case. Since the first of these inequalities is the same as in the case when it acts on only p variables, I always use $p_m = 1.5q_m$, which will avoid extrapolation entirely when I do not need to act to the right or left, and it will as good as possible comply with the other inequality.

8.1 Interpolation and extrapolation

As stated in the previous section, I will need to interpolate and extrapolate in order to evaluate the permutation operators. Here I describe how this is done in general terms.

Given a set of grid points $\{g_i\}_{i=1}^N$ and their values $\{v_i\}_{i=1}^N$ the values $\{y_j\}_{j=1}^M$ at the off-grid points $\{x_j\}_{j=1}^M$ is evaluated with the formula

$$y_j \approx \sum_{i=1}^N s(x_j; g_1, g_2, \dots, g_N) v_i. \quad (8.9)$$

This can be written as a matrix-vector multiplication,

$$\mathbf{y} \approx S \mathbf{v}. \quad (8.10)$$

In appendix B, I describe the different interpolation and extrapolation methods I have used.

8.2 Matrix representations of the permutation operator

By using the interpolation matrices defined in section 8.1, an explicit matrix representation can be created for the permutation operator. As an example, I will here consider the case of the permutation matrix acting on the p variables. In this case, the p variables need to be integration variables. In the partial-wave basis in momentum space I have

$$\begin{aligned} \int_0^\infty p^2 dp \int_0^\infty p'^2 dp' |pqL_\alpha\rangle \langle pqL_\alpha| \hat{P} |p'q'L'_\alpha\rangle \langle p'q'L'_\alpha| = \\ |\pi_p^1(q, q', x) q L_\alpha\rangle \int_{-1}^1 dx \frac{G_p(q, q', x, L_\alpha, L'_\alpha, L)}{\pi_p^1(q, q', x)^{L_p} \pi_p^2(q, q', x)^{L'_p}} \langle \pi_p^2(q, q', x) q' L'_\alpha|. \end{aligned} \quad (8.11)$$

Discretizing the x integration and using the interpolation scheme from section 8.1, the above expression is

$$\begin{aligned} \sum_p \sum_{p'} |pqL_\alpha\rangle \\ \overbrace{= \tilde{P}_p(p, q, L_\alpha; p' q' L'_\alpha)} \\ \times \sum_x \left[w_q(x) s(\pi_p^1(q, q', x); \mathbf{P}) \frac{G_p(q, q', x, L_\alpha, L'_\alpha, L)}{\pi_p^1(q, q', x)^{L_p} \pi_p^2(q, q', x)^{L'_p}} s(\pi_p^2(q, q', x); \mathbf{P}) \right] \langle p' q' L'_\alpha| \end{aligned} \quad (8.12)$$

Similar calculations can be done for the case when the permutation operator acts to one side.

In this way, matrix representations of the permutation operators are possible, allowing for fast calculations. The downside is that everything the permutation operators act on will be interpolated. When the permutation operator acts on the kinetic energy operator or on another permutation operator, it would not be necessary to interpolate since the exact expressions could be used instead.

9 Calculation of the binding energy

In the theory part, I reduced the problem of finding the binding energy to one of two cases. Either I diagonalize the hamiltonian directly, or find E so that the operator \hat{K}_i has eigenvalue 1. In this section I will describe how these equations are solved in the implementation.

9.1 Diagonalization in the harmonic-oscillator basis

The diagonalization is only done in the harmonic-oscillator basis. The only variable is n , which is discrete. This means that no integration weights should be added. The hamiltonian matrix \tilde{H} will then have elements $\tilde{H}_{ij} = \langle i | (\hat{V} + \hat{T}) | j \rangle$. This will be a real, symmetric matrix. Due to the spectral theorem for finite matrices, this means that the eigenvalues will all be real.

To diagonalize the matrix, I use the GSL function `gsl_eigen_symm`, which in turn uses a method from section 8.3 of the book *Matrix Computations* by Golub and van Loan [16].

This immediately gives all the eigenvalues, and the eigenvalues that are negative corresponds to bound states.

9.2 Solving the kernel equation

I need to find E such that the equation

$$\hat{K}(E)|\psi\rangle = |\psi\rangle, \quad (9.1)$$

has a non trivial solution. With non trivial I mean that $|\psi\rangle$ should not be zero. To do this, a matrix representation of $\hat{K}(E)$ is needed. This can be obtained by multiplying with $\langle\alpha|$ from the left and inserting a complete set of states,

$$\hat{1} = \int_{\alpha'} w_I(\alpha') |\alpha'\rangle \langle\alpha'|, \quad (9.2)$$

between $\hat{K}(E)$ and $|\psi\rangle$. α represents all the quantum numbers for the given problem. This gives the equation

$$\int_{\alpha'} w_I(\alpha') \langle\alpha| \hat{K}(E) |\alpha'\rangle \langle\alpha'|\psi\rangle = \langle\alpha|\psi\rangle. \quad (9.3)$$

With a choosen grid for α , $\{\alpha_i\}_{i=1}^N$, the matrix equation is

$$\tilde{K}(E)\psi = \psi. \quad (9.4)$$

Solving eq. (9.4) will be an iterative process, where different values of E needs to be tested. In order to do this, I need a piecewise continuous real valued function, $f: \mathbb{R} \rightarrow \mathbb{R}$, taking an energy value as argument and returning zero if and only if the equation has

a solution. If I have such a function, I can apply a root finding algorithm to it to find the binding energies. In the following sub sections I will describe some different such functions that I have used.

I have used a bracketing algorithm to find the root. Such an algorithm starts with two energy values E_0 and E_2 for which the function f has different signs and $E_0 < E_2$. If f is continuous in the interval $[E_0, E_2]$, then a root exists in that interval. It is found by calculating f at some point E_1 , $E_0 < E_1 < E_2$ and then continuing the process recursively with either the interval $[E_0, E_1]$ or $[E_1, E_2]$ depending on the sign of f at the three points.

Since f is only assumed to be piecewise continuous, I can get false roots with the bracketing algorithm if f has a discontinuity where the value at one side of the discontinuity has different sign than on the other. This is easily seen to be a false root since the function value does not approach zero.

I have used the Brent-Dekker bracketing algorithm, implemented in the GSL library as the algorithm `gsl_root_fsolver_brent`.

9.2.1 Determinant method

With this method, the function f described above is

$$f(E) = \det(\check{K}(E) - \check{I}). \quad (9.5)$$

This will return zero if and only if the equation

$$(\check{K}(E) - \check{I})\psi = \check{0} \quad (9.6)$$

has a non trivial solution, which is exactly what I want. This function f will also be continuous.

To calculate the determinant, I calculate the LU decomposition of the matrix $\check{K}(E) - \check{I}$,

$$\check{P}(\check{K}(E) - \check{I}) = \check{L}\check{U}, \quad (9.7)$$

where P is a permutation matrix. The determinant is then just the product of the diagonal elements of \check{U} times the sign of the permutation matrix \check{P} . The LU decomposition is done using the function `gsl_linalg_LU_decomp`, which in turn uses the algorithm 3.4.1 from the book Matrix Computations by Golub and Van Loan [16].

For large matrices, the determinant takes a long time to calculate, which makes it useful mostly for rather small matrices, with $N \lesssim 2000$ or when no other method works.

Another problem is that the value of the determinant could be too large or too small for the computer to represent the number. This can be avoided by, instead of calculating the value of the determinant from the LU decomposition, just calculate the sign. This will, however, make it harder for the bracketing algorithm, since it can not estimate in a good way where the zero is.

One of the advantages of the kernel \check{K}_1 over \check{K}_2 is that the value of the determinant stays relatively close to zero regardless of the matrix size.

9.2.2 Power iteration

A method to find the eigenvalue with the largest absolute value, is the power iteration method. The idea is simply to start with any vector \mathbf{x}_0 of norm 1, then repeatedly do

$$\mathbf{x}_n = \check{K} \mathbf{x}_{n-1}. \quad (9.8)$$

The goal is that the ratio

$$\frac{|\mathbf{x}_n|}{|\mathbf{x}_{n-1}|} \quad (9.9)$$

should converge to the value of the eigenvalue with largest absolute value. This can be seen by expanding \mathbf{x}_0 and \mathbf{x}_n in the eigenbase of \check{K} :

$$\mathbf{x}_0 = \sum_i C_i \mathbf{k}_i \quad (9.10a)$$

$$\mathbf{x}_n = \check{K}^n \sum_i C_i \mathbf{k}_i = \sum_i C_i \lambda_i^n \mathbf{k}_i, \quad (9.10b)$$

where \mathbf{k}_i are the eigenvectors of \check{K} and λ_i are the eigenvalues. Assuming λ_0 is an eigenvalue with largest absolute value, then by dividing by λ_0^n , I get

$$\frac{1}{\lambda_0^n} \mathbf{x}_n = \sum_i C_i \frac{\lambda_i^n}{\lambda_0^n} \mathbf{k}_i. \quad (9.11)$$

This means that the components i with $\lambda_i < \lambda_0$ tend to zero.

This can only solve the kernel equation if 1 is the largest eigenvalue. For systems with only one bound state, this has been observed to be the case for kernels K_1 and K_3 , which is an additional advantage of K_1 over K_2 .

When there are more than one bound state, lower eigenvalues need to be found. This can be done by first finding the highest eigenvalue, then start again, with a new \mathbf{x}_0 and in each step make the obtained vector orthogonal to the eigenvector \mathbf{k}_0 . In this way, the next largest eigenvalue is found.

9.2.3 Arnoldi iteration

Another way to find eigenvalues other than the one with largest absolute value, is to use Arnoldi iteration. It is similar to the technique used in power iteration. But instead of converging each eigenvector at a time, all the obtained vectors \mathbf{x}_i are orthogonalized to each other and normalized. Then the matrix \check{H} is formed, with matrix elements

$$\check{H}_{ij} = \mathbf{x}_i^T \check{K} \mathbf{x}_j. \quad (9.12)$$

If \check{K} had been symmetric, then the eigenvalues of \check{H} will converge to the largest eigenvalues of \check{K} . In this case it is called Lanczos algorithm. For non symmetric matrices, the theory is not as well developed, but it has been observed in practice that the same holds in the non symmetric case.

The eigenvalues of \check{H} can easily be determined in a fast way, since the size of this matrix will be very small, usually between ten and twenty.

This method is usually faster than the power iteration method, since fewer iterations are needed for convergence, usually between 10 and 20.

9.3 The Kernels

9.3.1 Two-particle kernels

The two kernels for two particles are $\hat{K}_1(E)$ and $\hat{K}_2(E)$, see section 5.3. Discretizing is done according to the rule in section 7.2, that is by inserting complete set of states between all operators and states:

$$\langle \alpha | \hat{K}_1(E) | \psi \rangle = \langle \alpha | \psi \rangle = \int \int_{\alpha' \alpha''} \langle \alpha | (E\hat{1} - \hat{T})^{-1} | \alpha' \rangle \langle \alpha' | \hat{V} | \alpha'' \rangle \langle \alpha'' | \psi \rangle. \quad (9.13)$$

In the harmonic oscillator, there are no integrations, and the discretized version of the kernel is

$$\check{K}_1(E) = (E\check{1} - \check{T})^{-1} \check{V}. \quad (9.14)$$

In the partial-wave basis, the operator \hat{T} is diagonal, so the operator $(E\hat{1} - \hat{T})^{-1}$ will also be diagonal. This means that the Dirac delta function will remove the integration over α' . Using that $\alpha = p$, the relative momentum, I can write eq. (9.13) as

$$\int_0^\infty p'^2 dp' (E - T(p, E))^{-1} V(p, p') \langle p' | \psi \rangle = \langle p | \psi \rangle. \quad (9.15)$$

The discretized kernel is then

$$\check{K}_1(E) = (E\check{I} - \check{T})^{-1} * V * \check{W}_p \quad (9.16)$$

The kernel $\hat{K}_2(E)$ can only be used in the harmonic oscillator basis, and the discretized version is just

$$\check{K}_2(E) = \frac{1}{E} (\check{V} + \check{T}). \quad (9.17)$$

9.3.2 Three-particle kernels

The only kernel is $\hat{K}_3(E)$. The expression for the kernel is

$$\hat{K}_3(E) = (E\hat{1} - \hat{T} - \hat{V})^{-1} (\hat{V}\hat{P} + \hat{U}) \equiv K_3^{(1)}(E) K_3^{(2)} \quad (9.18)$$

where $K_3^{(1)} = (E\hat{1} - \hat{T} - \hat{V})^{-1}$. This is the only part that depends on E , which means that the other part only needs to be calculated once. Discretizing the equation $\hat{K}_3(E) |\psi\rangle = |\psi\rangle$ in the usual way, I get

$$\check{K}_3(E) = (E\check{I} - \check{T} - \check{V} * \check{W}_p)^{-1} * (\check{V} * \check{W}_p \check{P} * \check{W}_{pq} + \check{U} * \check{W}_{pq}). \quad (9.19)$$

I need to choose which variables the permutation operator should act on. It can not act to the left, since \hat{V} is diagonal in the q variable. I can either let it act on the two p variables or just to the right. If it acts on the p variables, the \check{W}_p matrices will be removed due to the delta functions, and if I choose it to act to the right, the \check{W}_{pq} to the right of \check{P} will be removed. To simplify, I define the matrix \check{P}_w as

$$\check{P}_w = \begin{cases} \check{P}_p * \check{W}_q, & \text{if } \hat{P} \text{ acts on } p \text{ variables} \\ \check{W}_p * \check{P}_R, & \text{if } \hat{P} \text{ acts to the right} \end{cases}. \quad (9.20)$$

Using this, the discretized equation will look the same in both cases, and the expression will be

$$\check{K}_3(E) = (E\check{I} - \check{T} - \check{V} * \check{W}_p)^{-1} * (\check{V}\check{P}_w + \check{U} * \check{W}_{pq}). \quad (9.21)$$

Note that \check{T} depends on q and \check{V} depends on L_p , so there will be one $N_p \times N_p$ matrix to invert for each q and each L_p .

10 Calculation of low-energy scattering observables

To calculate the low energy scattering parameters a_0 and r_0 I first need to discretize eq. (5.11), which for $L_p = 0$ looks like

$$t_E(p, p') = V(p, p') + \int_{p''} dp'' \frac{V(p, p'') t_E(p'', p') p''^2 - V(p, p_0) t_E(p_0, p') p_0^2}{T(p_0) - T(p'')} + \frac{mp_0}{2} V(p, p_0) t_E(p_0, p') \left(\log \left(\frac{p_m + p_0}{p_m - p_0} \right) - i\pi \right). \quad (10.1)$$

Since the momentum p_0 will be off grid, that is not one of the quadrature points, the matrices must be interpolated to get the value at the desired momentum. This can be achieved using an interpolation vector \mathbf{s} , such that if \mathbf{x} is a vector with values at the grid points, $\mathbf{x} \cdot \mathbf{s}$ will be the value at the desired point. This means that the terms $V(p, p_0) t_E(p_0, p')$ when discretized will look like

$$V(p, p_0) t_E(p_0, p') \rightarrow \check{V} \mathbf{s} \mathbf{s}^T \check{t}_E \quad (10.2)$$

Using this, the discretized version will be

$$\check{t}_E = \check{V} + \check{V} (\check{W}_p * \check{T} + \alpha \mathbf{s} \mathbf{s}^T) \check{t}_E \quad (10.3a)$$

$$\check{T} = (T(p_0)\check{I} - \check{T})^{-1} \quad (10.3b)$$

$$\alpha = \frac{mp_0}{2} \left(\log \left(\frac{p_m + p_0}{p_m - p_0} \right) - i\pi \right) - p_0^2 \vec{W}_g^T \vec{T}. \quad (10.3c)$$

Solving for \check{t}_E , this becomes

$$\check{t}_E = (\check{I} - \check{V} (\check{W}_p * \check{T} + \alpha \mathbf{s} \mathbf{s}^T))^{-1} \check{V} \equiv \check{K}^{-1} \check{V}. \quad (10.4)$$

Since I am only interesting in the on shell value t_E , I want to calculate

$$t_E \equiv \mathbf{s}^T \check{t}_E \mathbf{s} = \mathbf{s}^T \check{K}^{-1} \check{V} \mathbf{s}. \quad (10.5)$$

Defining \mathbf{x} from the relation $\check{K} \mathbf{x} = \check{V} \mathbf{s} \equiv \mathbf{y}$, which is easily solved using for example LU factorization, the value for t_E will be

$$t_E = \mathbf{s}^T \mathbf{x} \quad (10.6)$$

So the only time consuming part will be solving $\check{K} \mathbf{x} = \mathbf{y}$. Note that \check{K} is a complex valued matrix.

This process then has to be repeated for several different values of E , then the parameters a_0 and r_0 can be calculated from a linear fit to eq. (5.41a). Since a_0 is determined from the value at very low E , an accurate value can be obtained simply by decreasing E sufficiently. This is not the case for r_0 , since the slope of the line must be resolved. When using too low values of E , numerical errors will dominate and the data points will not look like a straight line. For too large E , the taylor expansion will not hold, so care must be taken when choosing the values for E .

11 The SRG flow equation

11.1 In two-particle space

For a two-particle system, the total hamiltonian is just

$$\hat{H} = \hat{T} + \hat{V}. \quad (11.1)$$

Using eq. (6.12), I get the derivative

$$\frac{\partial \hat{V}}{\partial s} = S([\hat{T}, \hat{V}](\hat{T} + \hat{V})). \quad (11.2)$$

The evolution will be done in the partial-wave basis, so integration weights will only be needed between two \hat{V} terms, since \hat{T} is diagonal. This means that the discretized version can be written as

$$\frac{\partial \hat{V}}{\partial s} \rightarrow \frac{\partial \check{V}}{\partial s} = S((\check{T} * \check{V} - \check{V} * \check{T})(\check{T} + \check{W}_p * \check{V})). \quad (11.3)$$

This means that only one matrix multiplication is necessary.

The only approximation that has been done is the discretized integration. Apart from that eq. (11.3) will cause \check{V} to evolve unitarily. The discretized integration is not expected to cause any significant deviations from unitarity.

11.2 In three-particle space

For three particles, the potential is $\sum_i \hat{V}_i + \hat{U}$, and the SRG equation is

$$\left(\sum_{i=1}^3 \hat{V}_i + \hat{U} \right)' = S \left(\left[\hat{T}, \sum_{i=1}^3 \hat{V}_i + \hat{U} \right] \left(\hat{T} + \sum_{i=1}^3 \hat{V}_i + \hat{U} \right) \right). \quad (11.4)$$

Here the derivation sign is implicitly assumed to be with respect to the flow parameter s . The expression for the \hat{V}'_3 term is already known from the two particle case, and from eqs. (5.17a) and (5.17b) I can relate \hat{V}'_1 and \hat{V}'_2 to \hat{V}'_3 ,

$$\hat{V}'_1 = (\hat{P}_{23} \hat{P}_{12})^{-1} \hat{V}'_3 \hat{P}_{23} \hat{P}_{12} \equiv \hat{P}_1^{-1} \hat{V}'_3 \hat{P}_1 \quad (11.5a)$$

$$\hat{V}'_2 = (\hat{P}_{23} \hat{P}_{13})^{-1} \hat{V}'_3 \hat{P}_{23} \hat{P}_{13} \equiv \hat{P}_2^{-1} \hat{V}'_3 \hat{P}_2. \quad (11.5b)$$

It is expected that the differential equations for \hat{V}'_1 and \hat{V}'_2 are the same as for \hat{V}'_3 . This is indeed the case:

$$\begin{aligned} \hat{V}'_1 &= \hat{P}_1^{-1} S \left([\hat{T}, \hat{V}_3] (\hat{T} + \hat{V}_3) \right) \hat{P}_1 = S \left(\hat{P}_1^{-1} [\hat{T}, \hat{V}_3] \hat{P}_1 \hat{P}_1^{-1} (\hat{T} + \hat{V}_3) \hat{P}_1 \right) = \\ &= S \left([\hat{T}, \hat{P}_1^{-1} \hat{V}_3 \hat{P}_1] (\hat{T} \hat{P}_1^{-1} \hat{P}_1 + \hat{P}_1^{-1} \hat{V}_3 \hat{P}_1) \right) = S \left([\hat{T}, \hat{V}_1] (\hat{T} + \hat{V}_1) \right), \end{aligned} \quad (11.6)$$

where I used that \hat{P}_1 is hermitian and that it commutes with \hat{T} .

I want to evaluate the differential equation in the partial-wave basis. As was shown in section 5.2.1,

$$\langle pqL_p | \hat{P}_1 | p'q'L'_p \rangle = \langle pqL_p | \hat{P}_2 | p'q'L'_p \rangle = \frac{1}{2} \langle pqL_p | \hat{P} | p'q'L'_p \rangle, \quad (11.7)$$

where the last inequality holds since $\hat{P} = \hat{P}_1 + \hat{P}_2$. Furthermore, I will use the identities

$$\hat{P}_1^{-1} = \hat{P}_2 \quad (11.8a)$$

$$\hat{P}_1 \hat{P}_2^{-1} = \hat{P}_2 \quad (11.8b)$$

so that

$$\hat{V}_1 \hat{V}_2 = \hat{P}_1^{-1} \hat{V}_3 \hat{P}_1 \hat{P}_2^{-1} \hat{V}_3 \hat{P}_2 = \hat{P}_2 \hat{V}_3 \hat{P}_2 \hat{V}_3 \hat{P}_2 \quad (11.9)$$

Moving the $\sum_i V_i$ sum to the right hand side of eq. (11.4), dropping the index 3 on the two-body potential and using the expressions valid only in the partial-wave basis I

get

$$\begin{aligned}
\hat{U}' &= S \left(\left[\hat{T}, \hat{V} + \frac{1}{2} \hat{P} \hat{V} \hat{P} + \hat{U} \right] \left(\hat{T} + \hat{V} + \frac{1}{2} \hat{P} \hat{V} \hat{P} + \hat{U} \right) - \right. \\
&\quad \left. - [\hat{T}, \hat{V}] (\hat{T} + \hat{V}) - 2 \left[\hat{T}, \frac{1}{4} \hat{P} \hat{V} \hat{P} \right] \left(\hat{T} + \frac{1}{4} \hat{P} \hat{V} \hat{P} \right) \right) = \\
&= S \left([\hat{T}, \hat{U}] \hat{T} + [\hat{T}, \hat{V}] \left(\frac{1}{2} \hat{P} \hat{V} \hat{P} + \hat{U} \right) + \right. \\
&\quad \left. + \left[\hat{T}, \frac{1}{2} \hat{P} \hat{V} \hat{P} \right] \left(\hat{V} + \frac{1}{4} \hat{P} \hat{V} \hat{P} + \hat{U} \right) + [\hat{T}, \hat{U}] \left(\hat{V} + \frac{1}{2} \hat{P} \hat{V} \hat{P} + \hat{U} \right) \right) = \\
&= S \left([\hat{T}, \hat{U}] \hat{T} + [\hat{T}, \hat{V}] \left(\frac{1}{2} \hat{P} \hat{V} \hat{P} + \hat{U} \right) + \right. \\
&\quad \left. + \left[\hat{T}, \frac{1}{2} \hat{P} \hat{V} \hat{P} \right] \left(\hat{V} + \frac{1}{2} \hat{V} \hat{P} + \hat{U} \right) + [\hat{T}, \hat{U}] \left(\hat{V} + \frac{1}{2} \hat{P} \hat{V} \hat{P} + \hat{U} \right) \right).
\end{aligned} \tag{11.10}$$

The discretized version, valid only in the partial-wave basis, is

$$\begin{aligned}
\hat{U}' \rightarrow \check{U}' &= S \left([\check{T}, \check{U}] * \check{T} + [\check{T}, \check{V}] * \left(\frac{1}{2} \check{P}_p \check{V} * \check{P}_L + \check{W}_p * \check{U} \right) + \right. \\
&\quad \left. + \left[\check{T}, \frac{1}{2} \check{P}_R \check{V} * \check{P}_p \right] \left(\check{V} + \frac{1}{2} \check{V} * \check{P}_L + \check{W}_q * \check{U} \right) + \right. \\
&\quad \left. + [\check{T}, \check{U}] \left(\check{W}_p * \check{V} + \frac{1}{2} \check{W}_q * \check{P}_p \check{V} * \check{P}_L + \check{W}_{pq} * \check{U} \right) \right).
\end{aligned} \tag{11.11}$$

The first term in all the brackets is \check{T} , which means that the brackets can be calculated without using any matrix multiplications. Calculation of the term $\check{P}_p \check{V} * \check{P}_L$ requires one matrix multiplication, and using the fact that $\check{P}_R \check{V} * \check{P}_p = (\check{P}_p \check{V} * \check{P}_L)^T$ I need no extra matrix multiplication for that term. Two of the multiplications between bracket and parenthesis need a full matrix multiplication. This gives in total 3 matrix multiplications.

In eq. (11.11), deviations from a truly unitary transformation arises from the discretized integration, the cutoff in angular momentum values and the permutation matrices. The first two should both tend to zero as the cutoff values and density of grid points goes to infinity. The error from the permutation matrices is due to the interpolation and extrapolation, and this error should also decrease with the number of grid points.

Although \hat{T} and \hat{P} commute, the discretized matrices will not necessarily commute due to the interpolations and extrapolations in the permutation matrices. This means that by rewriting the SRG flow equation a better or worse expression could be obtained. For comparison, I have also tried the following expression, which is a reordering of the terms in eq. (11.10):

$$\begin{aligned}
\hat{U}' &= S \left([\hat{T}, \hat{U}] \hat{T} + \left(\frac{1}{2} \hat{I} + \frac{1}{8} \hat{P} \right) f(\hat{V} \hat{P}, \hat{V} \hat{P}) + f \left(\hat{U}, \frac{1}{2} \hat{P} \hat{V} \hat{P} + \frac{1}{2} \hat{U} + \hat{V} \right) \right) \\
f(\hat{A}, \hat{B}) &= \hat{T} \hat{A} \hat{B} - 2 \hat{A} \hat{T} \hat{B} + \hat{A} \hat{B} \hat{T}.
\end{aligned} \tag{11.12}$$

Discretizing this equation, I get

$$\begin{aligned} \check{U}' \rightarrow \check{U}' &= S \left([\check{T}, \check{U}] * \check{T} + \left(\frac{1}{2} \check{I} + \frac{1}{8} \check{P}_R \right) f \left(\check{V} * \check{P}_p, \check{V} * \check{P}_L \right) + \right. \\ &\quad \left. + f \left(\check{U}, \frac{1}{2} \check{W}_q * \check{P}_p \check{V} * \check{P}_L + \frac{1}{2} \check{W}_{pq} * \check{U} + \check{W}_p * \check{V} \right) \right) \quad (11.13) \\ f(\check{A}, \check{B}) &= \check{T} * \check{A} \check{B} + \check{A} \check{B} * \check{T} - 2 \check{A} * \check{T} \check{B}. \end{aligned}$$

This discretized version requires a total of 6 full matrix multiplications. Each f function requires two multiplications and then there are two more needed. This means that this implementation will take about twice as long to evaluate.

Part III

Results

12 Introduction

In this part of the report I present the results I have obtained by using some different potentials for systems of nucleons and helium atoms. When using the algorithms for a specific potential, there are a few things that need to be defined first. These choices will be discussed in the following sub sections.

12.1 Choice of units

First off, the units need to be specified. As stated in the beginning of the report, I always set $\hbar = c = 1$ and express all quantities in either length or inverse length. However, to show results I want to show energies in the unit of energy. For the nucleon potentials I will use MeV and fm. The relation between the units is

$$1 = \hbar c = 197.327 \text{MeV} \cdot \text{fm}. \quad (12.1)$$

During the calculations, I store all quantities in units of fm. This implies that energies are given in fm^{-1} and to obtain, for example, the binding energy in MeV, I just multiply with 197.327.

For the helium potentials I use the units Kelvin (K) and atomic length units (au). Note that Kelvin is used as a unit of energy by also setting $k_B = 1$. This means that the relation between the units is

$$1 = \frac{\hbar c}{k_B} = 4.327249141 \cdot 10^7 \text{K} \cdot \text{au}. \quad (12.2)$$

12.2 Choice of grid

Since the momentum variables are continuous suitable grids need to be chosen. By grid I mean a number of discrete momentum values that will be used by the quadrature when integrating. This means that the grid points will always be dictated by the quadrature rule that is used. For the momentum variables I always use finite-interval quadratures. I define the grid through a set of limiting momentum values $[p_1, p_2, \dots, p_N]$ and a set of integer values $[n_1, n_2, \dots, n_N]$. Then, for the interval $[0, p_1]$, I use a quadrature with n_1 points, and for $[p_1, p_2]$ I use n_2 points, and so on. N is the number of intervals.

In all cases presented here, I use $N = 2$. For the lower region, $[0, p_1]$, I use a Gauss-Radau quadrature including the value $p = 0$. For the upper region, $[p_1, p_2]$, I also use Gauss-Radau and include the upper value $p = p_2$. The end points are included so that I can do interpolation in the full range. To specify the grid used, I write it in the format (p_1, p_2, n_1, n_2) .

For a two-particle system, I only need one momentum variable p . In a three-particle system, both p and q has the type of grid described above. For a given p grid

(p_1, p_2, n_1, n_2) , the q grid is always $(p_1, 2p_2/3, n_1, n_2)$. The factor $2/3$ is there to avoid extrapolation as much as possible, as explained in section 8. All values of the angular momenta L_p are used up to a cutoff $L_{p,\max}$. Only even values of L_p are used, as explained in the theory part.

12.3 Error estimates

It is important to be able to give error bounds on the calculated values. This is achieved by performing the calculations on different grids. The calculation of an observable A – this could be the ground-state binding energy E_0 for example – will depend on the cutoff values \mathbf{M} used and on the density of grid points ρ for continuous quantum numbers. When all the variables \mathbf{M} and ρ tends to infinity, the calculated value $A(\mathbf{M}, \rho)$ is more exact. There could still be other sources of errors, such as numerical errors, but the error due to the limited size of the Hilbert space will tend to zero.

In order to get a good estimation of the finite-space error, the behaviour of $A(\mathbf{M}, \rho)$ need to be studied in detail for each observable A and for each potential. Since this is not the focus of this thesis, I will instead do a simpler error estimation. I will calculate $A(\mathbf{M}, \rho)$ for two different values of each M_i and each ρ_i and use the least rounded value which is a correctly rounded value for each calculation. Many significant digits in the presented value is an indication of a low error.

12.4 SRG evolution

For the SRG evolution I have used the explicit embedded Runge-Kutta-Fehlberg method to solve the ordinary differential equation. I have used the implementation in GSL, more specifically the stepper `gsl_odeiv2_step_rkf45`.

The method accepts a relative and an absolute error bound. For the two-body SRG evolution, I have used a relative error bound of 10^{-10} for all potentials and an absolute error bound of zero for all potentials except the LM2M2 potential where I used an absolute error bound of 10^{-14}au^{-1} . For the three-body evolution I have used a relative error bound of 10^{-4} . For the nucleon potentials I have used 10^{-8}fm^{-1} as absolute error. For the soft core helium potential I have used an absolute error bound of zero. For the LM2M2 potential I have not done a three-body evolution.

Of the two implementations of the three-body SRG flow equation, seen in eqs. (11.11) and (11.13), the second one produced better results so I have only used that version for all the results presented in this thesis.

13 Nucleon potentials

I will not include the spin degree of freedom for the nucleons, which means I can treat them as spinless bosons. I have looked at two different nucleon-nucleon potentials. The first one is a sum of a short-range repulsive and an intermediate-range attractive Yukawa

interaction. This two-body potential has the form

$$\begin{aligned} \langle \mathbf{r} | \hat{V} | \mathbf{r}' \rangle &= V_{\text{Nuc-1}}(r) \delta^3(\mathbf{r} - \mathbf{r}') \\ V_{\text{Nuc-1}}(r) &= V_R \frac{\exp(-\mu_R r)}{r} + V_A \frac{\exp(-\mu_A r)}{r}. \end{aligned} \quad (13.1)$$

The parameter values used for this potential are the same that Elster et al. have used in their article for the MT-V potential [17]. Since I work in the momentum basis, I need to do a Fourier transform of this expression. In this case, the transform can be done analytically. Using the results from section 4.2, and more specifically eq. (4.5), a general term of form $V_0 \exp(-\mu r)/r$ is transformed as

$$\begin{aligned} \langle \mathbf{p} | V_0 \exp(-\mu \hat{r}) \hat{r}^{-1} | \mathbf{p}' \rangle &= \\ &= \frac{1}{2\pi^2 q} \int_0^\infty dr V_0 \exp(-\mu r) (2i)^{-1} \left(\exp(irq) - \exp(-irq) \right) = \\ &= \frac{V_0}{4\pi^2 i q} \int_0^\infty dr \left(\exp(-r(\mu - iq)) - \exp(-r(\mu + iq)) \right) = \\ &= \frac{V_0}{4\pi^2 i q} \left(\frac{1}{\mu - iq} - \frac{1}{\mu + iq} \right) = \frac{V_0 2iq}{4\pi^2 i q} \frac{1}{\mu^2 + q^2} = \frac{V_0}{2\pi^2} \frac{1}{\mu^2 + q^2}, \end{aligned} \quad (13.2)$$

where $q = |\mathbf{p} - \mathbf{p}'|$. The values of the parameters V_R , V_A , μ_R and μ_A are shown in table 1.

The second potential is a modification of the momentum-space expression of the first one, with the expression

$$\langle \mathbf{p} | \hat{V} | \mathbf{p}' \rangle = V_{\text{Nuc-2}}(\mathbf{p}, \mathbf{p}') = \frac{g_R^2}{(2\pi)^3} \frac{1}{q^2 + m_R^2} F_R(q) - \frac{g_A^2}{(2\pi)^3} \frac{1}{q^2 + m_A^2} F_A(q) \quad (13.3a)$$

$$F_x(q) = \left(\frac{\Lambda_x^2 - m_x^2}{\Lambda_x^2 + q^2} \right)^2. \quad (13.3b)$$

The parameter values are presented in table 1 and are the same as the ones used by Liu et al. [18].

The momentum-space expressions are used to obtain the potentials in a partial-wave basis using eq. (4.4). The potentials for $L_p = 0$ and $L_p = 2$ in the partial-wave basis are shown in figure 2.

13.1 Three-body potential

No three-body force is used together with the Yukawa potential. However the modified Yukawa potential was used in combination with one of the three-body potentials presented in the paper by Liu et al. [18]. Using the coordinates defined in eq. (2.4), this

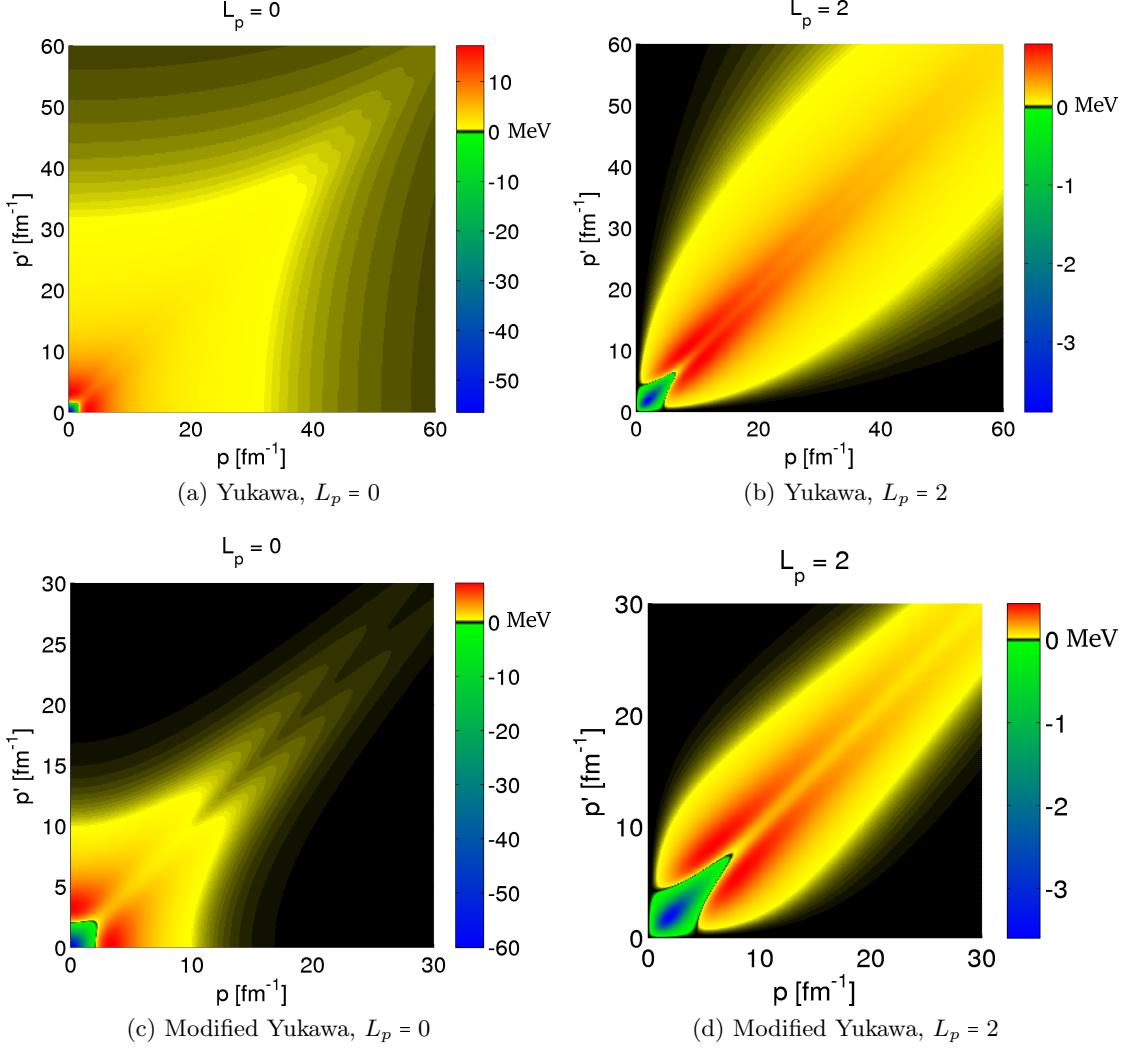


Figure 2: Matrix representations of the two nucleon potentials for $L_p = 0$ and $L_p = 2$. Note that I have used different momentum cutoff values for the two potentials. Each potential was produced using a total of 400 grid points, resulting in 400^2 matrix elements for each L_p . The modified Yukawa potential tends to zero faster for large p than the Yukawa potential due to the extra cutoff factor.

Table 1: Parameter values used for the nucleon potentials, both the two-body forces and the three-body force used with the modified Yukawa potential. The Yukawa potential with its parameter values is the same as in the paper by Elster et al. [17]. The modified Yukawa potential is identical to the one presented in the paper by Liu et al. [18]. The expressions for the two-body potentials are eqs. (13.1) and (13.3) and the three-body potential is eq. (13.4a).

Yukawa potential		Modified Yukawa potential			
		Two-body parameters		Three-body parameters	
V_R	1438.4812 MeV	$g_A^2/(4\pi)$	3.5775	$g_\alpha^2/(4\pi)$	5.0
μ_R	3.11 fm	m_A	330.2104 MeV	m_α	305.8593 MeV
V_A	-570.3316 MeV	Λ_A	1500.0 MeV	Λ_α	1000.0 MeV
μ_A	1.550 fm	$g_R^2/(4\pi)$	9.4086	a_α	-1.73
		m_R	612.4801 MeV		
		Λ_R	1500.0 MeV		

three-body potential has the form

$$\langle \mathbf{p}\mathbf{q} | \hat{U}_p | \mathbf{p}'\mathbf{q}' \rangle = U_{\text{Nuc-2,p}}(\mathbf{p}, \mathbf{q}, \mathbf{p}', \mathbf{q}') = \quad (13.4a)$$

$$= \frac{1}{(2\pi)^6} \frac{a_\alpha}{m_\alpha} g_\alpha^2 \frac{F_\alpha(Q)}{Q^2 + m_\alpha^2} \frac{F_\alpha(Q')}{Q'^2 + m_\alpha^2} = \frac{C}{G(Q)G(Q')} \quad (13.4b)$$

$$\mathbf{Q} = \mathbf{p} - \mathbf{p}' + \frac{1}{2}(\mathbf{q} - \mathbf{q}') \quad (13.4c)$$

$$\mathbf{Q}' = \mathbf{p} - \mathbf{p}' - \frac{1}{2}(\mathbf{q} - \mathbf{q}') \quad (13.4d)$$

$$C = \frac{1}{(2\pi)^6} \frac{a_\alpha}{m_\alpha} g_\alpha^2 (\Lambda_\alpha^2 - m_\alpha^2)^4 \quad (13.4e)$$

$$G(Q) = \frac{1}{(Q^2 + m_\alpha^2)(Q^2 + \Lambda_\alpha^2)^2}. \quad (13.4f)$$

The function F is defined in eq. (13.3b) and the parameter values are found in table 1. This is not the entire three-body potential, it is only one part of three, symmetric only in the two first particles. Using eqs. (2.5a) and (2.5b) the entire three-body potential can be written as

$$\begin{aligned} U_{\text{Nuc-2}}(\mathbf{p}, \mathbf{q}, \mathbf{p}', \mathbf{q}') &= U_{\text{Nuc-2,p}}\left(-\frac{1}{2}\mathbf{p} + \frac{3}{4}\mathbf{q}, -\mathbf{p} - \frac{1}{2}\mathbf{q}\right) + \\ &+ U_{\text{Nuc-2,p}}\left(-\frac{1}{2}\mathbf{p} - \frac{3}{4}\mathbf{q}, \mathbf{p} - \frac{1}{2}\mathbf{q}\right) + U_{\text{Nuc-2,p}}(\mathbf{p}, \mathbf{q}, \mathbf{p}', \mathbf{q}') = \quad (13.5) \\ &= C \left(\frac{1}{G(Q^{(1)})G(Q^{(1)'})} + \frac{1}{G(Q^{(2)})G(Q^{(2)'})} + \frac{1}{G(Q)G(Q')} \right). \end{aligned}$$

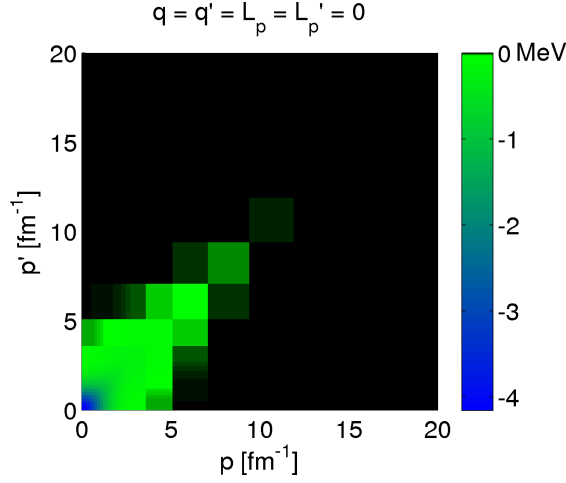


Figure 3: Modified Yukawa three-body potential for $q = q' = 0$ and $L_p = L_p' = 0$.

To simplify this, I note that

$$\mathbf{Q}^{(1)} = -(\mathbf{p} - \mathbf{p}') + \frac{1}{2}(\mathbf{q} - \mathbf{q}') = -\mathbf{Q}' \equiv \mathbf{X} \quad (13.6a)$$

$$\mathbf{Q}^{(1)'} = \mathbf{q} - \mathbf{q}' = -\mathbf{Q}^{(2)} \equiv \mathbf{Y} \quad (13.6b)$$

$$\mathbf{Q}^{(2)'} = -(\mathbf{p} - \mathbf{p}') - \frac{1}{2}(\mathbf{q} - \mathbf{q}') = -\mathbf{Q} \equiv \mathbf{Z}. \quad (13.6c)$$

Using these identities, the three-body force can be written as

$$\begin{aligned} U_{\text{Nuc-2}}(\mathbf{p}, \mathbf{q}, \mathbf{p}', \mathbf{q}') &= C \left(\frac{1}{G(X)G(Y)} + \frac{1}{G(Y)G(Z)} + \frac{1}{G(Z)G(X)} \right) = \\ &= C \frac{G(X) + G(Y) + G(Z)}{G(X)G(Y)G(Z)}. \end{aligned} \quad (13.7)$$

To transform this to the partial-wave basis, eq. (4.16) is used. The problem is that it is a five-dimensional integration which takes a long time. This means that I had to use fix-point integration which means no error bounds on the calculated matrix elements.

The three-body potential for $q = q' = 0$ and $L_p = L_p' = 0$ is shown in figure 3. The strength of the three-body force is lower than that of the two-body force, shown in figure 2c.

13.2 Two-body results

For the two-body system, I have calculated the binding energy, the scattering length and the effective range. In figures 4 and 5 it can be seen that the values of these observables are well converged for large enough grids. The converged values are presented in table 2.

Using too low values of the cutoff momenta will give poor results, since the important aspects of the potential are cut away. However, large values of the cutoffs will require

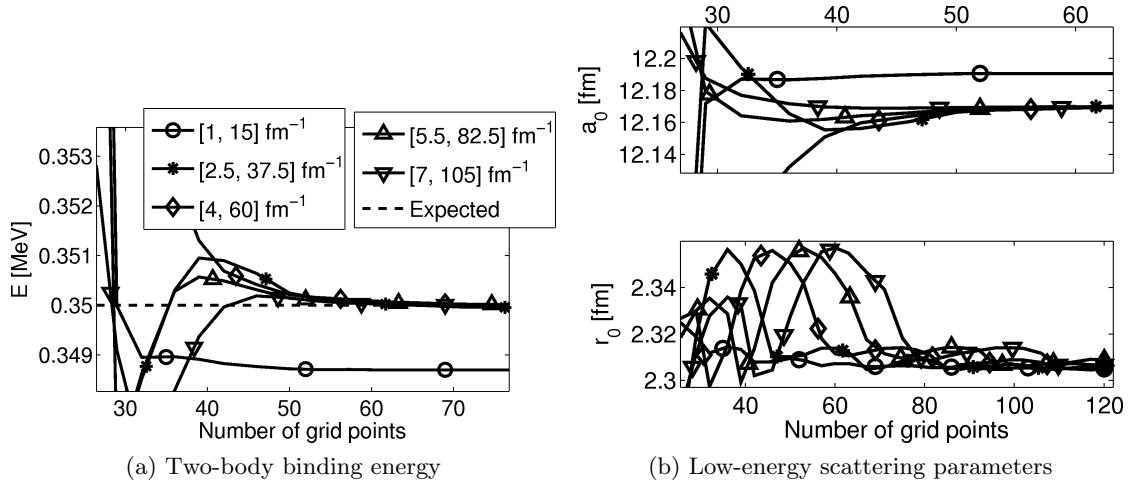


Figure 4: Yukawa potential. Convergence of two-body observables with the number of grid points and the momentum cutoffs. a_0 is the scattering length and r_0 is the effective range. With many enough grid-points convergence is achieved in all cases. The momentum cutoffs have only a small impact on the converged values in this case. The grids have $2/3$ of the grid points in the lower interval.

Table 2: Converged two-body observables for the nucleon potentials. Convergence can be defined in several ways, see subsection 12.3 for the used definition. To obtain the values, the two grids displayed in figures 4 and 5 with largest cutoff values were used, with a total of 360 and 720 grid points.

Yukawa		Reference	Modified Yukawa		Reference
E_0	0.35000 MeV	0.3500 MeV [17]	E_0	0.283951055 MeV	0.284 MeV [18]
a_0	12.1702 fm		a_0	13.310080 fm	
r_0	2.304 fm		r_0	2.228 fm	

more grid points to converge, because more points are needed to get a good resolution of the potential over the large momentum range. Therefore, I choose to work with the lowest cutoffs that still give good results.

13.2.1 Determination of the effective range

As mentioned in section 10, care need to be taken when choosing an energy range for the determination of r_0 . By testing different energy ranges, I got the best fit using the range 0.5 keV to 50 keV.

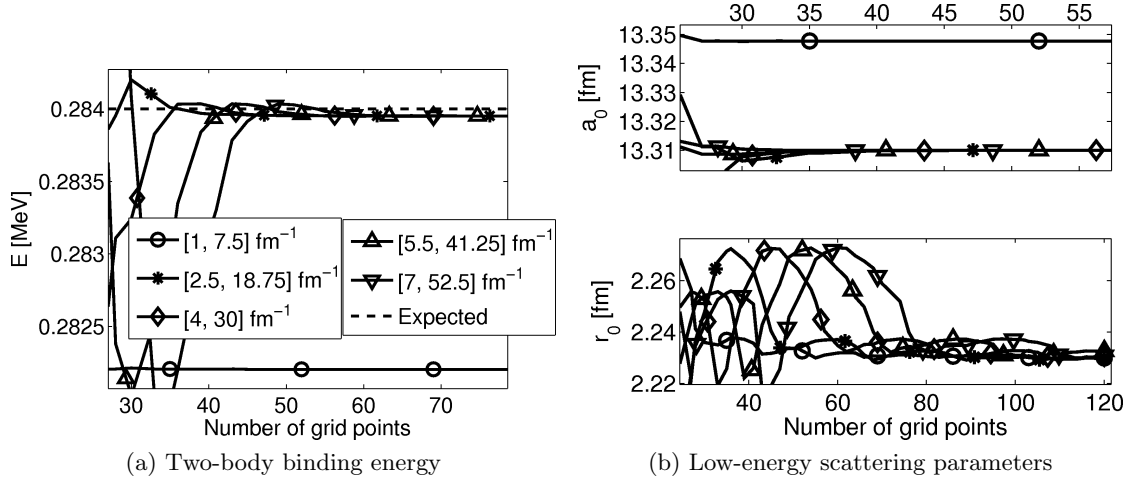


Figure 5: Modified Yukawa potential. Convergence of two-body observables with the number of grid points and the momentum cutoffs. It is seen that with large enough momentum cutoffs the same converged value is obtained. The grids have $2/3$ of the grid points in the lower interval.

13.2.2 Comparison with a harmonic-oscillator basis

I have compared the rate of convergence in the momentum-space partial-wave basis with the harmonic-oscillator basis presented in section 2.3. Of the nucleon potentials I have only considered the Yukawa potential. The position space expression (13.1) is used together with eq. (4.20) to get the potential in the harmonic-oscillator basis, $V_L(n, n')$.

A suitable value of r_0 , the oscillator length, need to be chosen to get good convergence. The optimal r_0 depends on the value of the cutoff in n . After some investigation I concluded that a good choice for r_0 is

$$r_0(n_{\max}) = 1.8 - 0.0008n_{\max} \text{ fm}. \quad (13.8)$$

The relative difference between the calculated two-body binding energy and the converged value in table 2 for the two bases are shown in figure 6. The figure shows that the momentum-space partial-wave basis converges much faster as a function of matrix size.

13.3 Three-body results

I have done similar convergence calculations for the three-body binding energy as for the two-body binding energy. In figures 7 and 8 are the results. An L_p cutoff of 4 or 6 is enough to get converged results.

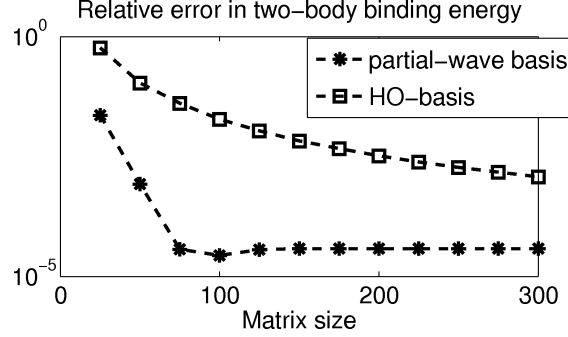


Figure 6: Yukawa potential. Comparison between convergence rate when using the harmonic-oscillator basis and the momentum-space partial-wave basis. The y -axis shows the relative difference between the calculated value and the converged value in table 2. The y -axis uses a logarithmic scale. The matrix size is equal to the cutoff in n and the number of grid points in p respectively. The oscillator length used is given by eq. (13.8) and the grid used is $(4.0, 60.0, 2x/3, x/3)$.

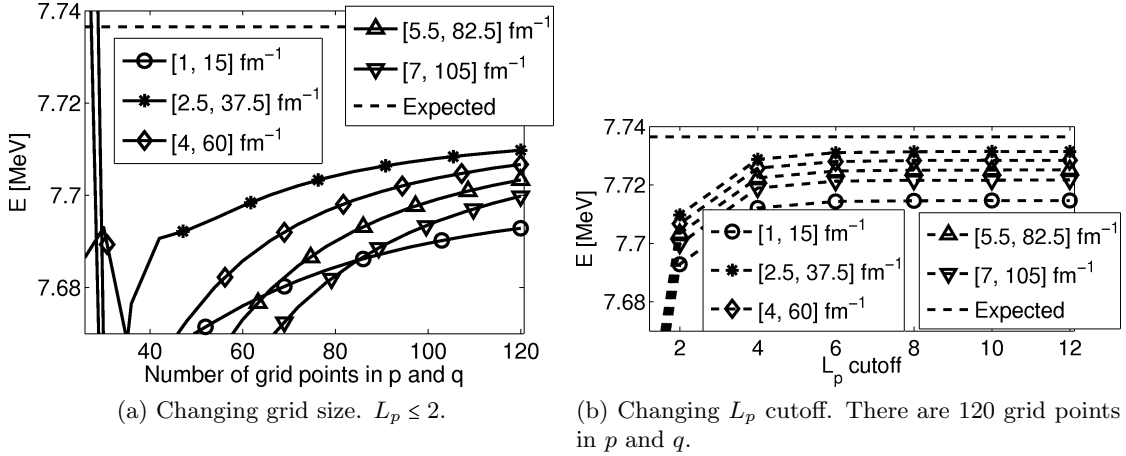


Figure 7: Yukawa potential. Convergence of the three-body binding energy with the number of grid points, the momentum cutoffs and the L_p cutoff. $2/3$ of the grid points are in the lower interval.

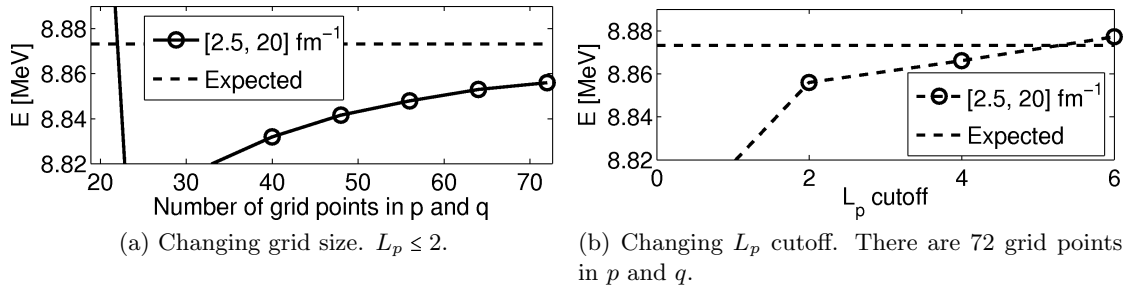


Figure 8: Modified Yukawa potential with three-body force. Convergence of the three-body binding energy with the number of grid points, the momentum cutoffs and the L_p cutoff. 2/3 of the grid points are in the lower interval. I have only used one grid here since the calculations take too much time. That is why I do not have more than 72 grid points. The three-body matrix elements were calculated using a fixed-point quadrature without error checking, using a total of 8^5 points.

13.4 SRG evolution of the potentials

13.4.1 Two-body evolution

The two-body SRG evolution is governed by eq. (11.3). The result of applying the transformation to the two potentials are shown in figures 9 and 10. The potentials display the expected behaviour of becoming band diagonal, and the width of the band is approximately given by the value of the flow parameter Λ .

The two-body observables are expected to be independent of Λ . In figures 11 and 12 it can be seen that the binding energy and the scattering length display no dependence on the flow parameter. The small errors are negligible. The effective range display a small dependence, but this is most likely due to the error in the calculation of the effective range, see section 13.2.1.

13.4.2 Three-body evolution

The three-body evolution is governed by equation 11.13. As seen in figures 7 and 8, many grid points are needed in p and q to get converged results. For the SRG evolution I have still used only 32 grid points in p and 32 grid points in q , in favour for using larger L_p cutoffs.

When doing the SRG evolution, I have considered two different L_p cutoffs. The first, $L_{p,V}$ is the cutoff in the potential, the second, $L_{p,I}$ is the cutoff in the induced three-body force. A large $L_{p,I}$ will reduce the deviation from unitarity in the SRG equation, while a large $L_{p,V}$ will give a more correct result.

In figure 13, the evolution for some different values of $L_{p,V}$ and $L_{p,I}$ have been plotted. Looking at the evolutions using $L_{p,V} = 0$ – figure 13a – it can be seen that the Λ dependency is indeed reduced with increasing values of $L_{p,I}$. With $L_{p,I} = 4$ the evolution is very close to unitary. The remaining error should be due to the relatively low number

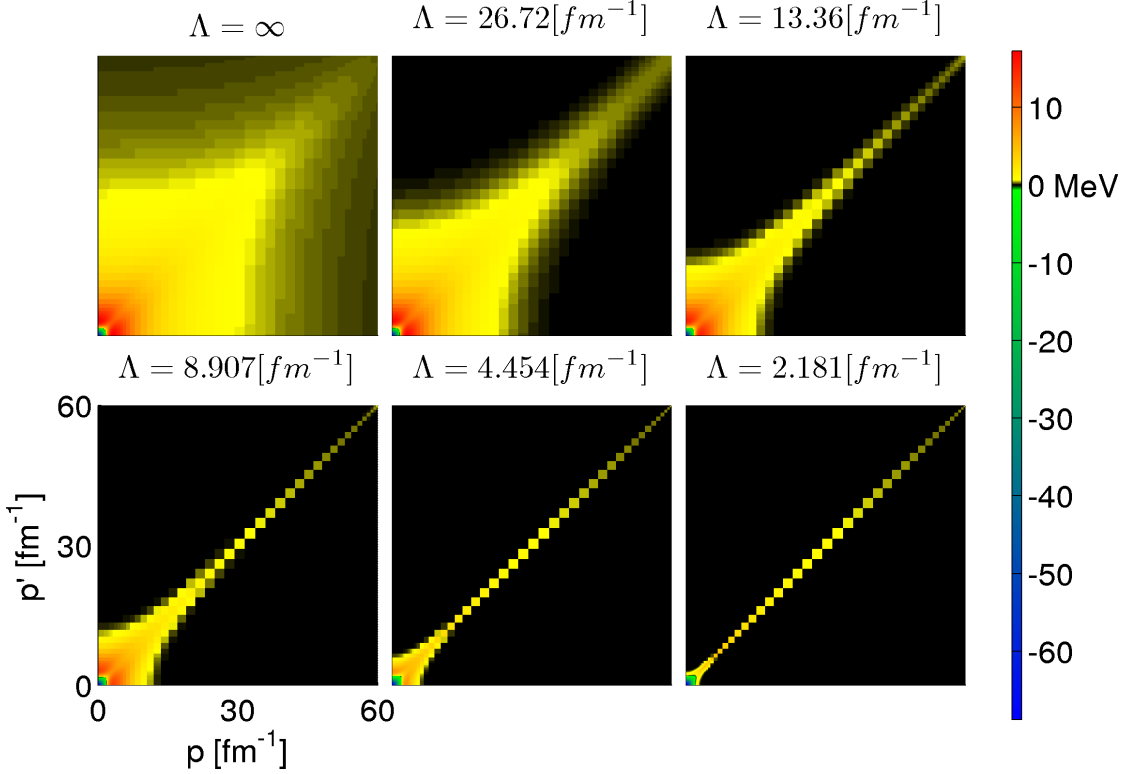


Figure 9: Yukawa potential. The potential depending on the SRG flow parameter Λ . The width of the band diagonal structure is approximately equal to Λ . The grid used is (4.0, 60.0, 80, 40)

of momentum grid points and the interpolation and extrapolation in the permutation matrices.

In figure 14 I show the evolution of the modified Yukawa potential. The behaviour is much like that of the Yukawa potential.

13.5 Decoupling

The purpose with the SRG transformation is to decouple the potential. I measure the degree of decoupling by cutting of the potential at different momentum values. All matrix elements with larger momentum values are set to zero, and the matrix elements with lower momentum values are unaffected. Good decoupling means that a large portion of the high-energy part of the potential can be set to zero without affecting the low-energy observables.

In figures 15 and 16 I have compared the unevolved potentials with evolved potentials. Since the three-body binding energy has a dependency on the SRG flow-parameter Λ , as seen in section 13.4.2, I have decided to measure the decoupling at a Λ -value which does not give too large deviation in the three-body binding energy. I have chosen values of

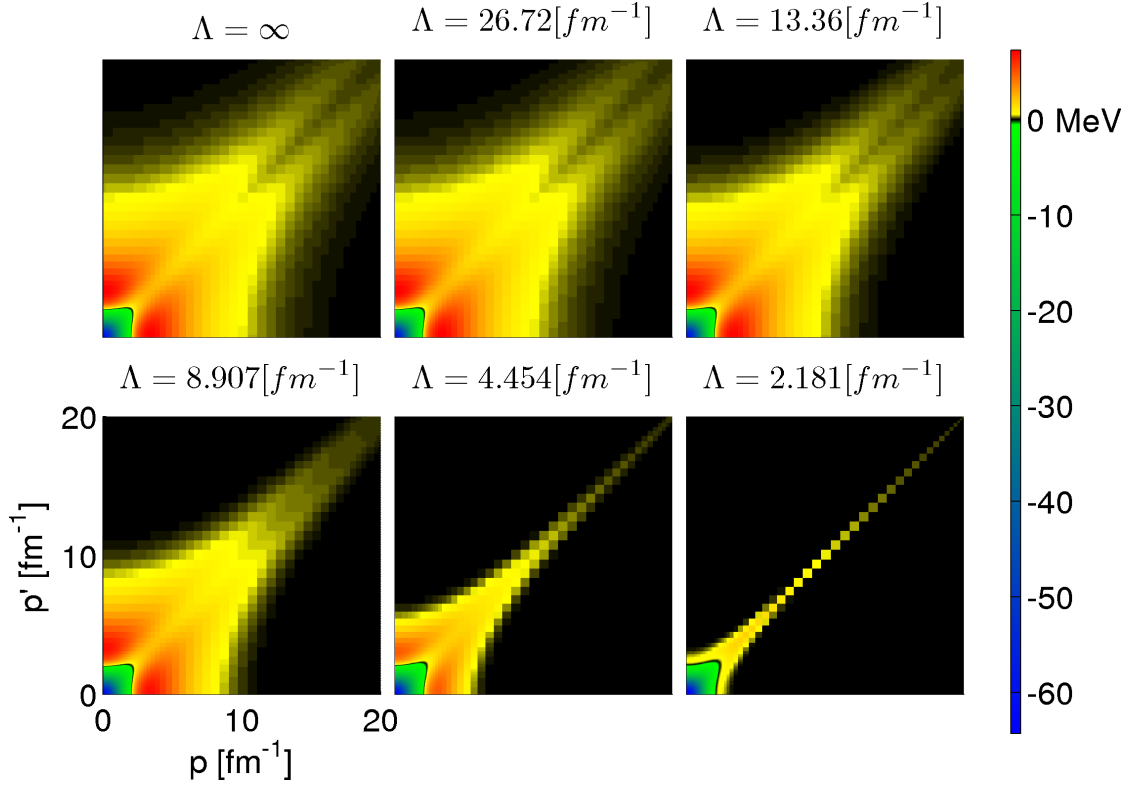


Figure 10: Modified Yukawa potential. The potential depending on the SRG flow parameter Λ . The width of the band diagonal structure is approximately equal to Λ . The grid used is (2.5, 20.0, 80, 40)

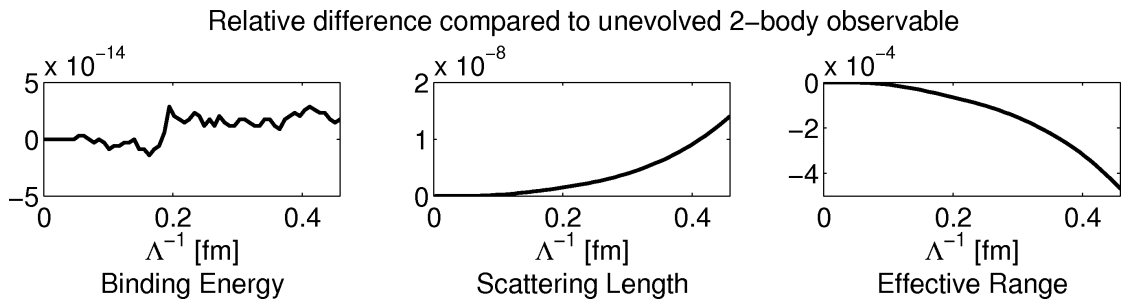


Figure 11: Yukawa potential. Two-body observables depending on the SRG flow-parameter Λ . The binding energy and scattering length have a very small error. The error in the effective range is probably due to the error in the calculation of the effective range, see section 13.2.1. The grid used is (2.5, 40.0, 21, 11)

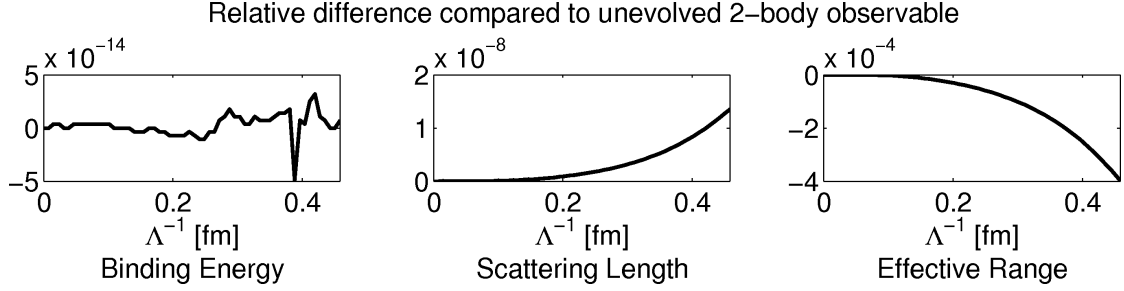
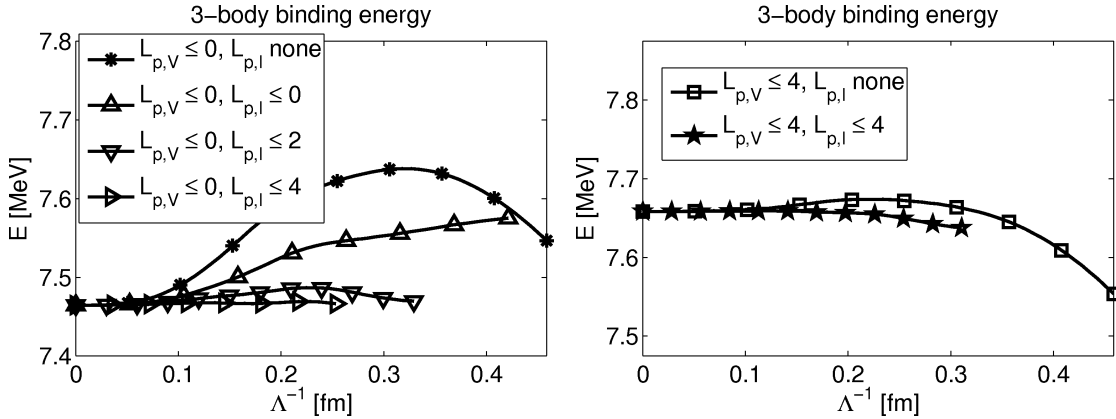


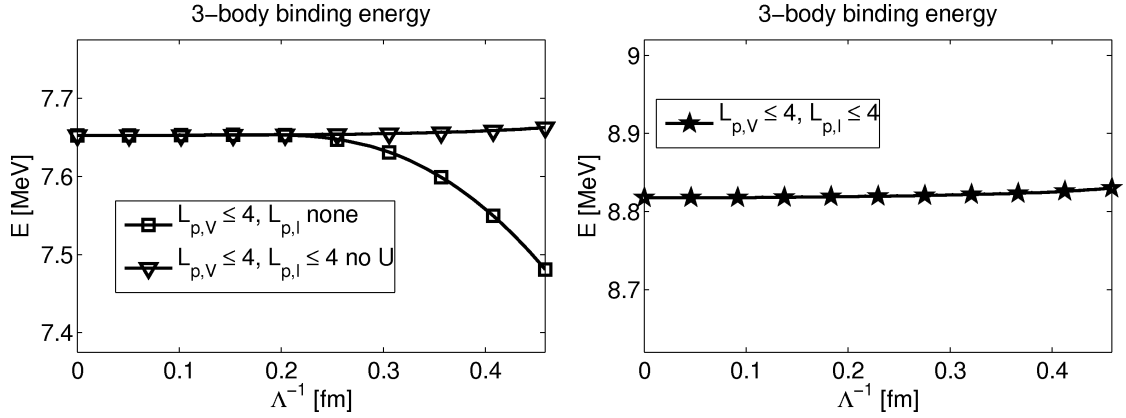
Figure 12: Modified Yukawa potential. Two-body observables depending on the SRG flow-parameter Λ . The binding energy and scattering length have a very small error. The error in the effective range is probably due to the error in the calculation of the effective range, see section 13.2.1. The grid used is (2.5, 20.0, 21, 11)



(a) Using $L_{p,V} = 0$. Without an induced three-body force there is a large Λ dependency. When an induced three-body force is included, the dependency decreases as the $L_{p,I}$ cutoff increases. The maximal deviations in the binding energy from the unevolved version is 2.3% without initial three-body force. With an $L_{p,I}$ cutoff of 0, 2 and 4 the maximal deviation is 1.5%, 0.30% and 0.060% respectively. Some curves are not evolved as far as others due to time constraints.

(b) Using $L_{p,V} = 4$. Without an induced three-body potential, the maximal deviation in the binding energy is 1.4%. This is reduced to 0.27% when including the induced three-body potential.

Figure 13: Yukawa potential. Three-body binding energy depending on the SRG flow-parameter Λ . The grid used is (2.5, 40.0, 21, 11) for the p variable.



(a) Without initial three-body potential. Three-body binding energy depending on the SRG flow-parameter Λ . Without an induced three-body force there is a large Λ dependency, but including the induced forces the deviation in the binding energy is 0.14%.

(b) With the initial three-body potential. Three-body binding-energy depending on the SRG flow-parameter Λ . With the initial three-body force the behaviour is the same as without, seen in figure 14a. The maximal deviation is 0.13%.

Figure 14: Modified Yukawa potential. Three-body binding energy depending on the SRG flow-parameter Λ . The grid used is (2.5, 20.0, 21, 11) for the p variable. The three-body matrix elements were calculated using a fix-point quadrature using a total of 12^5 points.

Λ where the deviation is about 0.1% from the unevolved value. In the figures I also show the decoupling at the lowest Λ value I have evolved to.

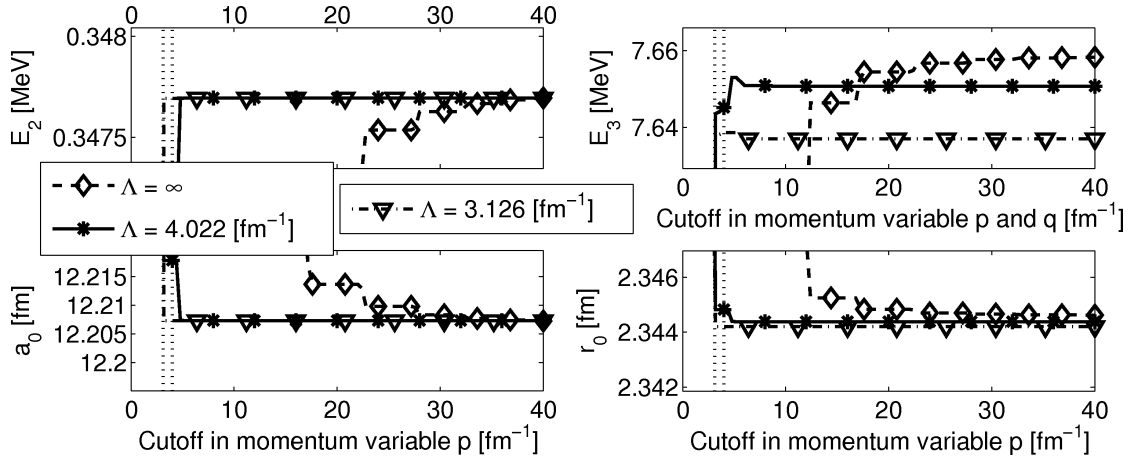


Figure 15: Yukawa potential. Two- and three-body observables depending on the cutoff in the momentum variables. The dotted vertical lines corresponds to the Λ values. The evolved potential has a greatly improved decoupling. Evolving from $\Lambda = 4.0\text{fm}^{-1}$ to $\Lambda = 3.1\text{fm}^{-1}$ increases decoupling slightly, but the three-body binding energy deviation is increased from 0.1% to 0.27%. The grid used is $(2.5, 40.0, 21, 11)$ with $L_p \leq 4$.

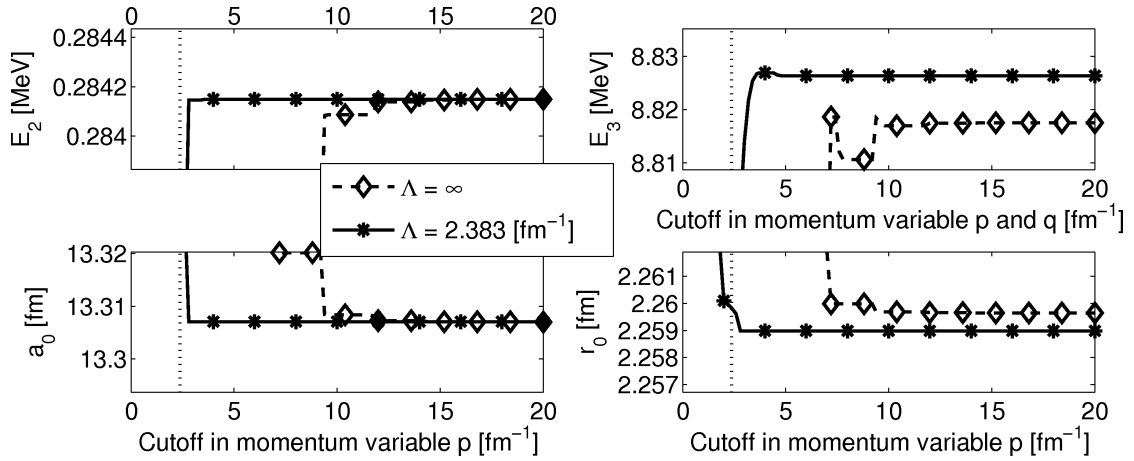


Figure 16: Modified Yukawa potential. Two- and three-body observables depending on the cutoff in the momentum variables. The evolved potential has a greatly improved decoupling, with an initial three-body binding-energy deviation of 0.13%. The dotted vertical line corresponds to the Λ value used. The grid used is $(2.5, 20.0, 21, 11)$ with $L_p \leq 4$.

14 Helium potentials

The soft core potential is simply a gaussian term, of the form

$$\langle \mathbf{r} | \hat{V} | \mathbf{r}' \rangle = V_{\text{He,soft}}(r) \delta^3(\mathbf{r} - \mathbf{r}') \quad (14.1a)$$

$$V_{\text{He,soft}}(r) = V_0 \exp\left(-\frac{r^2}{R^2}\right), \quad (14.1b)$$

and the mimic potential LM2M2 looks like

$$\langle \mathbf{r} | \hat{V} | \mathbf{r}' \rangle = V_{\text{He,hard}}(r) \delta^3(\mathbf{r} - \mathbf{r}') \quad (14.2a)$$

$$V_{\text{He,hard}}(r) = \epsilon \left(A^* \exp(-\alpha^* x + \beta^* x^2) - F(x) \left(\frac{C_6}{x^6} + \frac{C_8}{x^8} + \frac{C_{10}}{x^{10}} \right) + V_b(x) \right) \quad (14.2b)$$

$$x = \frac{r}{r_m} \quad (14.2c)$$

$$F(x) = \begin{cases} \exp\left(-\left(\frac{D}{x} - 1\right)^2\right) & , \quad x \leq 1 \\ 1 & , \quad x > 1 \end{cases} \quad (14.2d)$$

$$V_b(x) = \begin{cases} A_a \left(\sin\left(2\pi \frac{x-x_1}{x_2-x_1} - \frac{\pi}{2}\right) + 1 \right) & , \quad x_1 \leq x \leq x_2 \\ 0 & , \quad \text{otherwise} \end{cases}. \quad (14.2e)$$

The values of the parameters are presented in table 3. The coordinate space representations of the potentials are plotted in figure 17, where the strong repulsion of the LM2M2 potential can be seen.

The soft-core two-body potential expressed in momentum-space is

$$\langle \mathbf{p} | \hat{V} | \mathbf{p}' \rangle = \frac{V_0 R^3}{8\pi^{3/2}} \exp\left(-\frac{R^2}{4} q^2\right) \quad (14.3)$$

$$q = |\mathbf{p} - \mathbf{p}'|.$$

The LM2M2 potential can not be converted to momentum space analytically, instead eq. (4.6) is used. The double integral is not straight forward to evaluate, especially since

Table 3: Parameter values used for the helium potentials. The values for the soft core potential are the same as one of the parameter sets used by Gattobigio et al. [19]. The values for the LM2M2 potential are the ones that Aziz et al. used [9].

Soft core potential		LM2M2 potential			
		ϵ	10.97 K	C_6	1.34687065
V_0	-1.227 K	r_m	5.6115 au	C_8	0.41308398
R	10.03 au	A^*	$1.89635353 \cdot 10^5$	C_{10}	0.17060159
W_0	1.4742 K	α^*	10.70203539	A_a	0.0026000000
ρ_0	10.0 au	β^*	-1.90740649	x_1	1.0035359490
		D	1.4088	x_2	1.4547903690

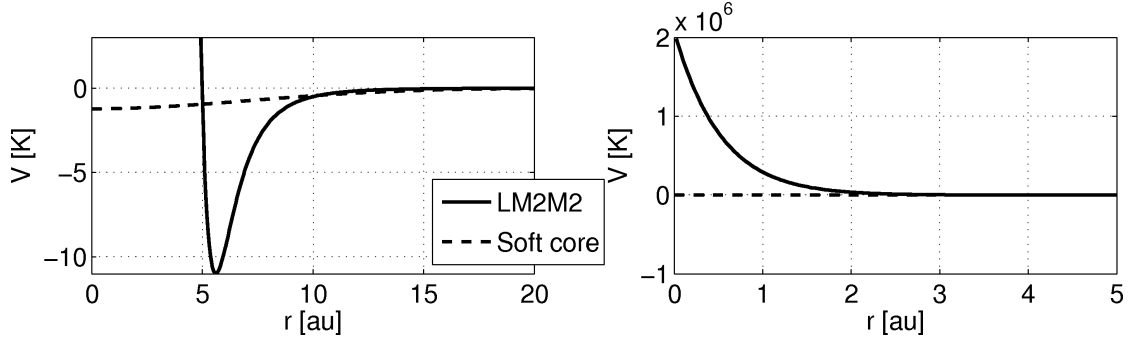


Figure 17: Coordinate space representations of the two helium potentials. Two different energy scales are used to emphasize the strong repulsion of the LM2M2 potential at close range.

the LM2M2 potential does not have an exponential decay for high values of r . The sine in eq. (4.6) will cause the integral to be very fluctuating for certain values of p , p' and t . I tried several different ways of integrating the function, and the method that worked best is to first do the t integration with an adaptive 31-point Gauss-Konrod rule, using the function `gsl_integration_qag`. If the argument to the sine function is zero, the x integration is done with the function `gsl_integration_qagi` for semi infinite intervals. Otherwise, it is done with a Gauss-Konrod rule up to the first zero of the sine function, then I use the specialized integrator `gsl_integration_qawf` for Fourier integrals for the rest of the interval.

Some of the terms in the LM2M2 potential can be calculated analytically. The $1/x^n$ terms for $x > 1$ can be calculated analytically. This did not improve the results however, so the numerical integration was used.

In figure 18 are the momentum space partial-wave representations. As seen in the figure, the soft-core potential is everywhere negative and has very low absolute values, compared to the LM2M2 potential which is positive with large values. The momentum scale is also very different.

14.1 Three-body potential

Since the soft-core potential is constructed just to give accurate results for low-energy two-body observables, it does not give accurate results when doing three-body calculations. For this reason, a three-body force is needed. The three-body potential expressed in the absolute coordinates \mathbf{x}_1 to \mathbf{x}_3 is [19]

$$\begin{aligned} \langle \mathbf{x}_1 \mathbf{x}_2 \mathbf{x}_3 | \hat{V}_3 | \mathbf{x}'_1 \mathbf{x}'_2 \mathbf{x}'_3 \rangle &= \\ &= U_{\text{He,soft}}(|\mathbf{x}_1 - \mathbf{x}_2|, |\mathbf{x}_2 - \mathbf{x}_3|, |\mathbf{x}_3 - \mathbf{x}_1|) \delta^3(\mathbf{x}_1 - \mathbf{x}'_1) \delta^3(\mathbf{x}_2 - \mathbf{x}'_2) \delta^3(\mathbf{x}_3 - \mathbf{x}'_3) \end{aligned} \quad (14.4a)$$

$$\tilde{U}_{\text{He,soft}}(r_{12}, r_{23}, r_{31}) = W_0 \exp\left(-\frac{4}{3\rho_0^2}(r_{12}^2 + r_{23}^2 + r_{31}^2)\right). \quad (14.4b)$$

The values I use for the parameters are presented in table 3.

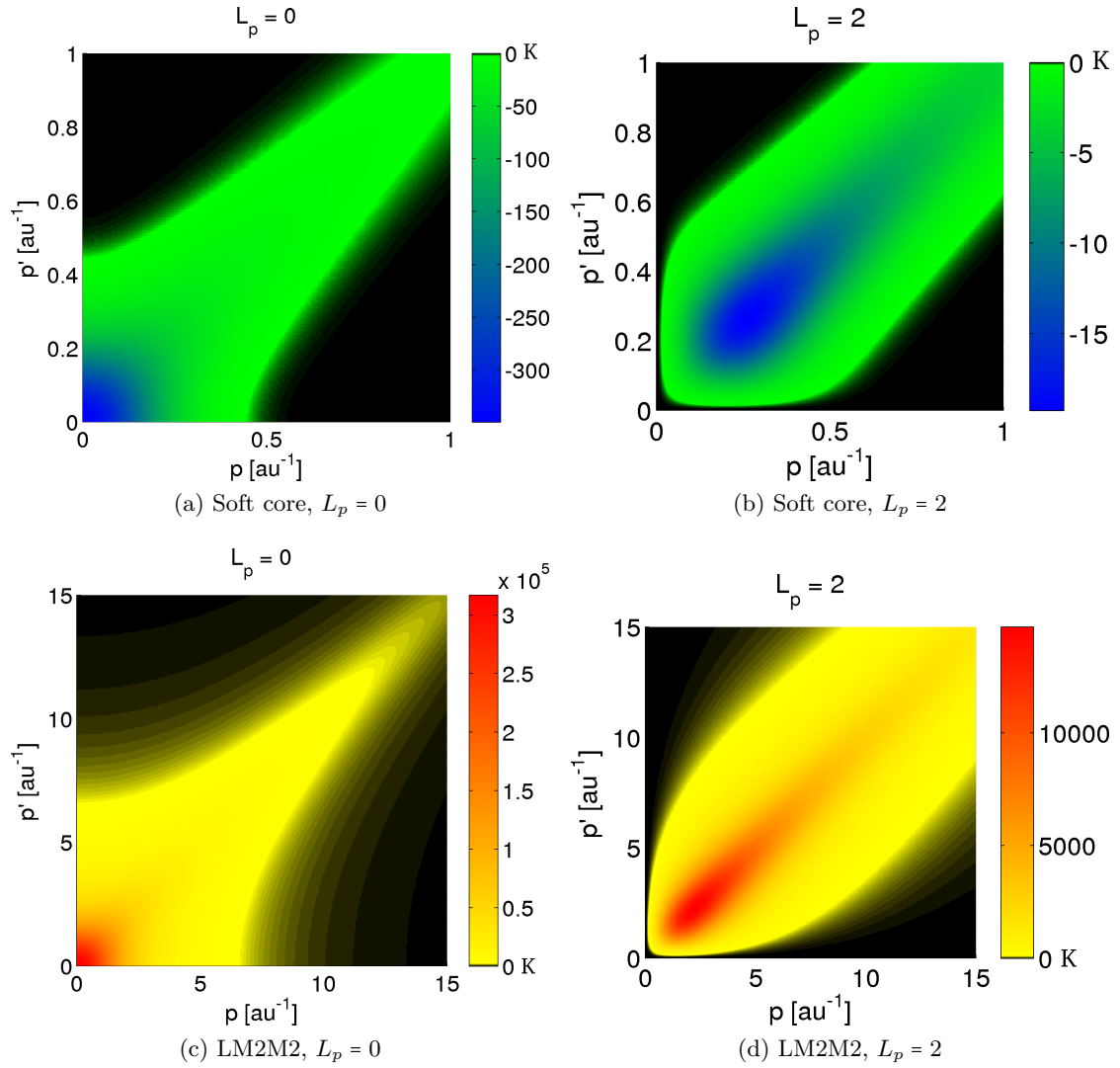


Figure 18: Matrix representations of the two helium potentials for $L_p = 0$ and $L_p = 2$. Each potential was produced using a total of 400 grid points, resulting in 400^2 matrix elements, for each L_p . Note the large difference in momentum scale and the magnitude of the potentials.

Expressed in Jacobi coordinates, $\tilde{U}_{\text{He,soft}}$ is

$$U_{\text{He,soft}}(r, s) = W_0 \exp(-\rho_0^{-2}(2r^2 + 8s^2/3)) \quad (14.5)$$

To express it in momentum coordinates, I need to do a Fourier transform of the expression. Since the potential is separable, I do the calculation for a general term $\exp(-\alpha r^2)$.

$$\begin{aligned} \langle \mathbf{p} | \exp(-\alpha \hat{r}^2) | \mathbf{p}' \rangle &= (2\pi)^{-3} \int_{\mathbb{R}^3} d^3 \mathbf{r} \exp(i(\mathbf{p}' - \mathbf{p}) \cdot \mathbf{r}) \exp(-\alpha r^2) = \\ &= \left((2\pi)^{-1} \int_{\mathbb{R}} dr \exp(i(p'_1 - p_1)r_1) \exp(-\alpha r_1^2) \right)^3 = \\ &= \left(\frac{1}{\sqrt{4\pi\alpha}} \exp\left(-\frac{1}{4} \frac{|p'_1 - p_1|^2}{\alpha}\right) \right)^3 = \\ &= (4\pi\alpha)^{-3/2} \exp\left(-\frac{1}{4} \frac{|\mathbf{p}' - \mathbf{p}|^2}{\alpha}\right) \equiv f(|\mathbf{p}' - \mathbf{p}|, \alpha). \end{aligned} \quad (14.6)$$

Thus, the entire expression will be

$$\begin{aligned} \langle \mathbf{p} \mathbf{q} | W_0 \exp(-\rho_0^{-2}(2\hat{r}^2 + 8\hat{s}^2/3)) | \mathbf{p}' \mathbf{q}' \rangle &= W_0 f(\overbrace{|\mathbf{p}' - \mathbf{p}|}^{\equiv \tilde{p}}, 2\rho_0^{-2}) f(\overbrace{|\mathbf{q}' - \mathbf{q}|}^{\equiv \tilde{q}}, 8\rho_0^{-2}/3) = \\ &= 3 \frac{W_0 \rho_0^6 \sqrt{3}}{2^{12} \pi^3} \exp\left(-\frac{\rho_0^2}{8} \left(\tilde{p}^2 + \frac{3}{4} \tilde{q}^2\right)\right) \end{aligned} \quad (14.7)$$

Eq. (4.18) is used to get the expression in the momentum-space partial-wave basis. Due to the simplicity of this three-body force however, the four-dimensional integral can be turned into a two-dimensional integration. Using eq. (4.18) and this three-body potential, I get

$$\begin{aligned} V(p, q, L_p, p', q', L'_p) &= 3 \frac{W_0 \rho_0^6 \sqrt{3(2L_p + 1)(2L'_p + 1)}}{2^{13} \pi^3} \int_{-1}^1 dt_2 P_{L_p}(t_2) \int_{-1}^1 dt_3 \\ &\times \int_{-1}^1 dt_4 \int_0^{2\pi} d\phi_2 \exp\left(-\frac{\rho_0^2}{8} \left(p^2 + p'^2 - 2pp't_3^2 + \frac{3}{4}(q^2 + q'^2 - 2qq'\tilde{S}_{24})\right)\right) \\ &\times \int_0^{2\pi} d\phi_3 P_{L'_p}(\tilde{S}_{34}), \end{aligned} \quad (14.8)$$

where

$$\tilde{S}_{ij} = \sqrt{(1 - t_i^2)(1 - t_j^2)} \cos(\phi_i) + t_i t_j. \quad (14.9)$$

To simplify, I will use

$$C = 3 \frac{W_0 \rho_0^6 \sqrt{3(2L_p + 1)(2L'_p + 1)}}{2^{13} \pi^3} \quad (14.10a)$$

$$\times \exp\left(-\frac{\rho_0^2}{8} \left(p^2 + p'^2 + \frac{3}{4} (q^2 + q'^2)\right)\right) \quad (14.10b)$$

$$\alpha = 2pp' \frac{\rho_0^2}{8} \quad (14.10c)$$

$$\beta = 2qq' \frac{\rho_0^2}{8} \quad (14.10d)$$

$$f(\alpha, \beta, L_p, L'_p) \equiv \frac{V(p, q, L_p, p', q', L'_p)}{C}. \quad (14.10e)$$

Now I need to calculate f ,

$$\begin{aligned} f(\alpha, \beta, L_p, L'_p) &= \int_{-1}^1 dt_2 P_{L_p}(t_2) \int_{-1}^1 dt_4 \exp(\beta t_2 t_4) \\ &\quad \times \underbrace{\int_0^{2\pi} d\phi_2 \exp\left(\beta \sqrt{(1-t_2^2)(1-t_4^2)} \cos(\phi_2)\right)}_{\equiv A} \\ &\quad \times \underbrace{\int_{-1}^1 dt_3 \exp(\alpha t_3^2) \int_0^{2\pi} d\phi_3 P_{L'_p}\left(\sqrt{(1-t_3^2)(1-t_4^2)} \cos(\phi_3) + t_3 t_4\right)}_{\equiv B} \end{aligned} \quad (14.11)$$

The factor A is just $2\pi I_0(\beta \sqrt{(1-t_2^2)(1-t_4^2)})$, where $I_0(x)$ is the regular modified cylindrical Bessel function of zeroth order, which I calculate with the GSL routine named `gsl_sf_bessel_I0`. D is a polynomial in $\cos(\phi_3)$. The integral from 0 to 2π is easy to compute analytically and an important property is that the integral will be zero for all odd powers. This means that B will be a polynomial in t_3 and the integral over t_3 can be calculated analytically.

Now I am left with only two integrals which can be calculated fast with an adaptive integration procedure. The potential also has the property that

$$V(p, q, L_p, p', q', L'_p) = V(p', q, L_p, p, q', L'_p) \quad (14.12a)$$

$$V(p, q, L_p, p', q', L'_p) = V(p, q', L_p, p', q, L'_p). \quad (14.12b)$$

which means that it is enough to calculate the potential for $p \geq p'$, $q \geq q'$ and $L_p \geq L'_p$, where the last inequality comes from that the potential is a hermitian operator.

In figure 19 is the three-body potential for $q = q' = 0$ and $L_p = L'_p = 0$. Worth noting is that the three-body force have larger values than the two-body force.

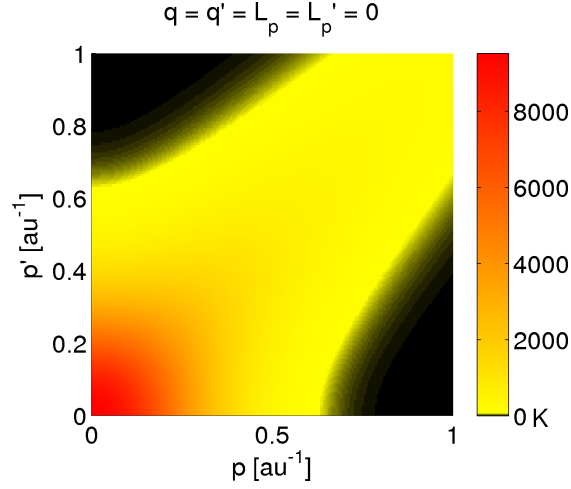


Figure 19: Soft core three-body potential. The potential for $q = q' = 0$ and $L_p = L_p' = 0$. The maximum value of the three-body force is larger than the maximum value of the two-body force in figure 18a.

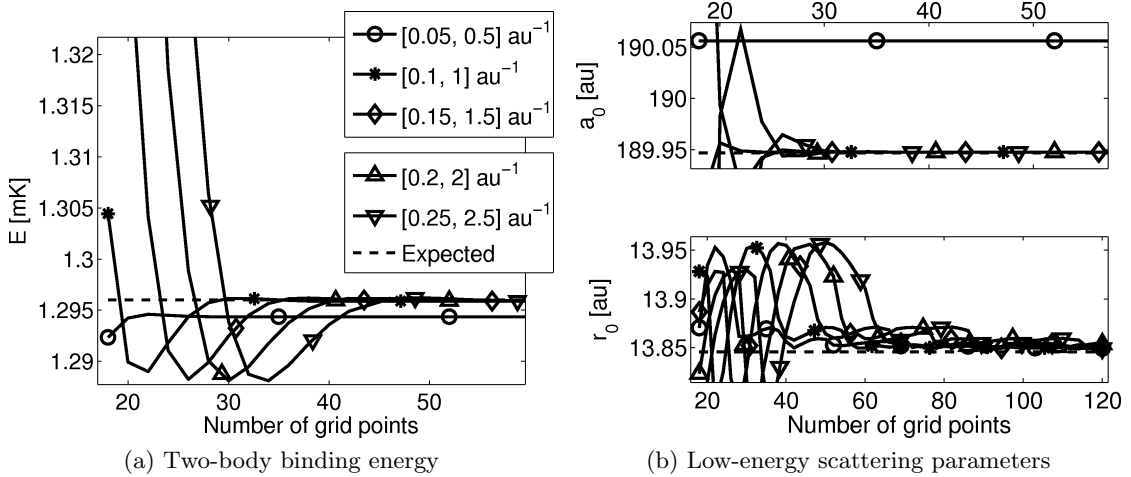


Figure 20: Soft core potential. Convergence of two-body observables with the number of grid points and the momentum cutoffs. It is seen that with large enough momentum cutoffs the same converged value is obtained. 1/2 of the the grid points are in each momentum interval.

14.2 Two-body results

In figures 20 and 21 are similar convergence plots as for the nucleon potentials. Interesting to note is that the LM2M2 potential needs considerably more grid points for converged results.

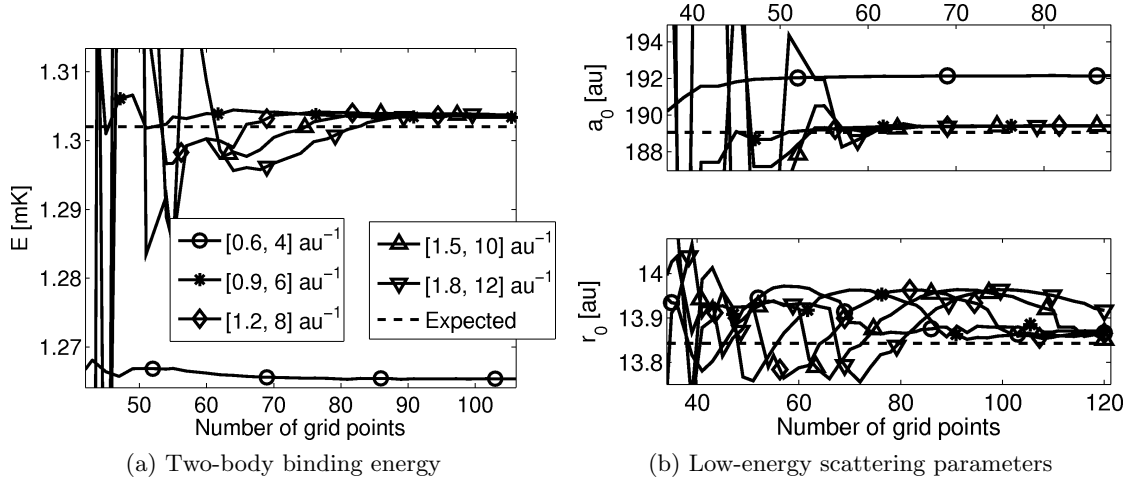


Figure 21: LM2M2 potential. Convergence of two-body observables with the number of grid points and the momentum cutoffs. It is seen that with large enough momentum cutoffs the same converged value is obtained. $2/3$ of the grid points are in the lower interval.

Table 4: Converged two-body observables for the helium potentials. To obtain the values, the five grids used in figure 20 and 21 were used with a total of 360 and 720 grid points. The digits that were the same for the two largest grid cutoffs and the two grid sizes are displayed. The number of significant digits is thus an indication of how fast the value is converging.

	Soft core	Reference	LM2M2	Reference
E_0	1.29589113343035 mK	1.296 mK [19]	E_0	1.3035 mK
a_0	189.947742 au	189.947 au [19]	a_0	189.414 au
r_0	13.848 au	13.846 au [19]	r_0	13.8 au

14.2.1 Comparison with a harmonic-oscillator basis

Just like in the case of the Yukawa potential in section 13.2.2 I have compared the rate of convergence in the momentum-space partial-wave basis with the harmonic-oscillator basis presented in section 2.3. Of the helium potentials I have only considered the soft-core potential.

The relationship between r_0 and n_{\max} I have used in this case is

$$r_0(n_{\max}) = 30 + 0.052n_{\max}\text{au}. \quad (14.13)$$

The relative difference between the calculated two-body binding energy and the converged value in table 4 for the two bases are shown in figure 22. The figure shows that the momentum-space partial-wave basis converges much faster as a function of matrix size.

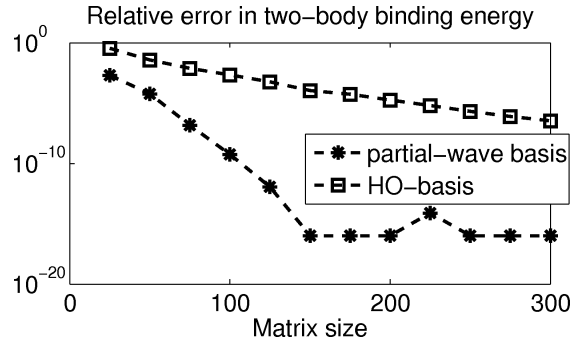


Figure 22: Soft-core potential. Comparison between convergence rate when using the harmonic-oscillator basis and the momentum-space partial-wave basis. The y -axis shows the relative difference between the calculated value and the converged value in table 4. The matrix size is equal to the cutoff in n and the number of grid points in p respectively. The oscillator length used is given by eq. (14.13) and the grid used is $(0.2, 2.0, x/2, x/2)$.

14.3 Three-body results

A big difficulty in obtaining the three-body binding energy for the LM2M2 potential is that the Arnoldi iteration method used to calculate the binding energy does not converge for this potential. The reason is that the kernel has many eigenvalues tightly packed close to one, which is the eigenvalue that need to be found. The other potentials have a simpler spectra of eigenvalues with a single eigenvalue close to one.

In figures 23 and 24 are the same type of convergence graphs for the three-body binding energy as for the nucleon potentials. In the case of the soft core potential a angular momentum cutoff of 2 is enough for converged results, whereas for the LM2M2 potential the binding energy does not seem to be completely converged even for a cutoff value of 6. More grid points in the momentum variables are also needed for the LM2M2 potential.

14.4 SRG evolution of the potentials

14.4.1 Two-body evolution

The result of applying the transformation to the two helium potentials are in figures 25 and 26. Just as the nucleon potentials, the potentials display the expected behaviour of becoming band diagonal. In the case of the LM2M2 potential there is an artifact left on the diagonal at the high end of the spectra. This is an edge effect, which is a result of the potential not being close enough to zero at the momentum cutoff. With a larger momentum cutoff value this side effect is not present.

As seen in figures 27 and 28, the two-body observables display the same kind of behaviour as they did for the nucleon potentials. The binding energy and the scattering length are independent of the flow parameter and the effective range display a small dependence on Λ .

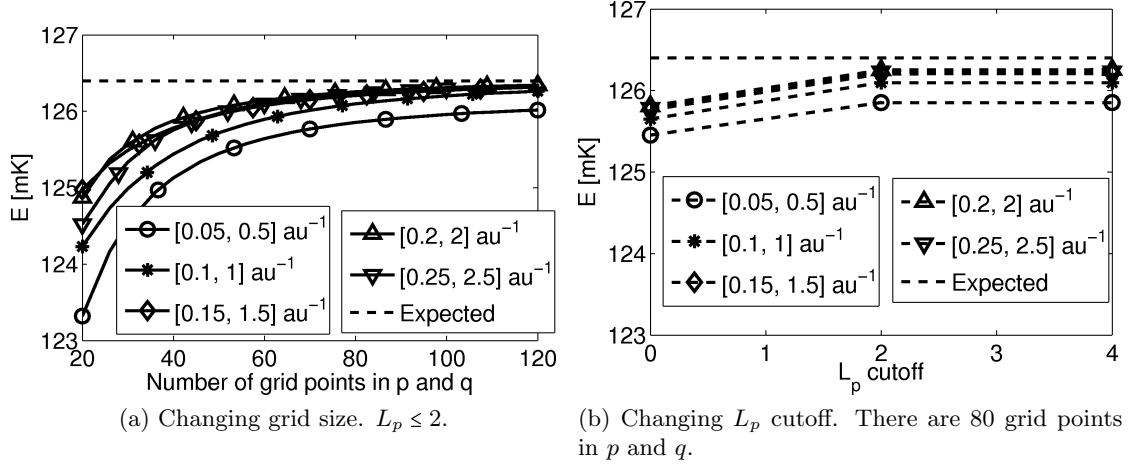


Figure 23: Soft-core potential. Convergence of the three-body binding energy with the number of grid points, the momentum cutoffs and the L_p cutoff. $1/2$ of the grid points are in each momentum interval.

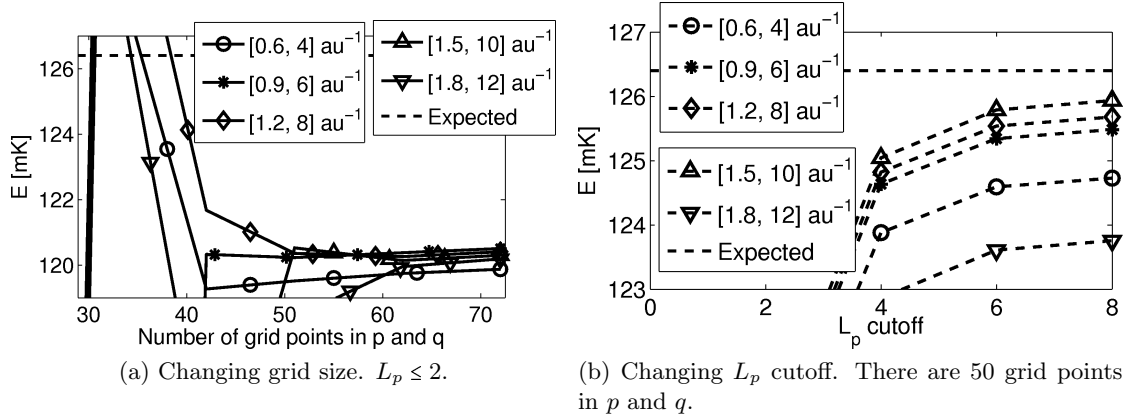


Figure 24: LM2M2 potential. Convergence of the three-body binding energy with the number of grid points, the momentum cutoffs and the L_p cutoff. $2/3$ of the grid points are in the lower interval.

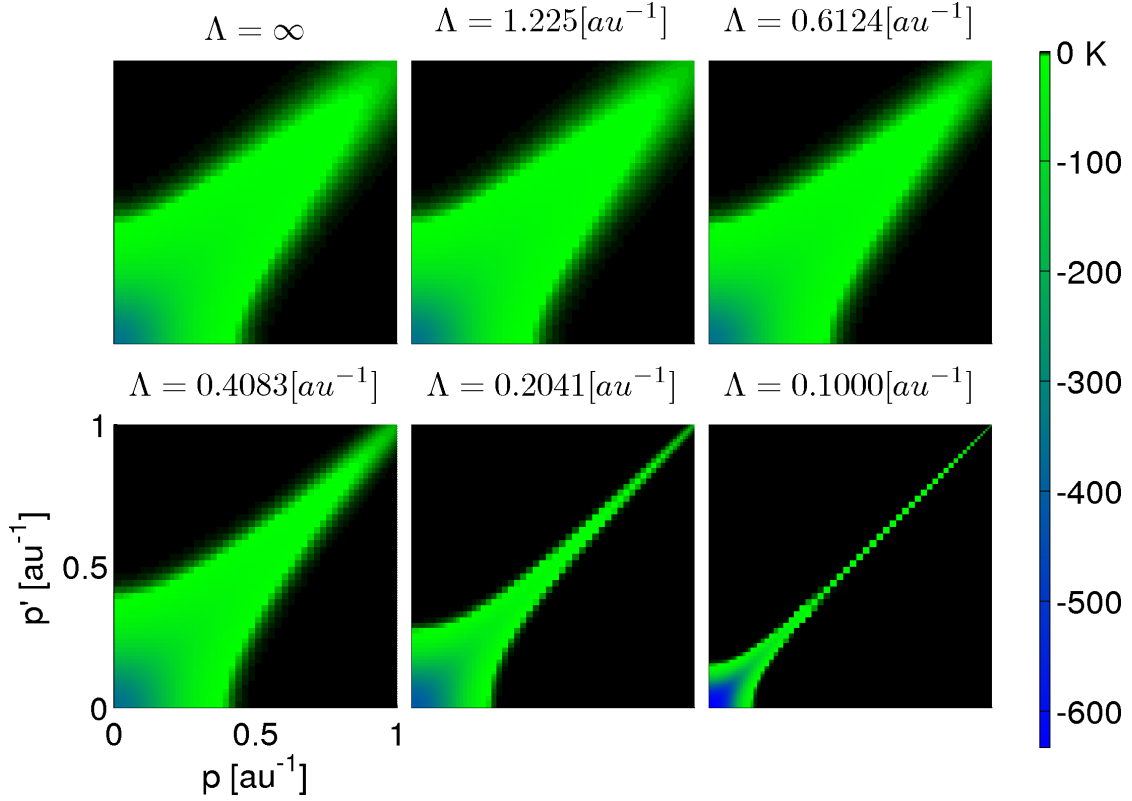


Figure 25: Soft core potential. The potential depending on the SRG flow parameter Λ . The width of the band diagonal structure is approximately equal to Λ . The grid used is (0.1, 1.0, 60, 60)

14.4.2 Three-body evolution

The behaviour of the two helium potentials are very different for the three-body evolution. The three-body binding energy as a function of the flow parameter is seen in figure 29. As seen, the behaviour is identical for all values of the angular momentum cutoff. However, even with induced three-body forces the binding energy has a large dependency on Λ . This is probably due to the large three-body force, which amplifies the errors in the SRG evolution caused by the discretization and the interpolation and extrapolation in the permutation matrices.

The three-body binding energy of the LM2M2 potential as a function of Λ is shown in figure 30. There is a large Λ dependency. I have not done a three-body SRG evolution with this potential. A relatively large grid is necessary to get reasonable good results which makes it difficult to do an SRG transformation.

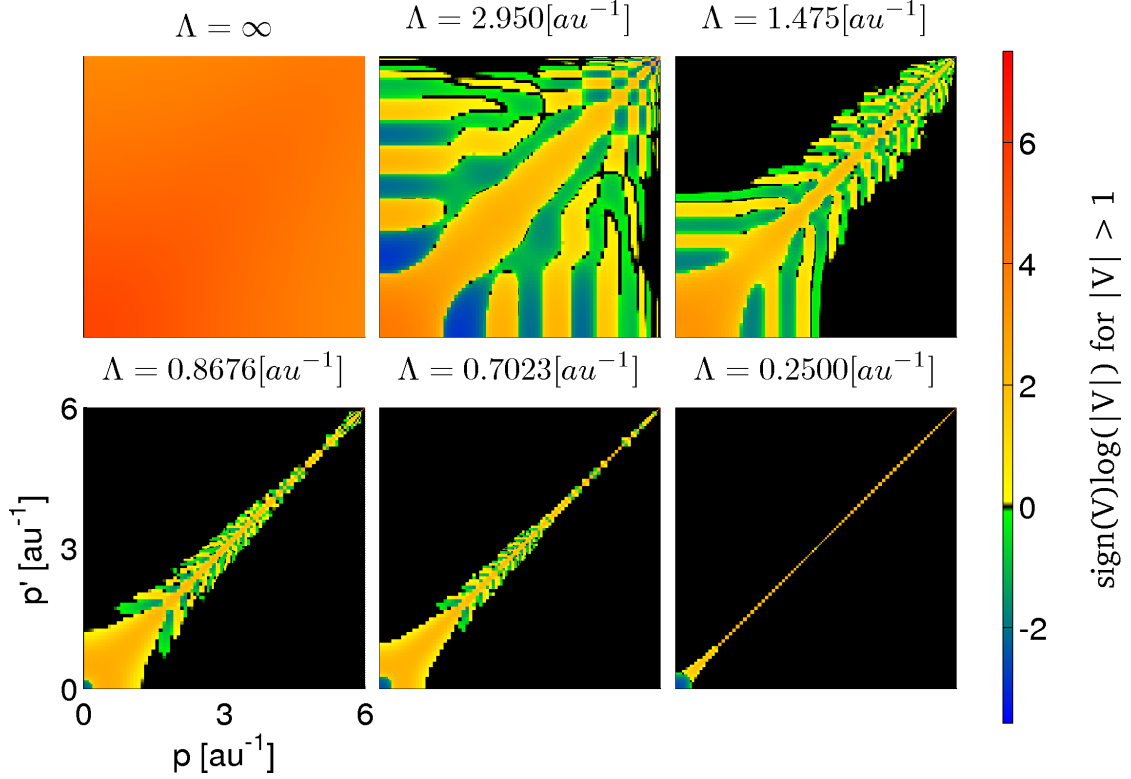


Figure 26: LM2M2 potential. The potential depending on the SRG flow parameter Λ . Due to the large differences in scale when evolving this potential, I have plotted $\text{sgn}(V)\log_{10}(|V|)$ for $|V| > 1$. Values with $|V| < 1$ are set to zero. The width of the band diagonal structure is approximately equal to Λ . The grid used is $(1.0, 20.0, 60, 60)$

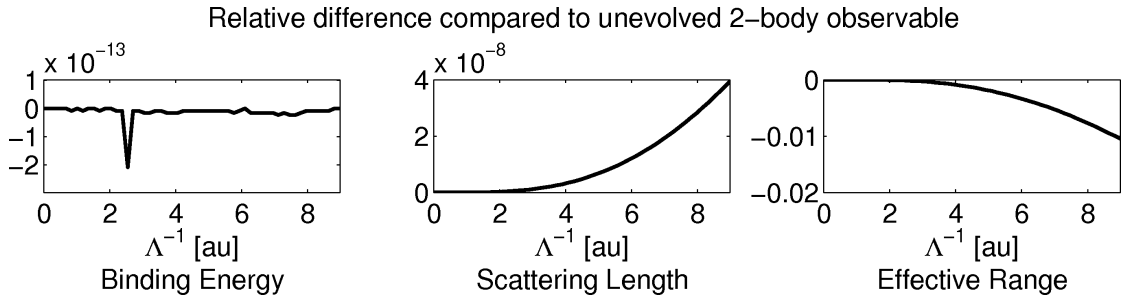


Figure 27: Soft core potential. Two-body observables depending on the SRG flow-parameter Λ . The binding energy and scattering length have a very small error. The error in the effective range is probably due to the error in the calculation of the effective range, see section 13.2.1. The grid used is $(0.1, 1.0, 16, 16)$

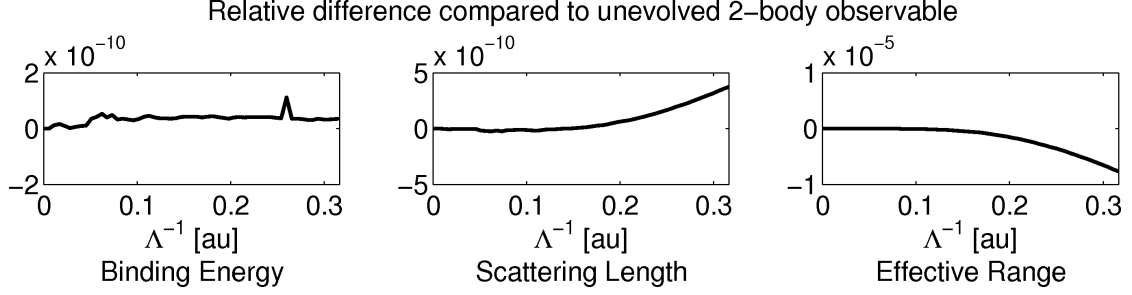
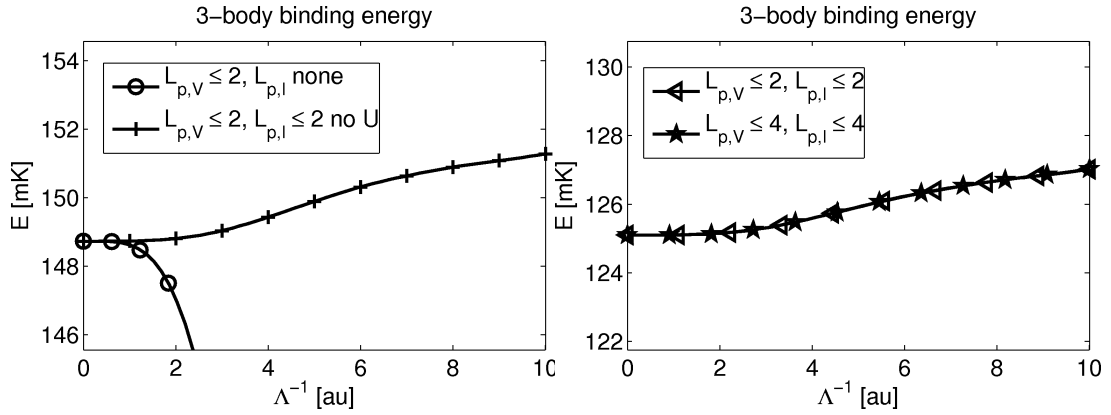


Figure 28: LM2M2 potential. Two-body observables depending on the SRG flow-parameter Λ . The binding energy and scattering length have a very small error. The error in the effective range is probably due to the error in the calculation of the effective range, see section 13.2.1. The grid used is (0.9, 6.0, 21, 11)



(a) Without initial three-body potential. Without(b) With initial three-body potential. When induced including the initial three-body potential, the Λ dependency is very large. Even with the induced three-body dependency is still large, with a deviation of 1.7% at the end. Just as in figure 23 there is no improvement of the other potentials, with a deviation of 1.5% at the end.

Figure 29: Soft-core potential. Three-body binding energy depending on the SRG flow-parameter Λ . The grid used is (0.1, 1.0, 16, 16) for the p variable.

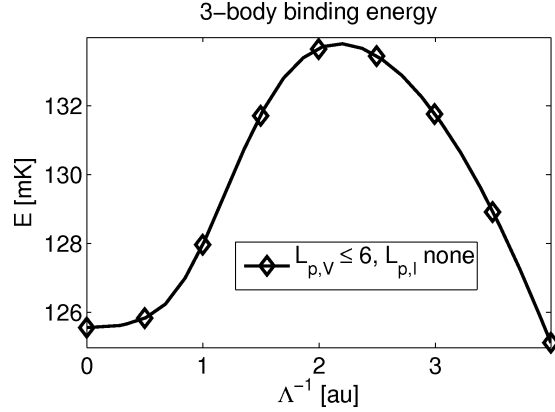


Figure 30: LM2M2 potential. Three-body binding energy depending on the SRG flow-parameter Λ . There is a large Λ dependency, with a maximal deviation of 6.6%. However, already at $\Lambda^{-1} \approx 1/3$ there is a greatly improved decoupling, as seen in figure 32. The grid used is (0.9, 6.0, 40, 20) for the p variable.

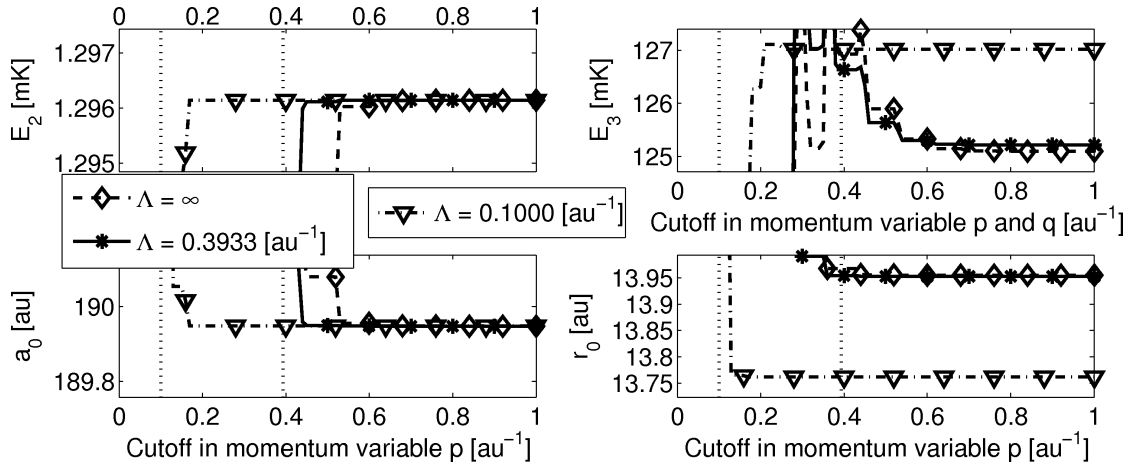


Figure 31: Soft core potential. Two- and three-body observables depending on the cutoff in the momentum variables. The evolved potential has a greatly improved decoupling. The grid used is (0.1, 1.0, 16, 16) with $L_p \leq 2$.

14.5 Decoupling

In figure 31 I have compared the unevolved potential with an evolved potential of the soft-core potential. The decoupling has been improved with the SRG transformation for the two-body observables.

The decoupling for the LM2M2 potential is shown in figure 30. The LM2M2 potential displays a greatly improved decoupling after the SRG transformation. Despite this, higher momentum values are still needed for the LM2M2 potential than for the soft-core potential.

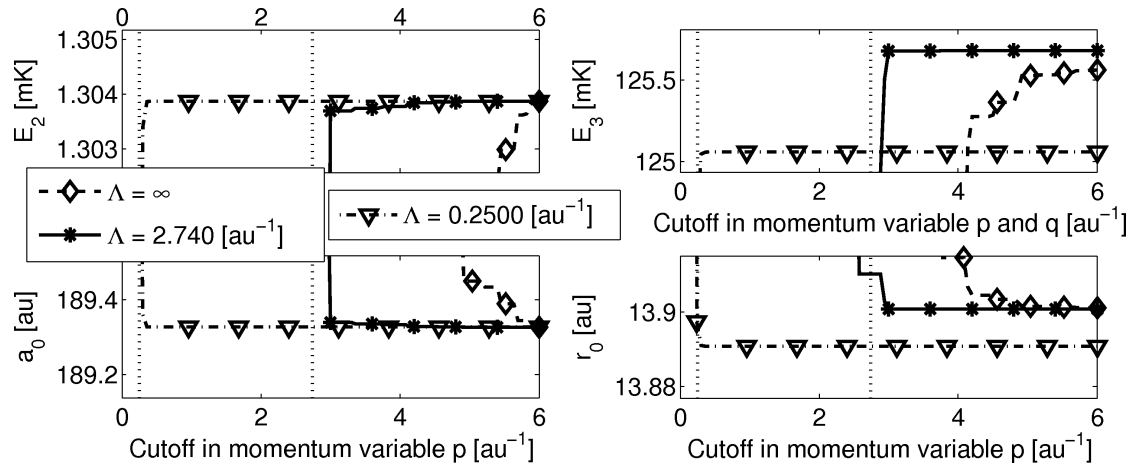


Figure 32: LM2M2 potential. Two- and three-body observables depending on the cutoff in the momentum variables. The evolved potential has a greatly improved decoupling for all observables. The grid used is $(0.9, 6.0, 40, 20)$ with $L_p \leq 6$.

Part IV

Conclusions

15 Algorithms

15.1 Faddeev equation

Using the Faddeev equation proved to be an effective method to calculate the three-body binding energy. The kernel matrix was fast to calculate since no full matrix multiplication is needed. The property that the eigenvalue 1 is the largest eigenvalue is an important property, which makes it easy to find the eigenvalue. It did not work so well for the LM2M2 potential however. As explained in section 14.3 the reason is that there are many eigenvalues close to one.

15.2 SRG flow equation

The SRG flow equation with the kinetic energy as generator for a two-particle system in a momentum space partial wave basis, implemented as in eq. (11.3), is fast and accurate. All observables retained their values, with the exception of the small change in the effective range, which likely comes from the way I calculated the effective range, and not from errors in the SRG flow equation. In all cases the potential attained a more band diagonal structure. The decoupling was increased compared to the unevolved potential in all cases.

For a three-particle system the results are not as good. For the nucleon potentials there were relatively small errors in the SRG evolution, but still significant. In the case of the soft-core helium potential the situation is not as good, where the three-body binding energy differed too much from the unevolved value. The reason for the large difference could be due to the difference in importance of the three-body forces. The soft-core helium potential has a very strong three-body force, while the nucleon potentials have relatively weak three-body potentials.

From figure 13a it is clear that increasing the maximum value of the angular momentum will improve the behaviour of the SRG transformation. It was also observed that different potentials need different high L_p values.

16 Results

16.1 Nucleon potentials

Since very large two-body grids can be used, it was easy to obtain converged values for the two-body observables. The effective range did however cause some problems, which resulted in a larger error in the converged value, as seen in table 2. The converged values agree with the reference values.

Making the three-body binding energy converge is harder, especially for the modified Yukawa potential due to the three-body potential. I had expected the three-body binding energy for the Yukawa potential to be closer to the reference value. Fully converged values are not the main focus however and I am not able to use the SRG transformation on the large matrices needed to get fully converged values.

Figure 6 shows that at least for the two-body binding energy, the momentum-space parial-wave basis is more suitable than the harmonic-oscillator basis.

The error in the SRG evolution could be controlled by increasing the L_p cutoff, as was expected.

16.2 Helium potentials

The two helium potentials – the soft-core potential and the LM2M2 potential – display very different behaviour. The soft-core potential does not need many grid points to get converged results and $L_p \leq 2$ is enough. Furthermore, it is sufficient with a momentum cutoff of 1.0 au to get good results. The LM2M2 potential, however, require a large state space to get converged results, both in the number of grid points in the momentum variables and in the L_p cutoff. This is not surprising, since the LM2M2 potential reproduces a lot of high-energy observables that require a detailed description of the potential.

The converged values of the two-body observables, shown in table 4, do not always agree with the reference values. Most notably is the scattering length a_0 for the LM2M2 potential. Also the effective range r_0 is not very well converged. The values are, however, rather good and compared with the harmonic-oscillator basis, see figure 22, the convergence is much faster.

The three-body binding energy converged relatively fast for the soft-core potential. The LM2M2 potential needed a high L_p cutoff, and $L_p = 8$ does not seem to be fully converged. The problem with the LM2M2 potential was also that I could not use as many grid points due to the problematic spectra of the Faddeev kernel, see section 14.3.

The decoupling of the LM2M2 potential was improved significantly with a low error in the observables without induced three-body forces. This was not the case with the soft-core potential, which immediately displayed large errors. However, the momentum grid for the soft-core potential was up to 1.0au^{-1} , while the LM2M2 still needed up to about 3.0au^{-1} without changing the three-body binding energy too much. For $\Lambda = 0.25\text{au}^{-1}$ the LM2M2 potential for low momentum values have matrix elements on the same order of magnitude as the soft-core potential.

17 Improvements

17.1 Momentum grids and angular momentum cutoff values

It is the size of the three-body state space that is the limiting factor. This suggests a couple of improvements. First off, the size of the two-body state space, used for the two-body potential for example, have only a small impact on the execution time of the algorithms. This means that a larger two-body state space can be used, possibly

improving convergence of the three-body binding energy and maybe also improving the SRG flow equation.

Another improvement to the grid structure could be to use different grids for different L_p values. Both the cutoff values and the number of grid points could be varied. Probably, larger cutoffs would be better for high L_p values, since the potentials for high L_p are localized at higher momentum values, as seen in for example figure 18. Also, fewer grid points could be used for higher L_p values, since the low L_p values are of greatest importance to the low-energy observables.

One could for example implement an algorithm that automatically chooses a suitable grid for each L_p value, by looking at the integration error using that grid. This, together with using different grids for the two- and three-body states spaces could improve the results without increasing the running time of the algorithms.

Using different grids for different L_p values could potentially improve the SRG results significantly, since the potentials for high L_p would be more accurately represented.

17.2 SRG flow equation

To decrease the error in the SRG evolution, the most important improvement is most likely to not precompute the permutation matrices so that interpolation and extrapolation of the kinetic energy operator and other permutation matrices can be avoided. If this would result in a too slow algorithm, a compromise could be to precompute permutation matrices where the kinetic energy is already included, which would remove some of the unnecessary interpolations and extrapolations.

In order to speed up the SRG flow equation, one possibility could be to take advantage of the band diagonal structure that arise. By using sparse matrices and dynamically remove elements that have become zero and also remove high momentum elements when they no longer affect the low-energy observables the SRG transformation should be faster and require less memory.

References

- [1] S.K. Bogner, R.J. Furnstahl, and A. Schwenk. From low-momentum interactions to nuclear structure. *Prog. Part. Nucl. Phys.*, 65(1):94 – 147, 2010. ISSN 0146-6410. doi:10.1016/j.ppnp.2010.03.001.
- [2] Franz Wegner. Flow-equations for hamiltonians. *Ann. Phys. (Berlin)*, 506(2):77–91, 1994. ISSN 1521-3889. doi:10.1002/andp.19945060203.
- [3] Stanisław D. Głazek and Kenneth G. Wilson. Renormalization of hamiltonians. *Phys. Rev. D*, 48:5863–5872, Dec 1993. doi:10.1103/PhysRevD.48.5863.
- [4] S. K. Bogner, R. J. Furnstahl, and R. J. Perry. Similarity renormalization group for nucleon-nucleon interactions. *Phys. Rev. C*, 75:061001, Jun 2007. doi:10.1103/PhysRevC.75.061001.
- [5] O. Åkerlund, E.J. Lindgren, J. Bergsten, B. Grevholm, P. Lerner, R. Linscott, C. Forssén, and L. Platter. The similarity renormalization group for three-body interactions in one dimension. *Eur. Phys. J. A*, 47(10):122, 2011. doi:10.1140/epja/i2011-11122-4.
- [6] K. Hebeler. Momentum-space evolution of chiral three-nucleon forces. *Phys. Rev. C*, 85:021002, Feb 2012. doi:10.1103/PhysRevC.85.021002.
- [7] E. D. Jurgenson, P. Navrátil, and R. J. Furnstahl. Evolving nuclear many-body forces with the similarity renormalization group. *Phys. Rev. C*, 83:034301, Mar 2011. doi:10.1103/PhysRevC.83.034301.
- [8] Robert Roth, Joachim Langhammer, Angelo Calci, Sven Binder, and Petr Navrátil. Similarity-transformed chiral $nn + 3n$ interactions for the *Ab Initio* description of ^{12}C and ^{16}O . *Phys. Rev. Lett.*, 107:072501, Aug 2011. doi:10.1103/PhysRevLett.107.072501.
- [9] Ronald A. Aziz and Martin J. Slaman. An examination of ab initio results for the helium potential energy curve. *J. Chem. Phys.*, 94(12):8047–8053, 1991. doi:10.1063/1.460139.
- [10] GNU. Gsl – gnu scientific library. <http://www.gnu.org/software/gsl/>, may 2012.
- [11] J. J. Sakurai. *Modern Quantum Mechanics*. Addison-Wesley, revised edition, 1994.
- [12] J. M. Blatt and V. F. Weisskopf. *Theoretical nuclear physics*. John Wiley and sons, inc., 1952.
- [13] M. Abramowitz and A. Stegun. *Handbook of mathematical functions*. Dover publications, inc., ninth edition, 1973.
- [14] Frederick W. Byron, Jr. and Robert W. Fuller. *Mathematics of classical and quantum physics*. Dover Publications, Inc, 1992.

-
- [15] W. Glöckle. *The Quantum Mechanical Few-Body Problem*. Springer-Verlag, 1983.
- [16] G. H. Golub and C. F. van Loan. *Matrix Computations*. The Johns Hopkins University Press, third edition, 1996.
- [17] Ch. Elster, W. Schadow, A. Nogga, and W. Glöckle. Three-body bound-state calculations without angular-momentum decomposition. *Few-Body Syst.*, 27:83–105, 1999. ISSN 0177-7963. doi:10.1007/s006010050124.
- [18] H. Liu, Ch. Elster, and W. Glöckle. Model study of three-body forces in the three-body bound state. *Few-Body Syst.*, 33:241–258, 2003. ISSN 0177-7963. doi:10.1007/s00601-003-0019-x.
- [19] M. Gattobigio, A. Kievsky, and M. Viviani. Spectra of helium clusters with up to six atoms using soft-core potentials. *Phys. Rev. A*, 84:052503, Nov 2011. doi:10.1103/PhysRevA.84.052503.
- [20] W. Glöckle, G. Hasberg, and A.R. Neghabian. Numerical treatment of few body equations in momentum space by the spline method. *Zeit. Phys. A*, 305:217–221, 1982. ISSN 0939-7922. doi:10.1007/BF01417437.
- [21] AMD. Amd core math library (acml). <http://developer.amd.com/libraries/acml/pages/default.aspx>, may 2012.
- [22] Intel. Math kernel library from intel. <http://software.intel.com/en-us/articles/intel-mkl/>, may 2012.
- [23] R. Clint Whaley. Automatically tuned linear algebra software (atlas). <http://math-atlas.sourceforge.net/>, may 2012.
- [24] OpenMP Architecture Review Board. Openmp.org. (<http://openmp.org/wp/>), may 2012.

Appendices

A Quadratures

As explained in section 7.2, all quadrature rules are defined over a finite interval, $[a, b]$, or an infinite interval. The associated discrete points are called $\{x_i\}_{i=1}^N$ and the weights are called $\{w_i\}_{i=1}^N$.

For the finite interval quadratures, the interval can be changed to any arbitrary, finite interval by means of the variable substitution

$$\tilde{x} = \tilde{a} \frac{b-x}{b-a} + \tilde{b} \frac{x-a}{b-a} = x \frac{\tilde{b}-\tilde{a}}{b-a} + \frac{\tilde{a}b-\tilde{b}a}{b-a} \equiv kx + m \quad (\text{A.1a})$$

$$d\tilde{x} = dx \frac{\tilde{b}-\tilde{a}}{b-a} = kx \quad (\text{A.1b})$$

which gives the quadrature

$$\int_{\tilde{a}}^{\tilde{b}} d\tilde{x} f(\tilde{x}) = \int_a^b dx kf(kx+m) \approx \sum_{i=1}^N w_i kf(kx_i+m) \implies \quad (\text{A.2a})$$

$$\tilde{x}_i = kx_i + m \quad (\text{A.2b})$$

$$\tilde{w}_i = kw_i. \quad (\text{A.2c})$$

The quadrature rules I have used are constructed in such a way that they will give exact results (numerical errors aside) for as high degree of polynomials as possible, for the given number of points N , times a weight function $g(x)$.

To check that a generated quadrature rule produces correct results, one can test the quadrature on functions that can be integrated analytically, and compare the numerical and analytical result. For all the quadrature rules, I did this check using the functions

$$f_0(x) = 1 \cdot g(x) \quad (\text{A.3a})$$

$$f_1(x) = xg(x) \quad (\text{A.3b})$$

$$f_2(x) = x^2g(x). \quad (\text{A.3c})$$

These functions should in theory give no error, assuming N is large enough. The errors will thus be an indication of the magnitude of the numerical errors.

A.1 Gauss-Legendre

This is the standard, finite interval quadrature. It has $g(x) = 1$, $a = -1$, $b = 1$ and the points for the N point rule are the roots of the Legendre polynomial of order N , $P_N(x)$. The weights are given by

$$w_i = \frac{2}{(1-x_i^2)(P'_N(x_i))^2}. \quad (\text{A.4})$$

The quadrature rule is exact for polynomials up to degree $2N - 1$.

The calculation of the points and weights were done using the Gnu Scientific Library.

A.2 Gauss-Lobatto

Gauss-Lobatto quadrature is a variant of Gauss-Legendre, where the end points -1 and 1 are included. It is exact for polynomials up to degree $2N - 3$. The points are $x_1 = -1$, $x_N = 1$ and for the other, x_i is root $(i - 1)$ of $P'_{N-1}(x)$, that is the derivative of the Legendre polynomial of degree $N - 1$. The weights are given by

$$w_i = \frac{2}{N(N-1)(P'_{N-1}(x_i))^2}. \quad (\text{A.5})$$

The points x_i are found by stepping – with small enough steps – over the interval $[-1, 1]$, and calculating the value of $P'_{N-1}(x)$ at each point. If there is a sign change, a simple bracketing root finder is used to locate the zero down to machine precision. The root finder calculates the value at the mid point and calls itself for the new sub interval that contains the root, until the interval is as small as it can be made. Although it is not an optimized algorithm, it runs in very short time, and it gives good results. It could fail if the step size is too large, but then one can just decrease the step size.

The Legendre polynomials are calculated using the recurrence relation

$$\begin{aligned} P_0(x) &= 1 \\ P_1(x) &= x \\ P_n(x) &= x \left(2 - \frac{1}{n} \right) P_{n-1}(x) - \left(1 - \frac{1}{n} \right) P_{n-2}(x). \end{aligned} \quad (\text{A.6})$$

A.3 Gauss-Radau

Gauss-Radau is another variant of Gauss-Legendre, where only one of the end points is included. It is exact for polynomials up to degree $2N - 2$. For the variant where the point $x_1 = -1$ is included, the rest of the points are the roots of the polynomial

$$\frac{P_{N-1}(x) + P_N(x)}{1+x}. \quad (\text{A.7})$$

The weights are given by the expression

$$w_i = \frac{1-x_i}{n^2(P'_{N-1}(x_i))^2}. \quad (\text{A.8})$$

To get the variant where the point $x_N = 1$ is included, I can just let $x_i \rightarrow -x_i$. The calculation of the points and weights are done in the same way as for the Gauss-Lobatto quadrature rule, see appendix A.2.

B Interpolation and extrapolation

Two different interpolation schemes have been implemented and compared. Both are of the form

$$y_j \approx \sum_{i=1}^N s_i(x_j; g_1, g_2, \dots, g_N) v_i, \quad (\text{B.1})$$

where y_j is the value at the intermediate point, x_j is the unknown point, v_i are the values at the grid points g_i .

The first one is a linear interpolation, where for a point x_j between the two grid points g_0 and g_1 the value of the s_i coefficients are

$$\begin{aligned} s_0 &= \frac{g_1 - x_j}{g_1 - g_0} \\ s_1 &= \frac{x_j - g_0}{g_1 - g_0} \\ s_2 &= s_3 = \dots = s_N = 0. \end{aligned} \tag{B.2}$$

This method has the advantages of being fast and requiring only a small amount of memory.

The other method is a global c-splines method, where each grid point is used to estimate the value at x_j [20].

The global c-splines method generally gives more accurate results, so I have used that method, since the time and memory used by the interpolation matrices were very low anyway.

Extrapolation is a tougher problem, since the behaviour need to be guessed. In my case, I know beforehand what the maximum value to extrapolate will be. The extrapolation was then done by assuming that there is another known point at the highest possible extrapolation point, with the value zero. For the extrapolation region linear interpolation was then used to get the value.

C Permutation operators

Here I present the factors G_p and G_R that appear in the permutation operators.

$$\begin{aligned} G_p(q, q', x, L_\alpha, L'_\alpha; L) &= \\ &= w_x(2L_p + 1)(2L'_p + 1)\sqrt{(2L_q + 1)(2L'_q + 1)} \\ &\times \sum_{\tilde{L}_p} \sqrt{\binom{2L_p}{2\tilde{L}_p}} \sum_{\tilde{L}'_p} \sqrt{\binom{2L'_p}{2\tilde{L}'_p}} q^{L_p + L'_p - \tilde{L}_p - \tilde{L}'_p} q'^{\tilde{L}_p + \tilde{L}'_p} \left(\frac{1}{2}\right)^{L_p - \tilde{L}_p + \tilde{L}'_p} \\ &\times \sum_f (2f + 1) \begin{Bmatrix} \tilde{L}_p & L_p - \tilde{L}_p & L_p \\ L_q & L & f \end{Bmatrix} \begin{pmatrix} L_p - \tilde{L}_p & L_q & f \\ 0 & 0 & 0 \end{pmatrix} \\ &\times \sum_{f'} (2f' + 1) \begin{Bmatrix} L'_p - \tilde{L}'_p & \tilde{L}'_p & L'_p \\ L'_q & L & f' \end{Bmatrix} \begin{pmatrix} \tilde{L}'_p & L'_q & f' \\ 0 & 0 & 0 \end{pmatrix} \\ &\times \sum_k (2k + 1) \begin{Bmatrix} f & \tilde{L}_p & L \\ f' & L'_p - \tilde{L}'_p & k \end{Bmatrix} \begin{pmatrix} k & \tilde{L}_p & f' \\ 0 & 0 & 0 \end{pmatrix} \begin{pmatrix} k & L'_p - \tilde{L}'_p & f \\ 0 & 0 & 0 \end{pmatrix} \\ &\times P_k(x). \end{aligned} \tag{C.1}$$

$$\begin{aligned}
G_R(p, q, x, L_\alpha, L'_\alpha; L) &= \\
&= w_x (2L'_p + 1)(2L'_q + 1) \sqrt{(2L_p + 1)(2L_q + 1)} \\
&\quad \times \sum_{\tilde{L}'_p} (-1)^{\tilde{L}'_p} \sqrt{\binom{2L'_p}{2\tilde{L}'_p}} \left(\frac{3}{4}\right)^{L'_p - \tilde{L}'_p} \\
&\quad \times \sum_{\tilde{L}'_q} \sqrt{\binom{2L'_q}{2\tilde{L}'_q}} p_1^{\tilde{L}'_p + \tilde{L}'_q} q^{L'_p + L'_q - \tilde{L}'_p - \tilde{L}'_q} \left(\frac{1}{2}\right)^{L'_q - \tilde{L}'_q + \tilde{L}'_p} \\
&\quad \times \sum_f (2f + 1) \begin{pmatrix} \tilde{L}'_p & \tilde{L}'_q & f \\ 0 & 0 & 0 \end{pmatrix} \\
&\quad \times \sum_{f'} (2f' + 1) \begin{Bmatrix} \tilde{L}'_p & L'_p - \tilde{L}'_p & L'_p \\ \tilde{L}'_q & L'_q - \tilde{L}'_q & L'_q \\ f & f' & L \end{Bmatrix} \begin{pmatrix} L'_p - \tilde{L}'_p & L'_q - \tilde{L}'_q & f' \\ 0 & 0 & 0 \end{pmatrix} \\
&\quad \times \sum_k (2k + 1) \begin{Bmatrix} L_p & f & k \\ f' & L_q & L \end{Bmatrix} \begin{pmatrix} L_p & f & k \\ 0 & 0 & 0 \end{pmatrix} \begin{pmatrix} L_q & f' & k \\ 0 & 0 & 0 \end{pmatrix} P_k(x).
\end{aligned} \tag{C.2}$$

The 3j-symbols are written with parenthesis and the 6j-symbols and 9j-symbols with curly brackets. P_k is the Legendre polynomial of degree k .

The summations over \tilde{L}'_p , \tilde{L}'_q and \tilde{L}'_q runs from 0 up to the corresponding angular momenta without the tilde. The other summation variables will be restricted by the 3j-, 6j- and 9j-symbols.

D Software

All implementations have been done in the programming language C. The implementation is heavily built around the open source library GSL – Gnu Scientific Library [10] – version 1.15.

BLAS routines have been used in order to get fast matrix and vector operations. The BLAS implementations used are ACML [21], MKL [22] and ATLAS [23] depending on availability.

openMP [24] was used to parallelize the code, together with POSIX threads.